Doctoral Thesis

Gd and B Based Integral Neutron Absorber for Spent Fuel Transportation and Storage System

Mi Jin Kim

Department of Nuclear Engineering

Graduate School of UNIST

2020

Gd and B Based Integral Neutron Absorber for Spent Fuel Transportation and Storage System

Mi Jin Kim

Department of Nuclear Engineering

Graduate School of UNIST

Gd and B Based Integral Neutron Absorber for Spent Fuel Transportation and Storage System

A thesis/dissertation
submitted to the Graduate School of UNIST
in partial fulfillment of the
requirements for the degree of
Doctor of Philosophy

Mi Jin Kim

01. 07. 2020
Approved by

Deokjung Lee
Advisor
Deokjung Lee

Gd and B Based Integral Neutron Absorber for Spent Fuel Transportation and Storage System

Mi Jin Kim

This certifies that the dissertation of Mi Jin Kim is approved.

01. 07. 2020

Advisor: Deokjung Lee

Co-advisor: Dong-Seong Sohn

Eisung Yoon

Changje Park

Hyunchul Lee

Abstract

This study presents the development of a new integral type neutron absorber design, characterized by the gadolinium (Gd) and boron (B) containing structural materials that enhance criticality safety and capacity for spent fuel transportation and storage system. The Gd and B stainless steel could act as both a structural member and a neutron absorbing member. It would help increase the storage capacity at equal volumes and decrease the manufacturing costs from removing the welding process between separate neutron absorber and sheathing.

The sensitivity studies were conducted for optimizing design parameters of the pitch between fuel assemblies, the inner width of the cell and the thickness of the cell wall in spent fuel transportation and storage system. The neutron multiplication factors reduce with increasing pitch and decreasing inner width due to the flux trap. The flux trap increases with increasing pitch and decreasing inner width. The flux trap enhances the neutron thermalization. However, the k_{eff} shows the minimum at optimum thickness according to the contents of neutron absorbing materials and design parameters. When thickness increases, the quantity of neutron absorbing materials increase and, on the other hand, the flux trap decreases. From competing for two phenomena, the optimum thickness is decided.

For reducing reactivity, the pitch should be maximum, and the inner width should be minimum when neutron absorber exists. The thickness of the cell wall is needed to be analyzed for specific neutron absorber content. However, large pitch occupies a large space to store the same amount of fuel assemblies. Only if the subcriticality is maintained, the pitch should be reduced for effective storage.

The new neutron absorber, Gd and B stainless steel with optimized dimension was applied to spent fuel transportation and storage cask and spent fuel pool storage rack. For the flux trap type transportation and storage system, the spent fuel pool of Shin-kori units 3 and 4 was selected for the spent fuel storage pool and the KORAD-21 was selected for spent fuel storage cask. The possible combination of Gd and B stainless steel and the optimized dimension were analyzed.

Maintaining subcriticality for accident conditions is critical. For SFP rack, the fuel assembly dropped in the region I and misloading of fresh fuel in region II were considered. For SFP cask, the eccentric position of the fuel assembly, flooding at various water height, flooding between pellet and cladding and loading of damaged fuel were analyzed. All accident conditions maintain subcriticality. The Gd and B stainless steel could ensure regulatory limits for accident conditions.

In conclusion, the Gd and B stainless steel with an optimized dimension could improve criticality control. This neutron absorber could applicable to both spent fuel cask and rack. Also, it could be stored more fuel assemblies in the same space.

Contents

List of the figures

List of Tables

Chapter 1. Introduction

Spent nuclear fuels (SNF) are continuously generated from nuclear reactors. After withdrawal from reactors, the SNFs are stored at the spent fuel pool storage within the nuclear power plant (NPP) site. The current status of SNF storage in Korea is summarized in Table 1 [1]. Most of the nuclear power plant units are already cumulated of spent fuel pool (SFP) storage over 80%. The shortage of spent fuel pool storage in NPP has been issued. The spent fuels are needed to be moved or stored at other systems. For extending storage capacity, existing storage has been replaced to high density storage rack. After withdrawing from SFP, the promising solution is interim storage of SNF before the final disposal of SNF. The interim storage is storing SNF at dry cask. Both SFP and dry cask needs to maintain safety requirements. The reactivity from SNF needs to be controlled.

The spent fuel pool storage stores spent fuel just right after burned in the reactor and during refueling periods. The fuel assemblies move from the reactor to the spent fuel storage pool along the bottom of water canals. Therefore, they always moved under water at least 20 m. It positions inside the nuclear power plant. The spent fuels are cooled by water reinforced by the pump. In spent fuel pool storage, there are two types of the region; region I and region II. Region I could store high reactive fuels and has two neutron absorber plates between fuel assemblies. The water between the two plates plays the role of a flux trap, a zone where neutron thermalization is enhanced and where the neutrons do not escape. Indeed, after entering a flux trap, the neutrons become thermalized in the water, and when “they attempt to” leave through the plates, they get “trapped” due to the high neutron-absorption cross-sections of the neutron-absorber plates in the thermal range. Region II is for low reactivity SNF and has one neutron absorber plate between fuel assemblies. For region II criticality-safety analysis, burnup credit is a commonly used methodology.

For dry cask, it could be stored after cooled by several years in spent fuel pool storage. Dry cask could be used in several ways; transport cask, storage cask, and dual-purpose cask. The transport cask is for transporting SNFs from SFP to an interim storage site. The SNF withdrawal from SFP moves to transport cask within the water and then, the transport cask contained SNF backfill with inert gas. From the transport cask, the canister moves to the storage cask. At the interim storage site, the form of the cask is storage cask. In these casks, the spent fuel would be cooled by dry air or inert gas by natural convection. The array of baskets is separated into the flux trap type and non-flux trap type. The flux trap type basket has two neutron absorbers between fuel assemblies and flux trap location to enhance the thermalization of the neutron. This structure could store much higher reactivity fuel assembly. The non-flux trap type basket has one neutron absorber between adjacent fuel assemblies. They could store SNF in a compact array, but it could store low reactivity fuel assemblies which needs burnup credit when criticality analysis performs.

For increasing the effectiveness of spent fuel storage systems, some solutions would be needed such as advanced neutron absorber and effective structure.

For effective storage of spent fuel, an advanced neutron absorber is needed. Commercially, boron (B) based neutron absorber is popularly used in the spent fuel storage systems such as BORAL®, METAMIC™ and borated stainless steel. Boron is 1/v absorber, so it well absorbs neutron overall energy range. However, boron could produce He bubble from $^{10}B(n,\alpha)\ ^{7}Li$ reaction. He bubbles could generate more swelling problems and make material degradation of boron neutron absorber so, it would not be good at long-term storage. Their problems have been noticed at several papers [2], [3].

The BORAL® and METAMIC™ are boron carbide (B_4C) and aluminum (Al) composite material. They have high B loading capability, however, poor mechanical properties. It needs to be attached to the wall and an additional welding process. Therefore, these materials are utilized in three layers. The neutron absorbers are attached to the cell wall and sheathing covers to protect them. From these three layers, the galvanic corrosion accelerates between neutron absorber and sheathing.

The borated stainless steel is boron alloyed stainless steel. It has enough ductility and impact resistance to be used as a structural material. It performs both structural and neutron absorbing member and used as a one-layer structure. However, it shows low solubility of B in stainless steel and manufacturing more than 2.25 wt% B is difficult.

Gadolinium (Gd) based neutron absorber has been developed called Ni-Cr-Mo-Gd alloy. This alloy was developed under DOE's National Spent Nuclear Fuel Program (NSNFP) inserted in the standardized canister for Yucca Mountain Repository. For long-term storage, high corrosion resistance neutron absorber has been investigated. A Ni-Cr-Mo base metal alloy was selected in order to provide long-term corrosion resistance. From the criticality safety requirements, the contents of Gd is about 2 wt%. This alloy is represented in ASTM B932-04 [4].

Therefore, it is essential to consider advanced neutron absorbing materials which have a higher neutron absorption cross section in the thermal energy region. The development of a new neutron absorber has been noticed. A rare-earth compound based neutron absorber has been described in [5]–[7]. They analyzed criticality with various vitrified form as neutron control elements. The shape of elements is cylinder which surrounds the whole edge of the fuel assembly and it is protected by stainless steel [7]. Also, cylindrical shape neutron absorbers are positioned at the guide tube site to control criticality [6]. However, this rare earth form neutron absorber is needed reprocessing in advance. Reprocessing has not been accepted in Korea and developing neutron absorber based on reprocessed fuel is in the far future. Also, installing the neutron absorber inside the guide tube needs much more works and process than using neutron absorber at plate or tube form in SNF storage systems.

Also, Gd based neutron absorber has been investigated for duplex stainless steel [8]–[11]. Duplex stainless steels have excellent corrosion resistance and mechanical properties [10]. The mechanical properties and corrosion resistance have been tested in [8], [11].

In this study, gadolinium (Gd), samarium (Sm), erbium (Er) and europium (Eu) have been considered for new advanced neutron absorbing materials which are widely utilized as burnable poison due to their high neutron absorption capability. Unlike boron, they do not produce the gas products when they react with neutrons.

In the design point of view, the spent fuel could separate into two types. The first one is the flux trap type. This type has two neutron absorber plates between fuel assemblies. So, it could store high reactivity fuels, but it needs a large space. The other type is a non-flux trap type. It has one neutron absorber between fuel assemblies. It could store low reactivity fuels. However, it could store in compact orientation.

The water gap between two neutron absorbers called the “flux trap”. Flux trap is a moderating region or island that nuclear fuel does not exist. Fast neutrons come out from nuclear fission reaction moderates in this region, therefore, in flux traps, we could get high thermal neutron flux. Hence, the flux trap has been utilized in research reactors.

High Flux Isotope Reactor (HFIR) reaches critical in 1965 at ORNL (Oak Ridge National Laboratory), USA. It performs the highest neutron flux among research reactors in the USA [12]. HFIR is a flux-trap type reactor operating at 85 MW and produces an average thermal neutron flux of $2.3 \times 10^{15}\ n/cm^2 \cdot s$. The flux trap located at the center of the reactor core and is surrounded by an annular region of fuel. The size of the flux trap is 12.70 cm in diameter. The thermalized neutrons trapped at the center and make it available for isotope production.

Advanced Test Reactor (ATR) operates from 1967 is developed for neutron radiation experiments. The maximum power of ATR is 250 MW and maximum thermal neutron flux is $1.0 \times 10^{15}\ n/cm^2 \cdot s$. It has a unique serpentine shape of fuel elements so it could have nine flux traps. The reactor core is about 121.92 cm (4 ft) diameter [13], [14]. For this reactor, the flux is high only at the flux trap position and the others are low flux.

Forschungs-Neutronenquelle Heinz Maier-Leibnitz (FRM-II) reactor went critical from 2004 by the Technical University of Munich in Germany. It has been designed to obtain high thermal neutron flux at the outer region of the reactor core with a large volume. It is ‘compact core’ that is used for cores with about 0.5 times smaller than ordinary cores. The active core size is between 6.75 and 11.2 cm in radius. The reactor power is 20 MW and maximum thermal neutron flux is $8 \times 10^{14}\ n/cm^2 \cdot s$ [6–8]. It has an inverse flux trap which has a flux trap outside of fuels. The best position of flux trap is at the center, however, it has a limit of reactor size. Therefore, they designed the inverse flux trap. In this concept, the lower reactor core performs the higher neutron flux at the same power. So, the reactor core is relatively smaller than any other research reactors.

High-Flux Advanced Neutron Application Reactor (HANARO) reached an initial critical in 1995 operated by the Korea Atomic Energy Research Institute (KAERI) in Korea. It was designed to utilize in a multi-purpose research reactor. The reactor power is 30 MW. The maximum neutron flux is

$5 \times 10^{14}\ n/cm^2 \cdot s$. It has three flux traps inside the core and the inside diameter is 7.44 cm of the same size with fuel assembly. The flux trap at the core is utilized for fuel/material test or radioisotope production [18], [19].

Unlike research reactors, the spent fuel storage system employs a flux trap for a different purpose. The neutrons generated from the fission reaction travels to the water gap. At the water gap, the water moderates the neutrons and it converts to thermal neutrons. These thermal neutrons have a short mean free path [20], therefore, they are absorbed by neutron absorbers and hard to escape from the water gap. Therefore, these neutrons are “trapped” in the water gap so-called “flux trap”. Flux trap type spent fuel storage enhances the thermalization of neutrons and reduces the reactivity of the system.

The neutron movement at the spent fuel storage pool had been studied in [21]. It describes the neutron movement and criticality with a stainless steel wall. Only one fuel assembly moderated by water had been studied. It is hard to explain the neutron movement and criticality when the array of fuel assembly rack has been stored in the spent fuel storage pool. Therefore, in this paper, the analysis of neutron movement and the effect of the flux trap have been studied with neutron absorbing material.

Through neutron absorbing materials and sensitivity studies, the new neutron absorber was applied to conventional spent fuel transportation and storage system.

Table 1 Spent fuel storage status in Korea (data until 2019 3rd quarter) [1]

Plant	Unit		Capacity	Stored FA	Saturation (%)
Kori	1		562	485	86
	2		799	652	82
	3		2103	1980	94
	4		2105	1997	95
	Shinkori-1		1273	564	44
	Shinkori-2		1273	662	52
Saeul	Shinkori-3		780	100	13
	Shinkori-4		780	0	0
Hanbit	1		2105	1713	81
	2		2100	1335	64
	3		1125	911	81
	4		1125	914	81
	5		1281	781	61
	6		1281	782	61
Hanul	1		957	869	91
	2		905	812	90
	3		1321	1118	85
	4		1321	1054	80
	5		1281	965	75
	6		1281	847	66
Wolsung	PWR	Shinwolsung-1	523	262	50
		Shinwolsung-2	523	189	36
	PHWR	1	44688	32728	73
		2	42408	35720	84
		3	42408	38068	90
		4	42408	35992	85
	Dry storage		330000	318480	97

Chapter 2. Analysis Methodology

2.1. Analysis code

To assure criticality safety, the 3D Monte Carlo computer codes are recommended such as SCALE/KENO, MCNP, and MONK in [22]. Among them, the KENO V.a. code in the SCALE code system is selected as an analysis code. That is the neutron transport code using the CSAS module. The ENDF/VII.0 library is selected as cross section library [23]. To evaluate neutron absorber and the effect of flux trap, criticality analysis has been performed. The analysis code was selected as KENO V.a. which is a neutron transport code that uses the Monte Carlo method.

2.2. Analysis model

2.2.1. Fuel assembly

The OPR-1000 reactor fuel assembly is selected as a fuel assembly model because it shows the most reactive fuel assembly in most fresh fuel cask [24]. The assembly design is characterized by a 16×16 fuel pin array. One instrumentation tube of size 2×2 fuel pins (in the center of the assembly) and four guide tubes of size 2×2 fuel pins are also present. The fuel rods are made of UO_2 fuel pellets surrounded by thin-walled zirlo cladding.

For the criticality analysis, the following modeling choices are adopted according to the guidelines of (U.S. NRC, 2010). These modeling choices are conservative for the purpose of evaluating the criticality of fuel assembly storage racks:

- all the fuel rods have the same initial enrichment of 4.5 wt% U-235;
- fresh fuel composition is applied;
- applied UO_2 density is 10.313 g/cm^3;
- spacer grids and top and bottom nozzles are ignored; they are replaced by water in KENO-V.a modeling;
- the fuel does not contain any burnable poisons; no control rod is used;
- the perfect cylindrical shape of fuel pellets is modeled without dishing or chamfer;
- zero boron concentration is assumed in the water coolant.

Replacing the spacer grids and nozzles by water is conservative because the modeled excess water increases neutron moderation. Since SF storage pools are under-moderated, the increased neutron moderation increases the reactivity. Not modeling the dishing and chamfer of fuel pellets is also conservative because it comes down to increase (very slightly) the fuel volume and therefore the total fissile content in the pool.

2.2.2. Spent nuclear fuel transportation and storage system

The spent fuel transportation and storage system is separated into two types of flux trap design and non-flux trap design as described in Figure 1. The flux trap type design consists of two neutron absorbers between fuel assemblies. On the contrary, the non-flux trap type design is composed of one neutron absorber between fuel assemblies.

The basic component of the spent fuel transportation and storage system is a cell wall which is a square structure of stainless steel that surrounds fuel assembly, neutron absorbers that absorb neutron for criticality control and attached at the cell wall and sheathing which covers neutron absorbers to protect them.

The dimensions of SNF transportation and storage system varies according to the type of fuel assembly. The normal inner width of the cell wall is 21 cm to 23 cm, the thickness of the cell wall is 0.19 cm to 0.75 cm. The thickness of the neutron absorber is 0.12 cm to 0.3 cm. The pitch between fuel assemblies is 26 cm to 29 cm as summarized in Table 2. The dimensions used in this study are described in Table 2.

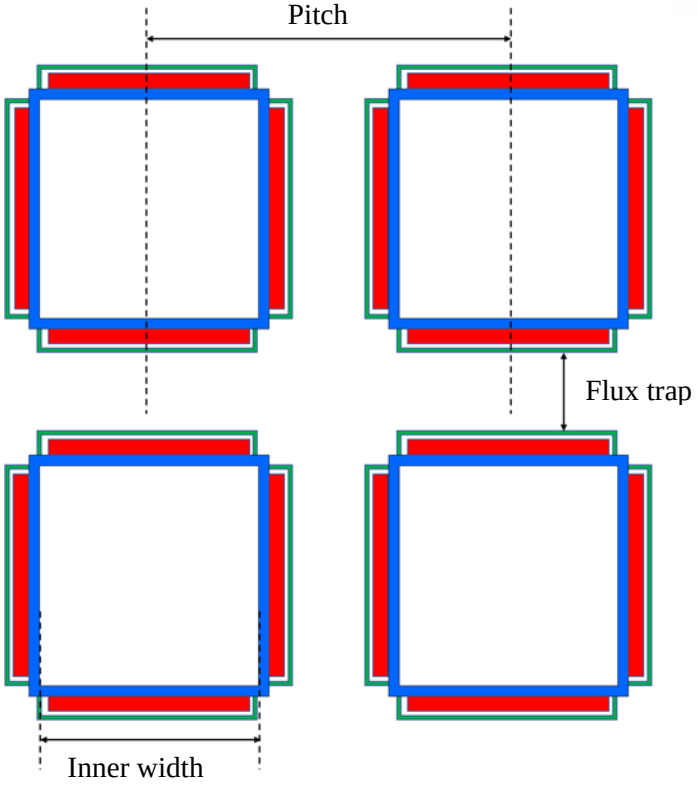

(a)

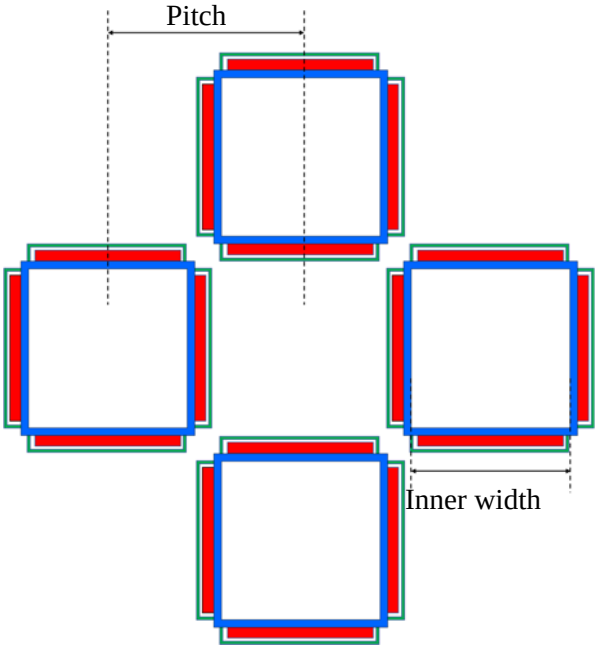

(b)

Figure 1 Cross section of a typical SNF transportation and storage system (a) Flux trap type (b) Non flux trap type

Table 2 Dimensions of general storage system and utilized in the calculation

Description	Dimension (cm)	Used in the analysis (cm)
Cell wall		
Inner width	21 to 25	22.35
Thickness	0.19 to 0.75	0.2
Pitch	26 to 29	28
Neutron absorber		
Width	18 to 20	19
Thickness	0.12 to 0.3	0.2
Sheathing		
Width	18 to 20	19
Thickness	0.05 to 0.1	0.1

2.3. Application to conventional cask

2.3.1. KSC-1

KSC-1 is a transport cask designed to shipping one fuel assembly at once. The general description and dimensions are described in Figure 2 (a). The target fuel assembly is an initial enrichment of 3.5 wt% and a burnup of 45 GWd/tU for Ulchin units 2. General dimensions are summarized in Table 3. It uses lead as a gamma shield and 50% ethylene glycol aqueous solution as a neutron shield. The basket is stainless steel and there's no neutron absorber.

In the criticality calculation, the conditions underneath were used and described in Figure 2 (b).

- Enrichment of U-235: 4.3 wt%
- Fresh fuel
- Neglect fuel basket
- Ethylene glycol aqueous solution as water
- Outer closure and inner closure and bottom plate as water

2.3.2. KSC-7

KSC-7 is a transport cask that could ship seven fuel assemblies. The design-based fuel assembly is 17x17 4.2 wt% enriched PWR fresh fuel as summarized in Table 4. The fuel basket is borated stainless steel and additional neutron absorber is B_4C rods or BORAL plates.

The fuel assemblies are fresh fuel conditions without control rods or burnable poisons for conservative calculations. The description of KSC-7 is described in Figure 3 (a). The upper and lower sides of the cask were filled with water. In the report, there are seven cases of neutron absorber combination. Among the seven cases, case number 7 was selected which that of the k_{eff} is lower than 0.95.

The neutron absorber orientation is described in Figure 3 (b). Basket is borated stainless steel of 9 mm and 68 B_4C rods and Boral plates. The KENO V.a. modeling of KSC-7 is described in Figure 3 (c).

2.3.3. KORAD-21

KORAD-21 could accommodate 21 fuel assemblies as described in Figure 4 (a). The fuel assemblies are stored at the center of the basket and the array of baskets is positioned inside the canister. Outside of the canister is a cask body, neutron shield, and outer shell. The cask body is carbon steel, the neutron shield is NS-4-FR resin and the canister and lids are stainless steel. The neutron absorber is METAMIC attached to the basket and sheathing covers it to protect. The dimensions and materials of KORAD-21 are summarized in Table 5. The fuel assembly stored in KORAD-21 is Westinghouse (WH) Optimized Fuel Assembly (OFA) 17x17 as depicted in Figure 4 (b). The dimensions of WH OFA 17x17 are summarized in Table 6.

Table 3 Fuel assembly dimension of 17x17 Ulchin unit 2

Content	dimension
Pellet diameter	0.82 cm
Fuel rod diameter	0.95 cm
Cladding thickness	0.57 cm (Zircaloy-4)
Active fuel height	370 cm
Pellet density	96 %TD*
Enrichment	4.3%
Number of fuel rod per fuel assembly	264
Weight of UO_2 per fuel assembly	528 kg

*TD: Theoretical density

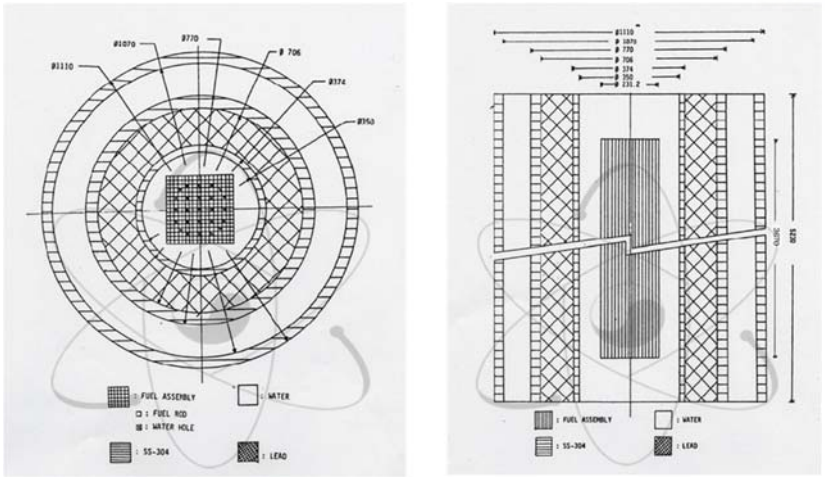

(a)

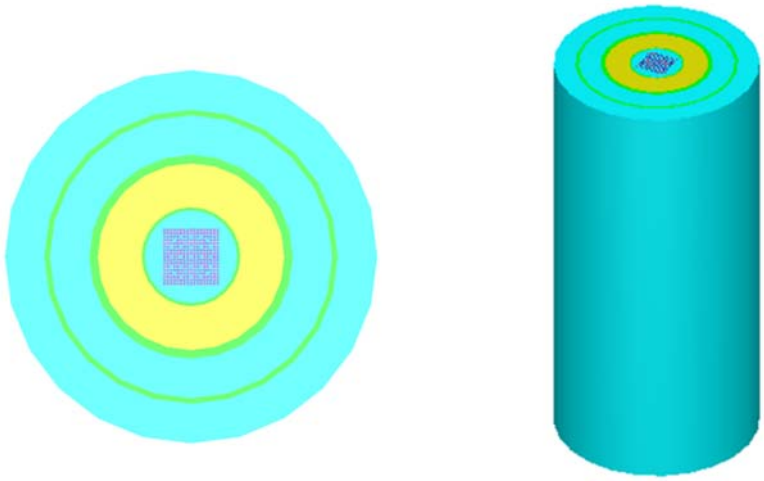

(b)

Figure 2 KSC-1 (a) Description and dimension (b) KENO V.a. model

Table 4 Description of 17x17 4.2 wt% enriched fuel

Content	Dimension
Weight of fuel assembly	639.44 kg
Weight of UO2 per fuel assembly	462.45 kg
Enrichment	4.2 w/o
Number of fuel rods	264
Active fuel height	365.76 cm
Fuel rod diameter	0.95 cm
Fuel rod pitch	1.26 cm
Cladding thickness	0.057 cm
Pellet diameter	0.819 cm
UO_2 density	95 % TD*

*TD: Theoretical density

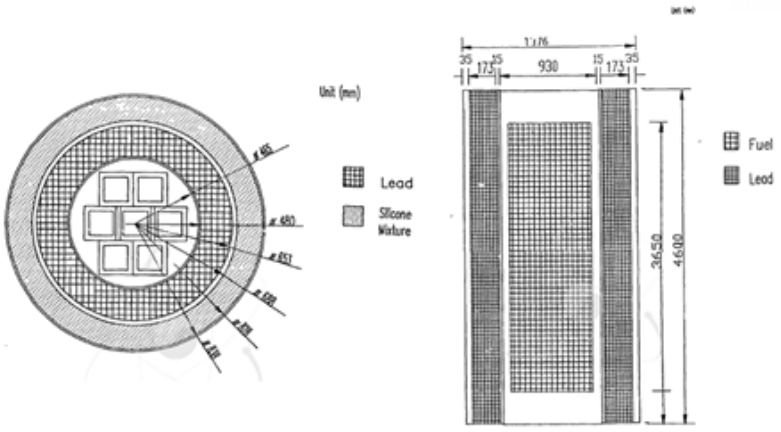

(a)

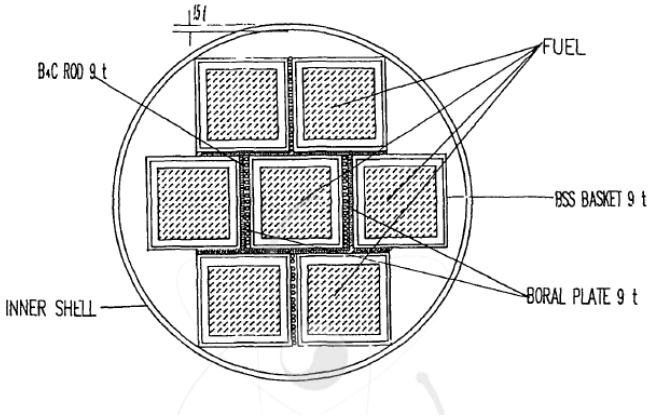

(b)

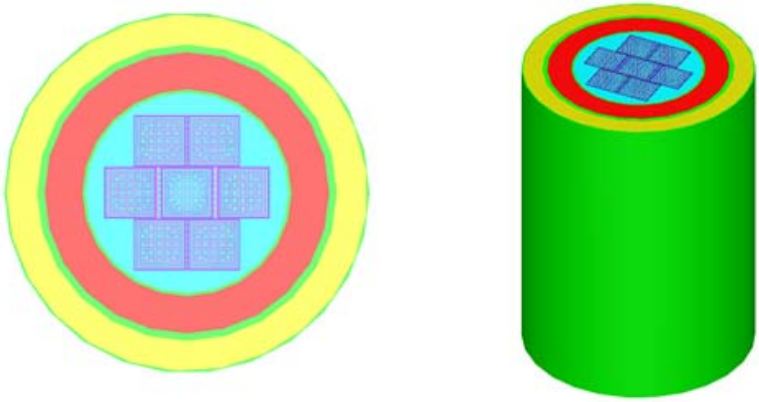

(c)

Figure 3 KSC-7 (a) Description and dimension (b) Detailed description of CASE 7 (c) KENO V.a. modelling

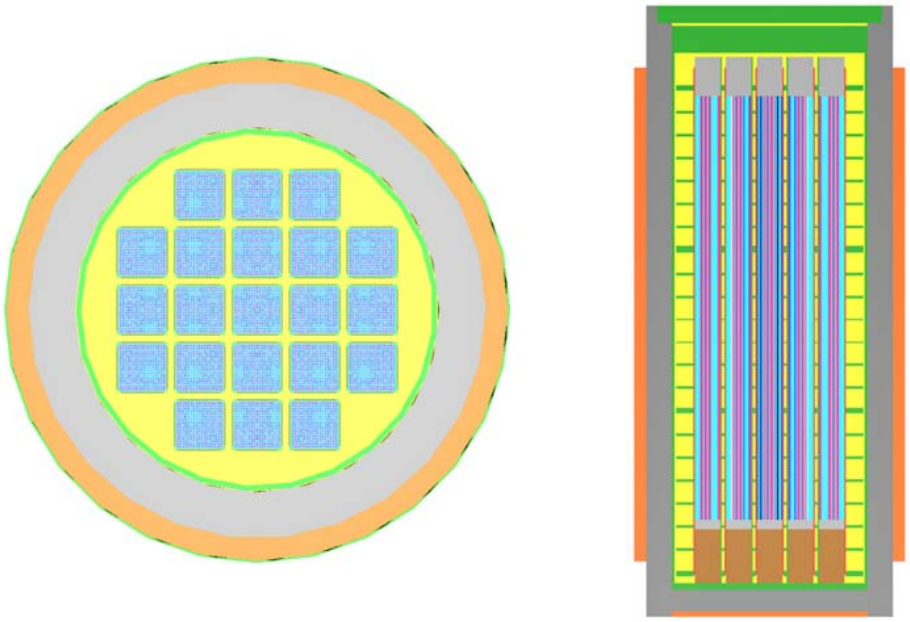

(a)

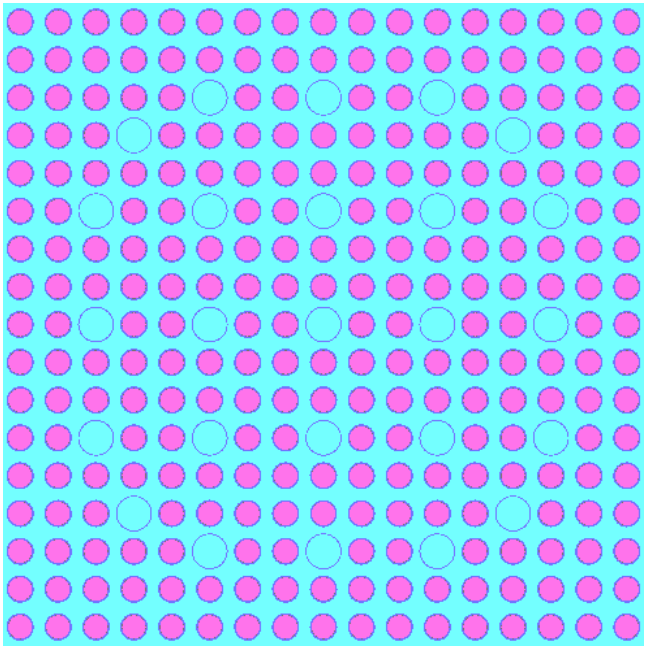

(b)

Figure 4 (a) KORAD-21 KENO-V.a. modeling (b) Description of the fuel assembly of WH OFA 17x17

Table 5 Description of material and dimension of KORAD-21

	Material	Dimension (cm)
Neutron absorber		
Thickness	B_4C + Aluminum	0.28476
Width		19.64252
Basket		
Thickness	SA240 TP 304	0.5
Inner width		22.2
Flux trap		3.55
Canister		
Upper thickness		24
Body thickness	SA240 TP 304	2.5
Lower thickness		6
Radius		163.6
Cask body		
Body thickness	SA350 LF. 3	21.5
Neutron shield thickness	NS-4-FR	10.4
Outer thickness		1
Inner diameter		169.6

Table 6 Description of WH OFA 17x17

Component		Dimension [mm]
UO_2 fuel	Diameter	7.84
	Height	3658
	Pitch	12.6
Cladding	Thickness	0.57
	Outer diameter	9.14
Guide thimble / Instrumentation tube	Inner diameter	11.23
	Outer diameter	12.04

Chapter 3. Study of new neutron absorber for spent fuel transportation and storage system

3.1. Conventional-type neutron absorber

The conventional-type neutron absorber used the boron carbide composite material has 3 layers; the cell wall, neutron absorber, and sheathing. The neutron absorbers are attached to the cell wall and sheathing covers them as described in Figure 5.

The representative examples of this type are BORAL and METAMIC. The BORAL is aluminum boron carbide cermet. Figure 6 shows the core and cladding regions. The core of BORAL has been manufactured with between 35 wt% to 65 wt% B_4C. Alloy 1100 aluminum box contains a mixture of ASTM C750 Type 3 B4C/Alloy 1100 Al powder. The blister problem has been observed in the cladding of BORAL in spent fuel rack. This blister occurs in cell wall degradation. These blisters do not reduce the neutron absorption capability; however, it changes the configurations of racks. For the region I of PWR fuel racks, the formation of blister causes that water is displaced by blister at the flux trap region. This could result in reactivity increase due to the reduction of thermalization of neutrons by flux traps. For region 2 PWR fuel racks, blister producing under the wrapper plate can cause reducing the free clearance in the cells of fuel assemblies. If several blisters occur at BORAL panels, the removal of fuel could become difficult. For dry storage and transportation case, the blister causes the wrapper to deform inward. The inward deformation of the wrapper reduces the free clearance of the cell for fuel assemblies. The porosity within the core is less likely to produce blister formation. The wetting/vacuum drying conditions would be more likely to result in blisters. Several blisters are noticed at full-size tests in ENSA as described in Figure 7. Therefore, the BORAL is suitable for storage-only canister which has only one or two wetting/drying cycles. For transportation casks, the wetting/drying cycles are too many due to producing blisters.

METAMIC is an aluminum boron carbide metal matrix composite. It produced by the powder metallurgy process of alloy 6061 aluminum and ASTM C-750 Type 1 isotopically-graded B_4C. The loading of B4C is from 0 to around 40 wt%. From accelerated corrosion testing, some coupons show localized pitting corrosion [25]. Also, the white spots have been noticed in the METAMIC surveillance coupons from KHNP. The degradation of METAMIC coupons shows the loss of boron or surface corrosion, although the B-10 areal density of the coupons was less than -5% limit. The continuous monitoring is needed for every cycle [26].

The main benefit for this type is high boron loading about 30 wt% of B_4C. However, it is needed for an additional welding process of neutron absorber to the cell wall. This could make a welding problem during radiation conditions. Also, the thickness of the total (cell wall+neutron absorber+sheathing) occupies large space in SNF transportation and storage system. When the space occupied by separate

neutron absorber or sheathing, the water at the flux trap decreases as the thickness increases. This could decrease the total thermalization of neutrons in the storage system.

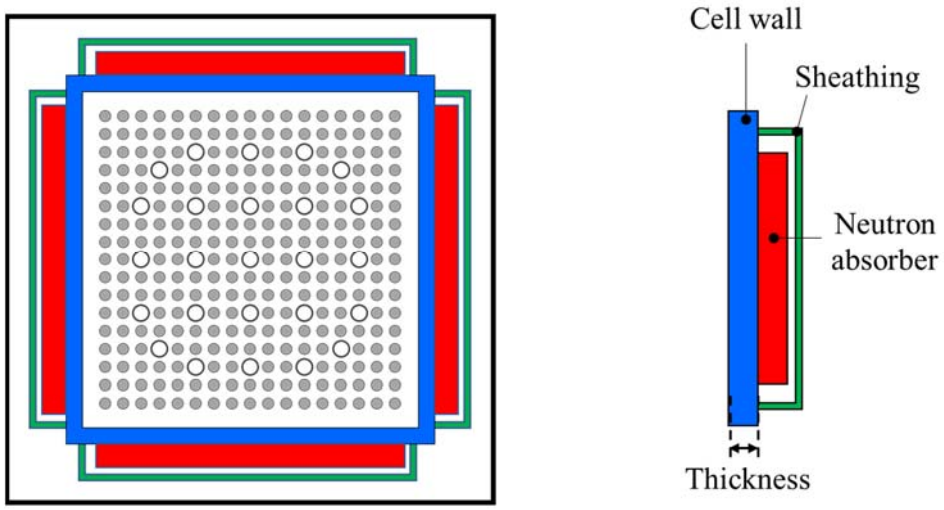

Figure 5 Description of conventional type

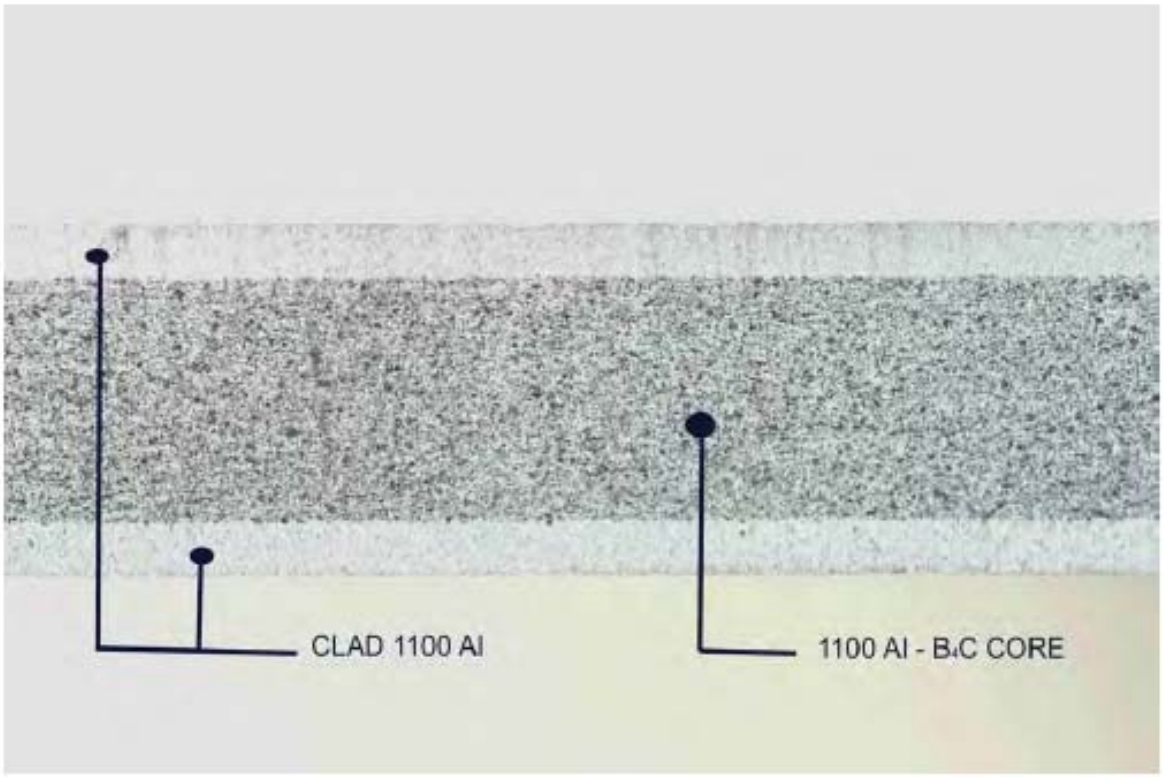

Figure 6 Microphotograph of the Trimmed Edge of BORAL [27]

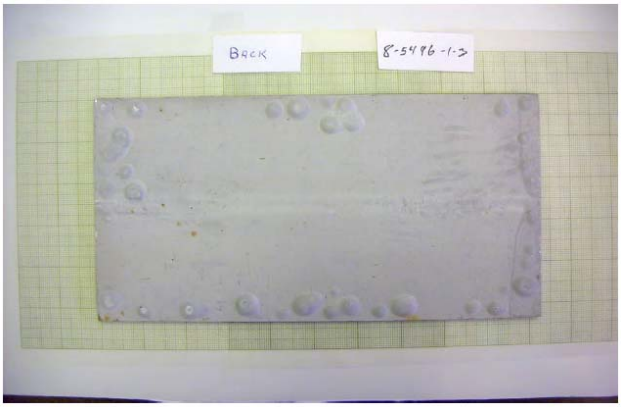

(a)

(b)

(c)

Figure 7 Blister in BORAL (a) a BWR BORAL Coupon Manufactured in the 1970s (b) Single Blister in BORAL (Full-Scale Tests at ENSA) (c) Section with Multiple Blisters (Full-Scale Tests at ENSA) [27]

(a)

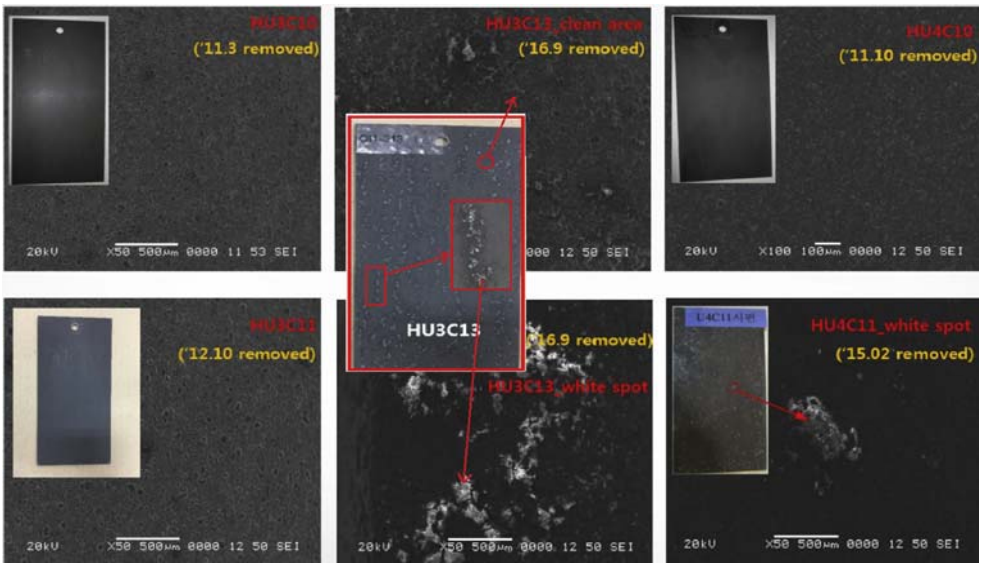

(b)

Figure 8 Metamic (a) Basket composed of Metamic [28] **(b) Surface micrographs of METAMIC coupons** [26]

3.2. New integral-type neutron absorber

A new neutron absorber would be an integral type which has a single layer of a wall without separate neutron absorber and sheath. The representative type is described in Figure 9. This wall acts as both a structural component and a neutron absorber at the same time. The wall is composed of stainless steel with neutron absorbing material. This type reduces the additional welding process of separate neutron absorber and sheathing. It would be reducing the degradation of welding.

The representative example is borated stainless steel (BSS) which is defined in ASTM A887-89 [29]. Stainless steel is a stable matrix because it has good resistant to radiation and corrosion resistance to either water or boric acid in spent fuel pools. Also, stainless steel shows excellent mechanical and structural stability. However, the solubility of boron in stainless steel is low. The manufacturing above 2.25 wt% is difficult. The BSS is divided into two grades of Grade “A” and Grade “B” according to the homogeneity of B. Grade “A” alloys are improved mechanical properties than Grade “B” alloys. The BSS shows a decrease in ductility with an increase of B loading.

Another example is Ni-Mo-Cr-Gd that is described in ASTM B932-04 [4]. This material is being developed to be used in final waste disposal at Yucca Mountain Repository project [30]. The purposes are to develop a new neutron absorber with improved reactivity control ability and improved corrosion resistance compared to borated stainless steel. Therefore, a Ni-Cr-Mo base metal alloy was selected to provide long-term corrosion resistance. The metallurgical properties decrease with increasing of the Gd content in the alloy. The maximum content of Gd is in the range of 2 wt% in Ni-Cr-Mo-Gd alloy [31].

3.2.1. Effect of new neutron absorbing materials

As described earlier, boron is the main neutron absorber used in the spent fuel storage system. However, some materials have higher neutron absorption cross section at thermal region than that of B. Candidate materials were gadolinium (Gd), samarium (Sm), erbium (Er) and europium (Eu) that are generally utilized in nuclear fuel as burnable poison due to their high neutron absorption capability.

Gd is broadly used as a fixed burnable absorber in fuel assemblies. Gd has two principal nuclides of Gd-155 and Gd-157 that have substantially high thermal neutron absorption cross sections. The thermal neutron absorption cross-section of Gd-157, respectively Gd-155, is approximately 60 times higher, respectively 16 times higher, than that of B-10, and the abundance of Gd-155 and Gd-157 is approximately 1.5 times higher than that of B-10.

Next, Sm previously used as control rods. Sm-149 has the largest thermal neutron absorption cross section of 40137.6 barn among Sm isotopes. The thermal neutron absorption cross section is 10 times larger than B-10. The abundance of Sm-149 is 13.8 slightly smaller than that of B-10.

Er is suggested as a burnable poison alternative than Gd.

Europium has two isotopes of Eu-151 and Eu-153. Both europium nuclides have a high neutron

absorption cross section. The possibility of Eu as a burnable absorber has been studied in [32], [33]. The Eu used integral burnable absorber in oxide form, Eu_2O_3. It uses as $UO_2 + Eu_2O_3$ and 2 wt% of Eu_2O_3. When Eu used as the burnable absorber, it is more effective than Gd as a burnable absorber for a long cycle.

The neutron absorbers of Gd, B, Sm, Er, and Eu are independently inserted in the stainless steel. The base alloy was selected as 304 stainless steel. The composition of 304 stainless steel is described in Table 11. In calculations, the density of stainless steel with neutron absorbing materials is calculated by mixture law in Eq. (1). The density of each material is described in Table 12. All the materials are inserted in natural composition as described in Table 13.

$$\rho_{mix} = \frac{1 - w_{abs}}{\rho_{SS}} + \frac{w_{abs}}{\rho_{abs}} \tag{1}$$

$\rho_{mix} = density\ of\ mixture$

$w_{abs} = weight\ percent\ of\ absorber$

$\rho_{SS} = density\ of\ stainless\ steel$

$\rho_{abs} = density\ of\ absorber$

All the calculations are conducted in moderation by water. The weight percent of absorber materials is calculated 0 to 2 wt%. Within a 2 wt% range of absorber contents, Gd shows the best performance among Gd, B, Sm, Er and Eu as described in Figure 10. Then, the following order of performance is B, Sm, Eu and Er. Above 1.7 wt% of absorber content, the B shows slightly better performance than that of Gd. The following order of performance is Gd, Sm, Eu and Er. The k_{eff} exponentially decreases with Gd addition. In other words, the effectiveness of Gd decreases as an increase of Gd content. The k_{eff} of other absorbers such as B, Sm and Eu decreases exponentially as the addition of absorber contents. The k_{eff} proportionally decreases as an absorber addition for the Er case. When using only Gd, it needs that the content of Gd should be at least 2 wt%. The Gd 2 wt% is hard to manufacture. The Gd burned out faster than any other materials.

Using one neutron absorbing material is not good for the manufacturing point. Therefore, using dual neutron absorbing material has been studied. B, Sm, Er and Eu were mixed with Gd 2 wt%. The density of mixture was calculated by mixture law in Eq. (2).

$$\rho_{mix} = \frac{1 - w_{Gd} - w_{abs}}{\rho_{SS}} + \frac{w_{Gd}}{\rho_{Gd}} + \frac{w_{abs}}{\rho_{abs}} \tag{2}$$

$\rho_{mix} = density\ of\ mixture$

$\rho_{SS} = density\ of\ stainless\ steel$

$$\rho_{Gd} = density\ of\ gadolinium$$
$$\rho_{abs} = density\ of\ absorbing\ material$$
$$w_{Gd} = weight\ percent\ of\ Gd$$
$$w_{abs} = weight\ percent\ of\ absorbing\ material$$

Among them, B shows the best performance as shown in Figure 11. Therefore, B is selected as the second neutron absorbing material. For being used in the spent fuel systems, the mixture content of Gd and B have been calculated in Figure 12. The contents of Gd and B are calculated in various combinations. The selected B contents are 0.225, 0.6 and 1.0 wt%. The k_{eff} continuously decreases with increasing Gd and B contents. With a large amount of B, the required Gd contents decrease. The possible contents which are possible should be determined by specific the SNF transportation and storage system and fuel assembly. Also, the manufacturability must be considered when determining the composition of neutron absorbing materials.

The manufacturability of Gd and B stainless steel was tested from HANSCO Co. and KITECH. The description of specimens is summarized in Table 14. The six alloys are manufactured and hot rolled. The specimens after hot rolling at 1050 ℃ are presented in Figure 13. From alloy 1 to 3, the B content is constant at 0.8 wt%. The Gd content is variant in 0.5 to 1.1 wt%. Only alloy 3 with Gd 1.1 wt% and B 0.8 wt% showed edge crack from hot rolling. From alloy 4 to 6, the various contents of Gd (0.32 to 0.51 wt%) and B (0.8 to 1.2 wt%). Only alloy 6 with Gd 0.51 wt% and B 1.2 wt% was noticed a huge crack. Therefore, the constraints of Gd and B content is set as 1.0 wt% for both nuclides.

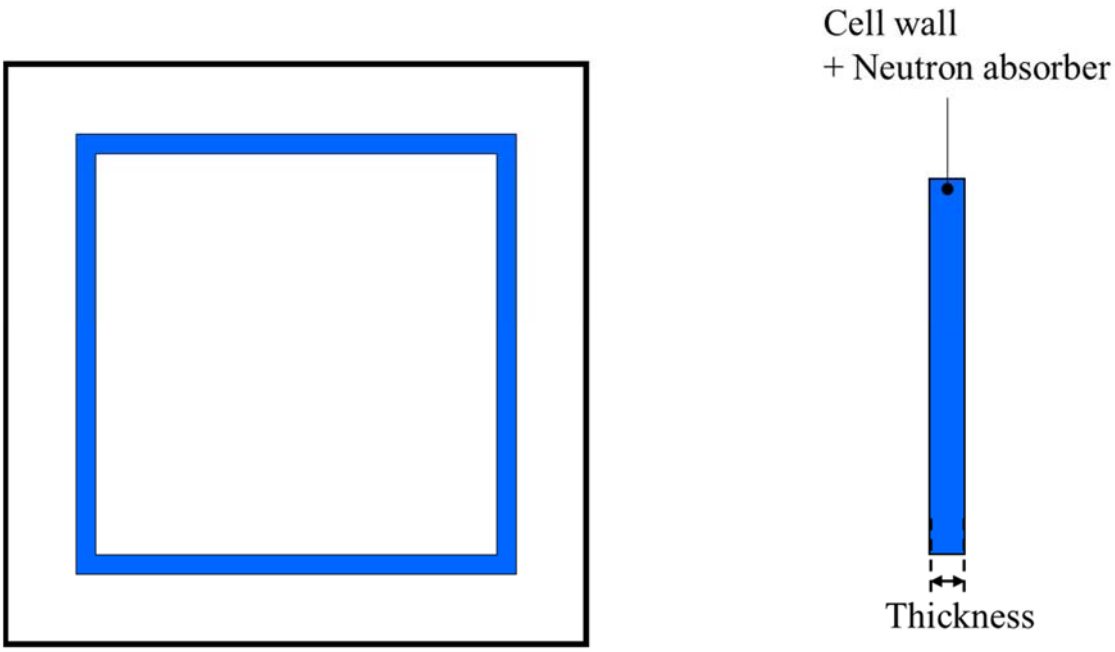

Figure 9 Description of integral type

Table 7 Thermal neutron absorption cross section of Gd (at 0.0253 eV)

Nuclide	Thermal neutron absorption cross section (barn)	Relative abundance (a/o)
Gd-152	735.005	0.2
Gd-154	85.1898	2.18
Gd-155	60886.3	14.8
Gd-156	1.79460	20.47
Gd-157	254071	15.65
Gd-158	2.20202	24.84
Gd-160	1.40991	21.86

Table 8 Thermal neutron absorption cross section of Sm (at 0.0253 eV)

Nuclide	Thermal neutron absorption cross section (barn)	Relative abundance (a/o)
Sm-144	1.63004	3.1
Sm-147	56.9844	15
Sm-148	2.40015	11.3
Sm-149	40137.6	13.8
Sm-150	99.9961	7.4
Sm-152	205.925	26.7
Sm-154	8.32259	22.7

Table 9 Thermal neutron absorption cross section of Er (at 0.0253 eV)

Nuclide	Thermal neutron absorption cross section (barn)	Relative abundance (a/o)
Er-162	18.9111	0.14
Er-164	12.9514	1.61
Er-166	16.8715	33.6
Er-167	649.000	22.95
Er-168	2.74124	26.8
Er-170	8.85071	14.9

Table 10 Thermal neutron absorption cross section of Eu (at 0.0253 eV)

Nuclide	Thermal neutron absorption cross section (barn)	Relative abundance (a/o)
Eu-151	9200.73	47.8
Er-153	358.001	52.2

Table 11 Composition of 304 stainless steel

Element	Composition (wt%)
Carbon (C)	0.07
Chromium (Cr)	17.50 - 19.50
Manganese (Mn)	2
Silicon (Si)	1
Phosphorous (P)	0.045
Sulphur (S)	0.015
Nickel (Ni)	8.00 - 10.50
Nitrogen (N)	0.1
Iron (Fe)	Balance

Table 12 Density of materials

Material	Density (g/cm^3)
Base alloy (304 SS)	8.03
Gd	7.9
B	2.08
Sm	7.52
Er	9.066
Eu	5.264

Table 13 Natural atomic abundances (in at%) of Gd, B, Sm, Er and Eu [34]

Gd		B		Sm		Er		Eu	
Gd-152	0.2	B-10	19.9	Sm-144	3.07	Er-162	0.139	Eu-151	47.81
Gd-154	2.18	B-11	80.1	Sm-147	14.99	Er-164	1.601	Eu-153	52.19
Gd-155	14.80			Sm-148	11.24	Er-166	33.503		
Gd-156	20.47			Sm-149	13.82	Er-167	22.869		
Gd-157	15.65			Sm-150	7.38	Er-168	26.978		
Gd-158	24.84			Sm-152	26.75	Er-170	14.910		
Gd-160	21.86			Sm-154	22.75				
Total	100	Total	100	Total	100	Total	100	Total	100

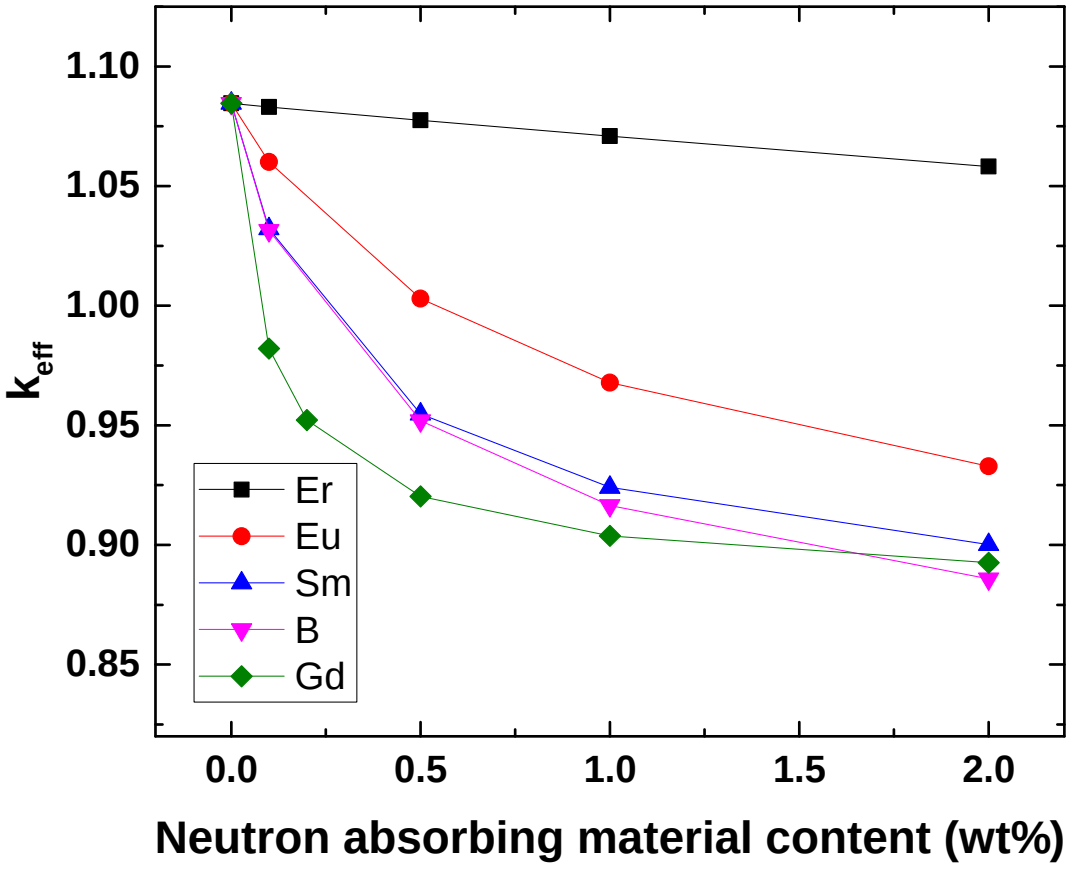

Figure 10 k_{eff} vs Gd, Sm, Er, Eu and B with 304 SS

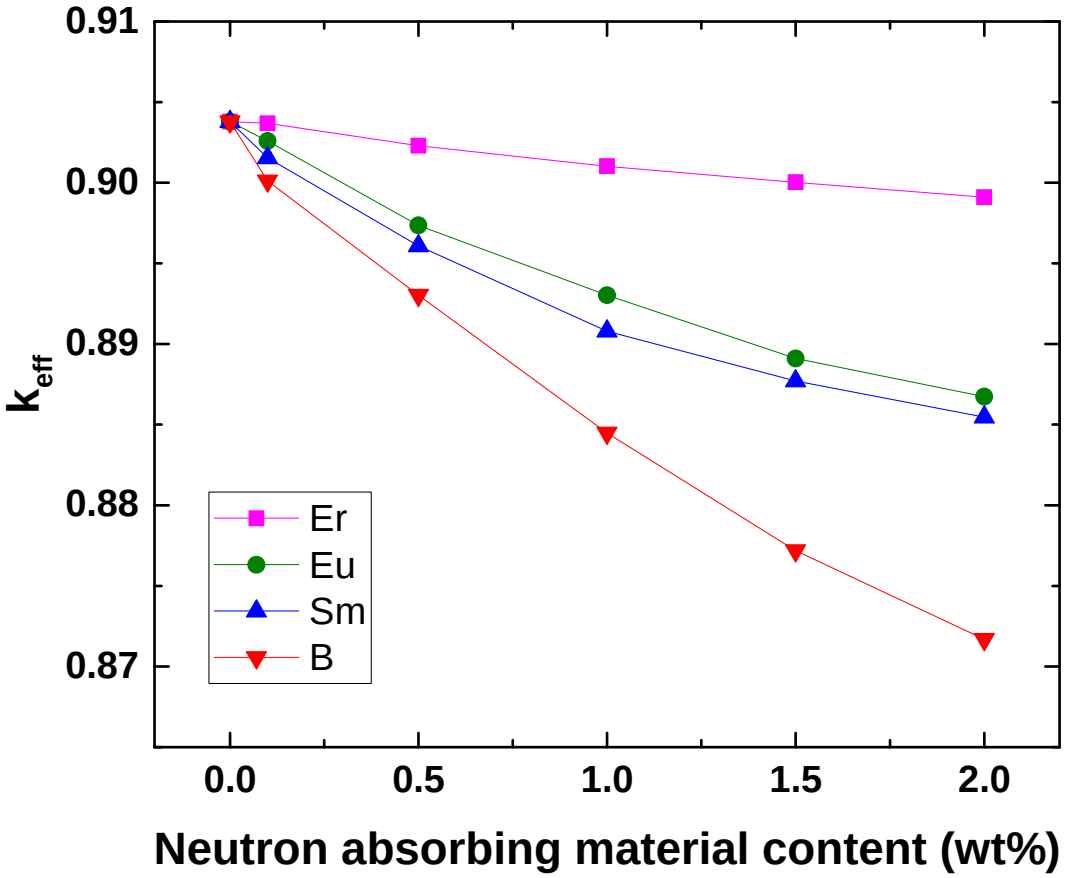

Figure 11 k_{eff} vs B, Sm, Er and Eu with Gd 1 wt% and stainless steel

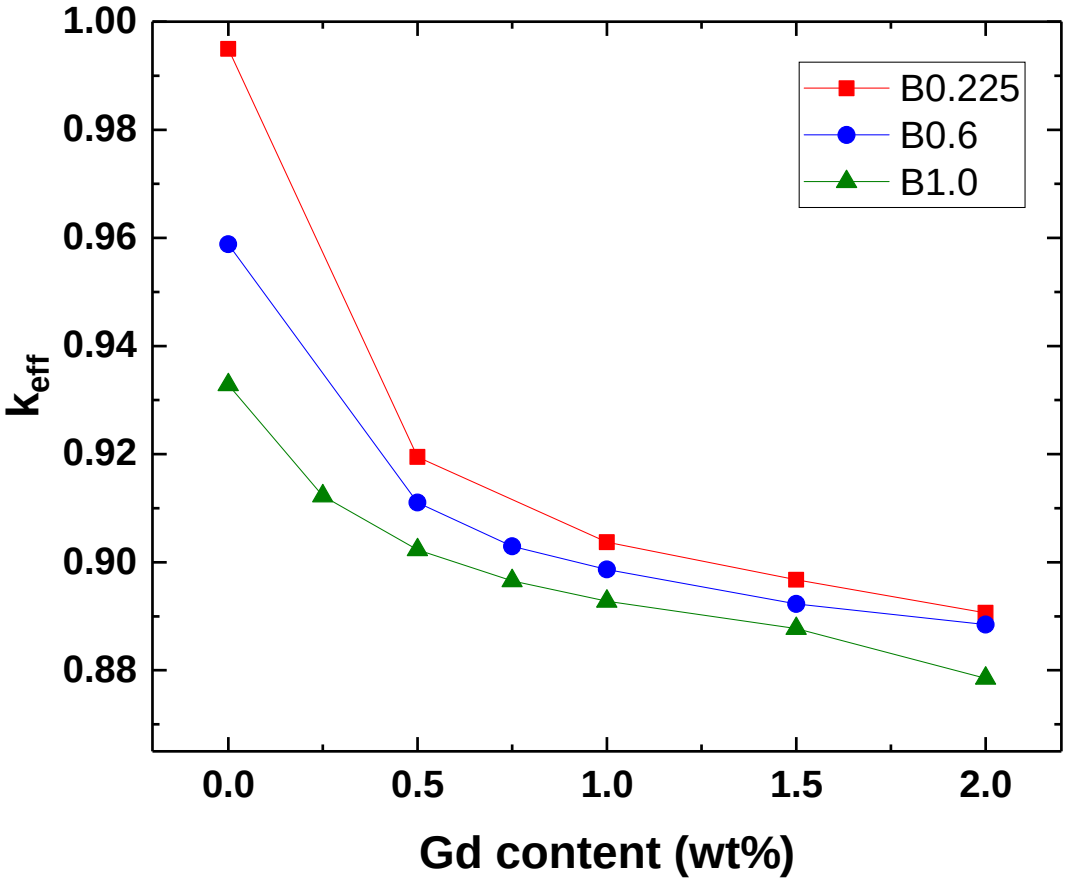

Figure 12 k_{eff} in various Gd and B combination

Table 14 Description of specimens and hot workability

	Gd (wt%)	B (wt%)	Hot workability
Alloy1	0.5	0.8	Good
Alloy2	0.7	0.8	Good
Alloy3	1.1	0.8	Bad (Crack)
Alloy4	0.32	0.8	Good
Alloy5	0.63	1.0	Good
Alloy6	0.51	1.2	Bad (Crack)

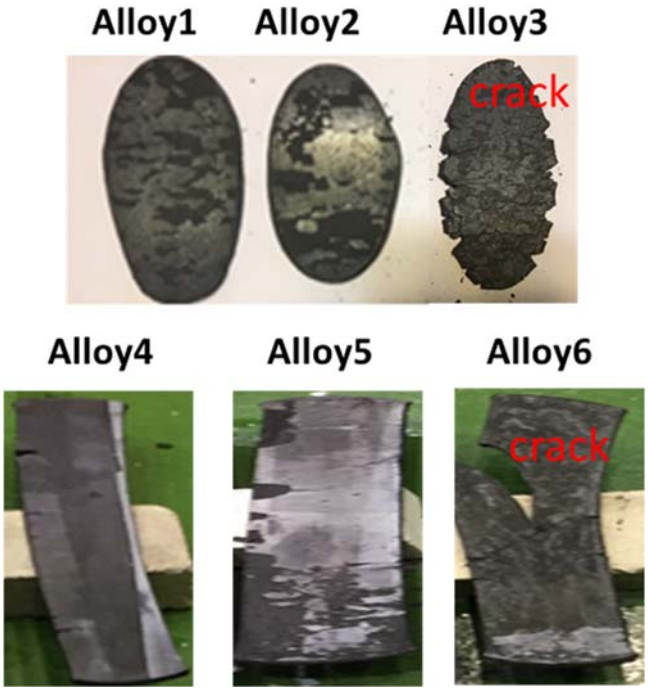

Figure 13 Specimen after hot rolling at 1050 ℃

Chapter 4. Sensitivity analysis in spent fuel transportation and storage system

The neutron movement around fuel assembly in water and cell structure is important to figure out the neutron reactions which affect the criticality analysis. The neutrons from the source or generated from fission reactions move around the medium and it reacts with surrounded structures by the interaction probabilities. These neutrons are absorbed or scattered by materials. Also, the array of fuel assemblies is stored in the SNF storage system. The neutrons come out from one fuel assembly that affects other fuel assemblies nearby. Therefore, understanding these neutron movements are important that is needed to be figured out neutron multiplication factor to maintaining subcritical.

In the SNF storage system, SNF is cooled by water for the rack, however, the SNF is cooled by inert gas for cask. However, the SNF moderated by water is needed to be analyzed for the loading of SNF to dry cask or accident casks for storage and transportation cask. Therefore, in this chapter, the neutron flux variation when fuel assembly with water and fuel assembly surrounded by cell structure with water is calculated.

The calculated regions are about 0.5 cm intervals and 7 or 8 points are calculated. The 0 cm depicts the fuel assembly edge. For the cell structure case, the cell located at 0.895 to 1.095 cm, which is 0.2 cm. It directly describes at 0.995 cm point within the results. The central location between the two fuel assemblies is 3.75 cm. The energy group is divided into thermal, Epithermal and fast regions to analyze the neutron phenomenon. Thermal energy region is $5 * 10^{-5}$ to 1 eV. Epithermal energy region is above 1 to 10^4 eV. Fast energy region is above 10^4 eV. Total energy explains the summation of all energy regions.

4.1. Neutron movement in spent fuel transportation and storage system

4.1.1. Neutron flux variation of fuel assembly case under water

Firstly, the neutron flux variation with only one fuel assembly surrounded by wide water moderation has been analyzed without installing any cell structure or neutron absorbers. The model is a finite model that has only fuel assembly within the water as described in Figure 14. The 0 cm is the edge of the fuel assembly and 70 cm is the water layer from the fuel assembly. The neutron flux of a 5 cm interval from fuel assembly to the edge of the water layer has been calculated. For the finite water only model, the neutron flux decreases abruptly that the position is far from the fuel assembly as described in Figure 15. After 30 cm from fuel assembly, the neutron flux variation is negligible. Therefore, in this case, the neutrons generated from one fuel assembly could travel until 30 cm without encountering any other materials. The fuel assembly envelop is almost 20 cm. Therefore, it could be concluded that if the pitch

between fuel assemblies is longer than 40 cm, the neutrons could hardly affect neighboring fuel assemblies. In this case, the neutron absorbers may not need to maintain subcriticality.

However, the pitch of the SNF storage system is much shorter than 40 cm. The pitch is about 23 cm to 30 cm [7], [27]. Also, as explained in the introduction, the shortage of SNF noticed so, it is inevitable to shrink the pitch between fuel assemblies for condense storage. Therefore, the neutron movement around fuel assembly surrounded by water condition at 28 cm pitch has been calculated. The fuel assembly is stored at the center and only water covers around fuel assemblies. The mirror boundaries are selected for horizontal direction due to repeated arrays in spent fuel storage. The outermost distance from the fuel assembly is 3.735 cm. For the case of a repeated array of fuel assemblies, the neutron movement shows a different configuration with the finite one fuel assembly model. In Figure 16, the total neutron flux gets higher as the distance gets far from the fuel assembly. The center position between fuel assemblies has the highest neuron flux.

For analyzing neutron flux in detail, the neutron flux is needed to be separated into the energy range of the thermal, epithermal and fast region. The variation of neutron flux at the thermal energy region was analyzed as shown in Figure 17. The neutron flux gets higher as the distance increases from fuel assembly. It shows the same configuration of the total energy region. The main neutron flux is from thermal neutron flux. The difference between the lowest and highest value is about $4 * 10^{-5}\ \#/\mathrm{cm}^2$.

At the epithermal energy region, the neutron flux gets lower when the position gets far from the fuel assembly. The difference between the maximum and the minimum value is only $0.5 * 10^{-5}\ \#/\mathrm{cm}^2$.

In the fast energy region, the neutron flux variation has a similar configuration with the epithermal energy region. As the distance far from the fuel assembly, the neutron flux decreases the amount of $1.5 * 10^{-5}\ \#/\mathrm{cm}^2$.

Both the epithermal and fast energy region, the neutron flux decreases as far from the fuel assembly. Therefore, the treatment of thermal neutrons is important for criticality control.

4.1.2. Neutron flux variation of fuel assembly with spent fuel transportation and storage case under water

The neutron flux variations were calculated for cell exists between fuel assembly. The fuel assembly and SNF storage systems are moderated with water. The cell with stainless steel and stainless steel with neutron absorbing materials cases have been studied.

4.1.2.1. Stainless steel plate

The calculated model is square-tube type stainless steel stored fuel assembly at the center and all the other remained site is filled with water. There are no any other materials except fuel assembly, stainless steel, and water. From Figure 18, the total neutron flux decreases until the stainless steel cell after that

point neutron flux increases. It is similar between neutron flux at the edge of the fuel assembly and that at the center region of the flux trap. The thermal neutron flux shows a similar configuration when only fuel assembly exists in the water in Figure 19. The thermal neutron flux decreases until the stainless steel cell and after that point neutron flux increases as total neutron flux variation. The neutron flux increases as the position far from the fuel assembly from the overall range point of view. In Figure 20, the neutron flux of epithermal and fast energy decreases as the position far from the fuel assembly.

4.1.2.2. Neutron absorber case

The Gd 1 wt% case has been selected for a representative neutron absorber case. The Gd 1 wt% is inserted in a stainless steel cell. From the same way of Chapter 3, the contents of Gd 1 wt% absorber and the density of absorber were applied.

For better understanding, the results of the Gd 1 wt% case and stainless steel case were represented at the same time in figures. The total neutron flux of Gd 1 wt% is much lower than that of stainless steel within the cell wall as shown in Figure 18. This is because the Gd 1 wt% cell wall absorbs neutrons much better than stainless steel due to its high neutron absorption cross section. The neutron flux depression at the cell wall could be more obviously noticed for Gd 1 wt% case than the stainless steel case. The outer region of the cell wall shows higher neutron flux than the inner region of the cell wall.

The thermal neutron flux of inside cells is low compared with the neutron flux of the cell outer region even more than total neutron flux as shown in Figure 19. Inside the cell, the fission reactions are dominant from reacting thermal neutrons and U-235. From fission reaction of $^{235}U(n,f)2.5n$, fast neutrons are generated, and it moves to the outside of the cell. These fast neutrons are moderated to thermal neutrons at the flux trap region with a large amount of water which has a high slowing down ratio. The Gd 1 wt% case has lower thermal neutron flux than the stainless steel case for the whole region. This would be seen that the cell wall is composed of Gd which has very high neutron absorption cross sections, so, the thermal neutrons are absorbed by Gd inside the cell. The high elevation of thermal neutron flux in the outer region is due to the flux traps. The thermal neutrons are gathered at the flux trap region and hard to escape.

The epithermal and fast neutron flux shows a similar configuration as described in Figure 20. They decrease as distance far from the fuel assembly. The neutron flux of Gd 1 wt% is lower than that of stainless steel, however, it does not show much difference.

The thermal neutron flux of stainless steel is 10 times higher than that of the Gd 1 wt%. On the other hand, the epithermal and fast neutron fluxes are $1 \times 10^{-4}\ \#/\mathrm{cm}^2$ higher than that of Gd 1 wt%. This is because the flux trap enhances the thermalization of neutron and fast neutrons and epithermal neutrons are moderated by this phenomenon. From these results, it could be concluded that flux traps are enhanced by the cell of high neutron absorption cross section.

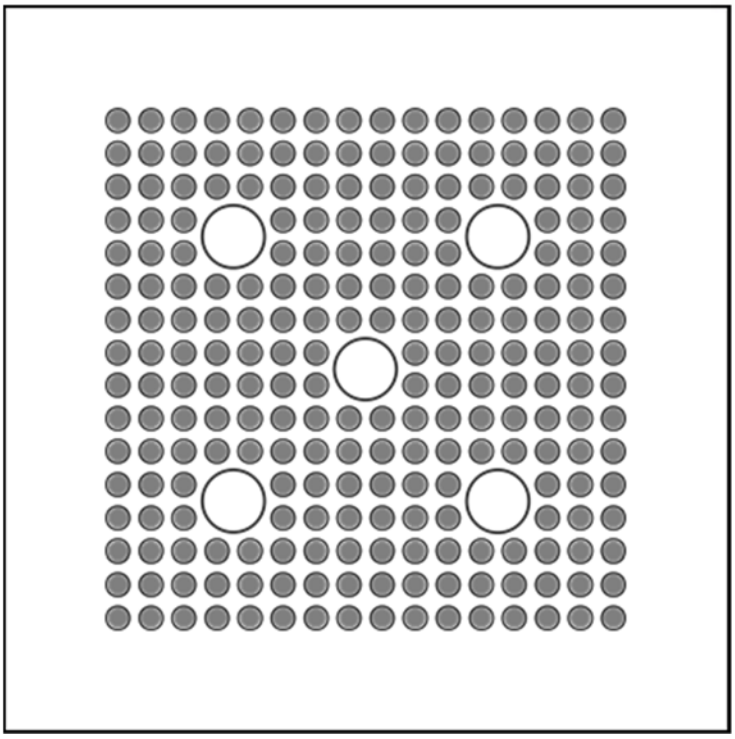

Figure 14 Description of one fuel assembly surrounded by water moderator

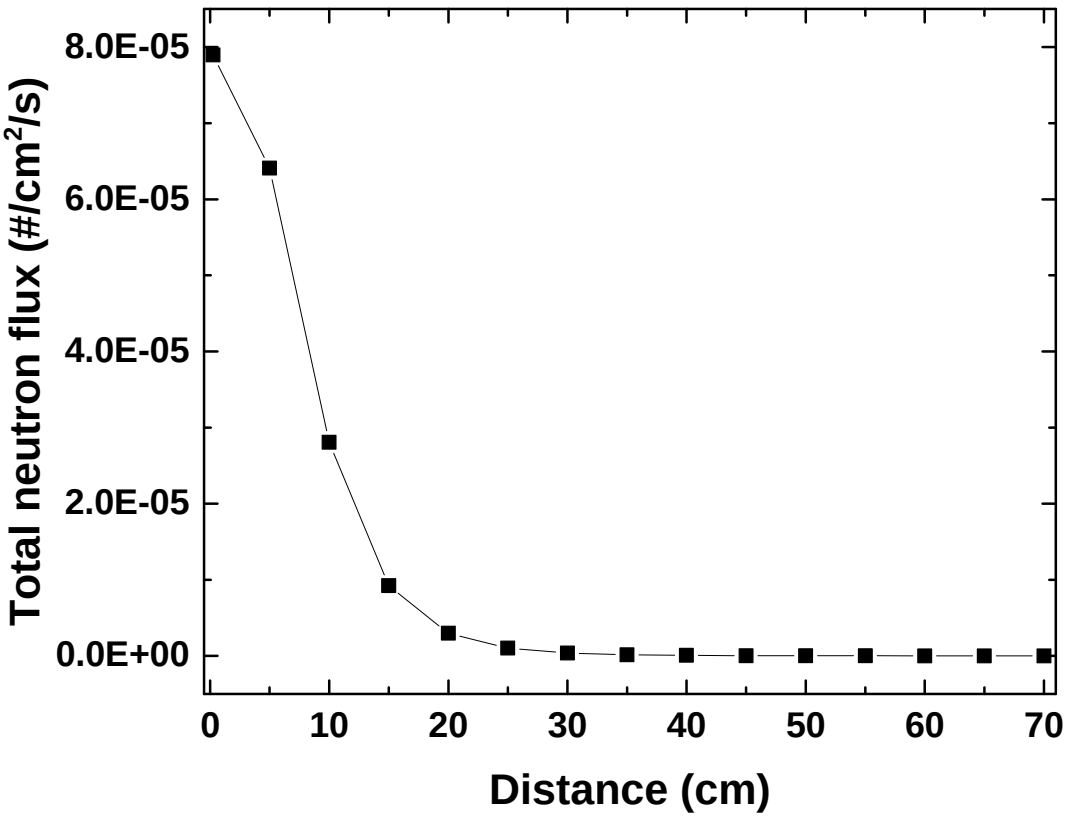

Figure 15 Neutron variation for one finite fuel assembly model

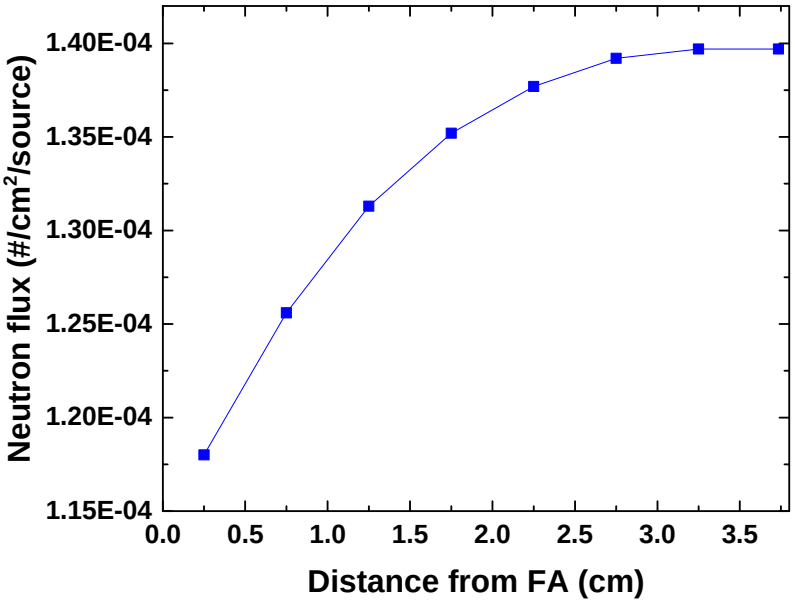

Figure 16 Total neutron flux for infinite array of fuel assemblies

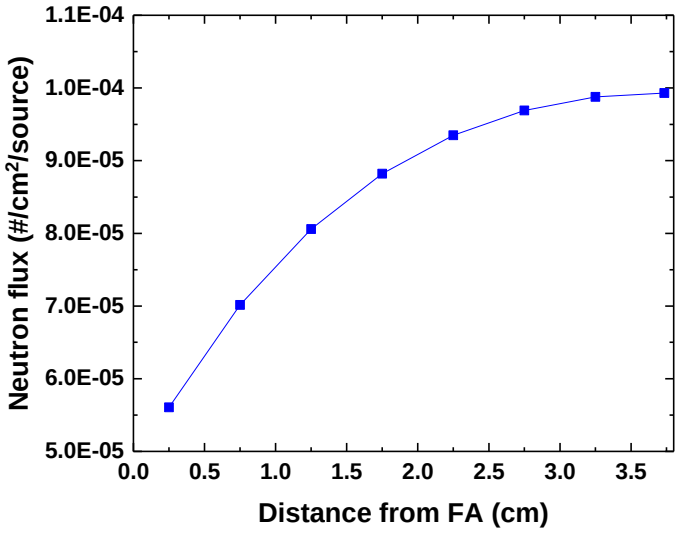

(a)

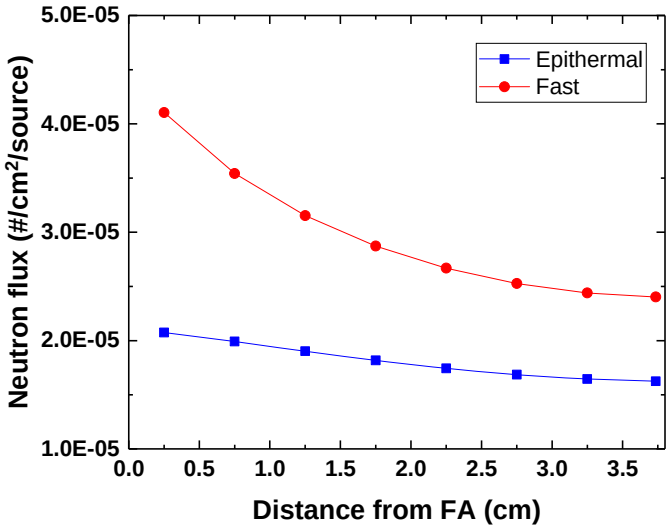

(b)

Figure 17 Neutron flux distribution for infinite array of fuel assemblies (a) Thermal (b) Epithermal and fast

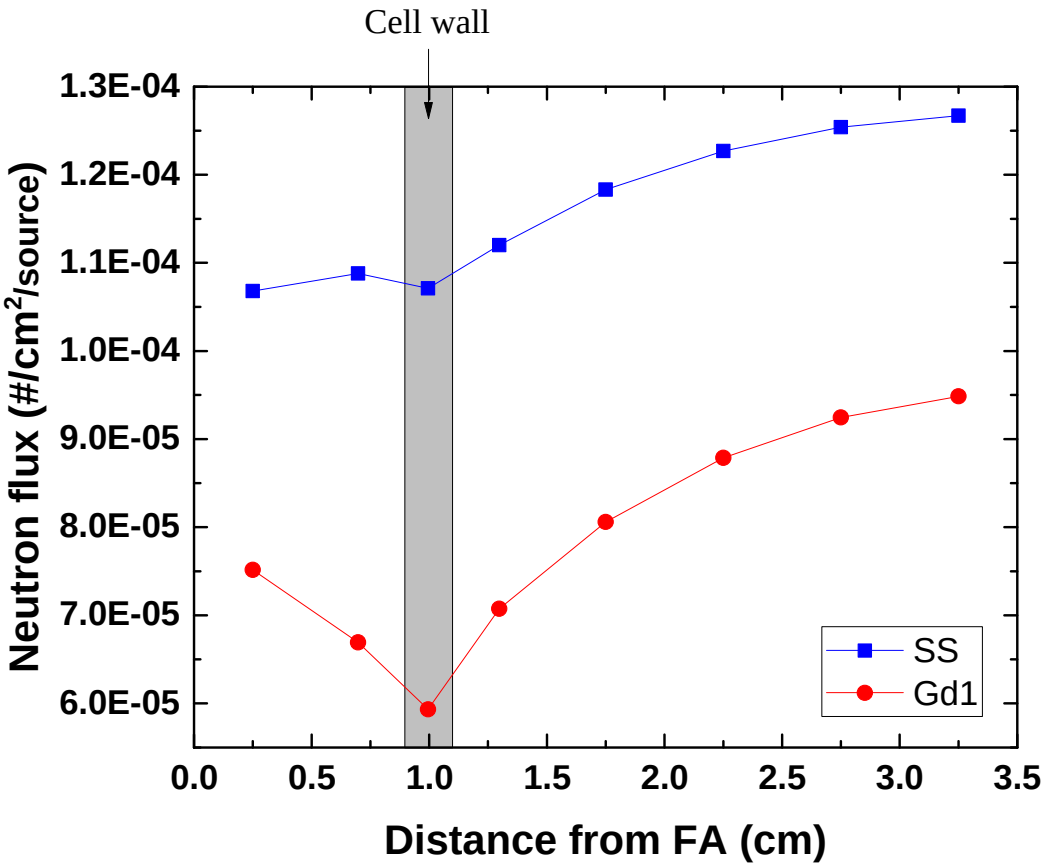

Figure 18 Total neutron flux of stainless steel and Gd 1 wt% case

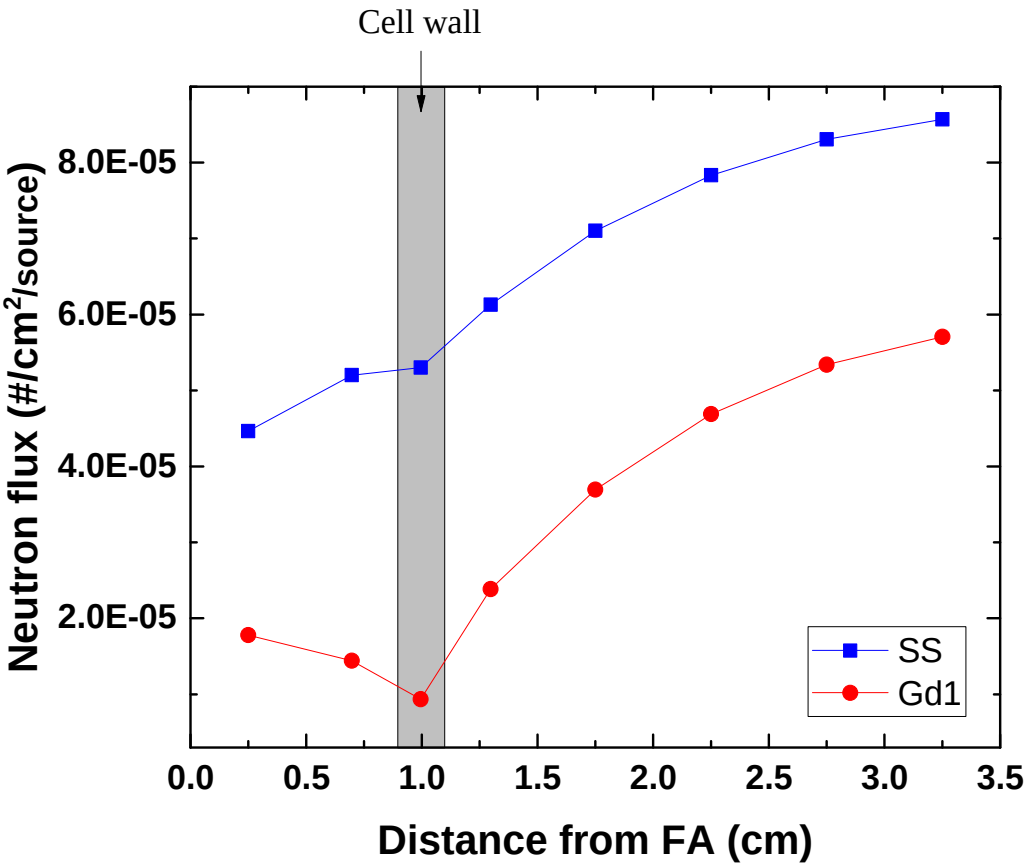

Figure 19 Thermal neutron flux of stainless steel and Gd 1 wt% case

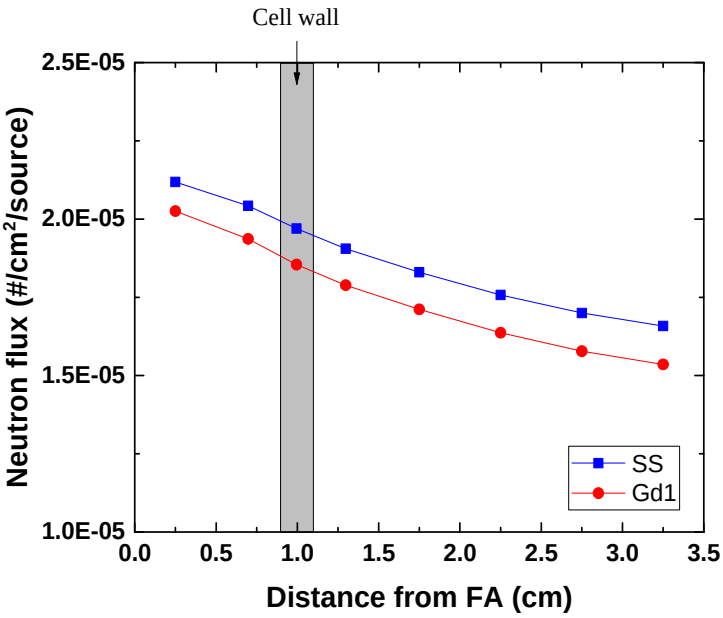

(a)

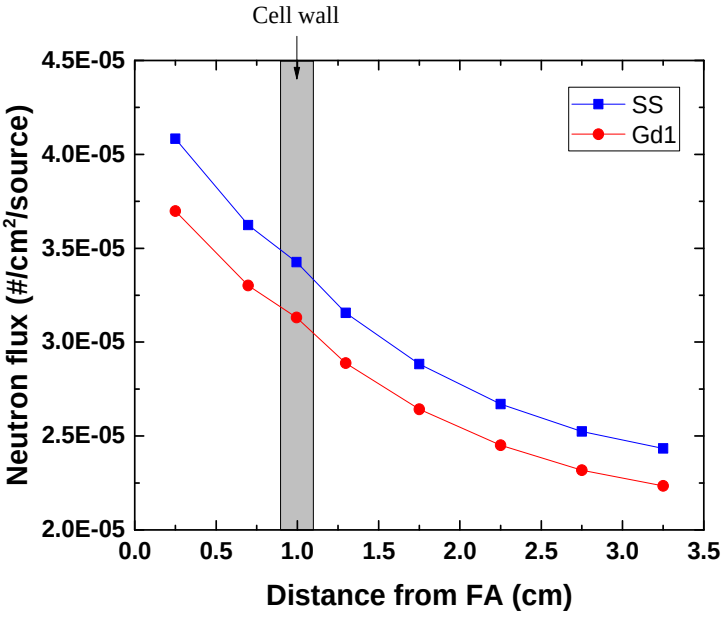

(b)

Figure 20 Neutron flux with stainless steel and Gd 1 wt% case (a) Epithermal (b) Fast

4.2. Sensitivity analysis of flux trap type for criticality control

The sensitivity analysis of flux trap type was performed for main parameter impact on criticality; pitch between fuel assemblies, inner width of cell wall and thickness of cell wall. The water gap between neutron absorbers is depicted as a “flux trap” as its functioning. The neutron multiplication factors have been calculated as a function of each parameter; thickness, inner width, and pitch. The tendency of neutron multiplication factors is confirmed with PLUS7 and Westinghouse OFA 17x17 fuel assemblies.

4.2.1. Pitch

Firstly, the neutron multiplication factor versus pitch change has been calculated in Figure 21 at the constant inner width of 22.35 cm and pitch of 28.03 cm. The pitch size used in the calculations is from 22.75 cm to 34.03 cm. The 22.75 cm of pitch depicts that the adjacent cell walls are attached to each other. The k_{eff} proportionally decreases with pitch increment for both stainless steel and the Gd 1 wt% cases. The neutron flux for stainless steel case has been studied in Figure 22. The distance from 0 to 1 cm is the inner region of the cell wall and the cell wall itself. In this region, the neutron flux slightly increases or continuously decreases. As pitch increases, the region of flux trap water continuously increases. The neutron flux with high pitch size shows lower than that with low pitch size at a whole distance. The outer region of the cell wall shows an increment of total neutron flux from pitch 25.03 to 28.03 cm. However, the case that pitch is larger than 31.03 cm shows increases the total neutron flux at a certain distance and decreases until the center of the flux trap. To simplifying the figures, the parameters are depicted in figures as CW (cell wall), W (Water) and FT (flux trap). The absorption rate at flux trap water increases as pitch increases because the amount of water increases as shown in Figure 23.

For the stainless steel case, the total neutron flux at the cell wall gets low as pitch increases as described in Figure 22, however, the neutron energy spectrum at the cell wall does not change according to pitch without pitch 22.75 cm case that does not have water gap in Figure 24 (a). The neutron thermalization at the flux trap enhances as pitch increase as described in Figure 24 (b). When pitch increases, the amount of water at flux trap increases and also, the distance between fuel assembly increases. Therefore, the multiplication factor gets low as pitch increases and neutron thermalization enhances.

In Figure 21, the k_{eff} for Gd 1 wt% also shows continuous decrement as a function of pitch. The trend of both cases is almost the same and Gd 1wt% has higher absorption cross sections than that of stainless steel so, the two graphs are parallel. The total neutron flux gets low as increase of pitch as explained in Figure 25. The depression of neutron flux at the cell wall is huge for Gd 1 wt% case. Also, the neutron flux slightly decreases after 4 cm distance from FA for pitch 34.03 cm. The absorption rate at the cell wall increases with pitch until 28.03 cm as shown in Figure 26. Above 28.03 cm of pitch, the absorption rate at the cell wall gradually decreases as the pitch increases. However, the absorption rate at the flux

trap continuously increases as the pitch increases.

For Gd 1 wt% case, the thermal neutrons are almost absorbed by Gd as shown in Figure 27 (a) due to high neutron absorption cross section in thermal energy region. At the flux trap, the neutron thermalization gets strong as pitch increases like stainless steel case as described in Figure 27 (b).

4.2.2. Inner width

Secondly, the multiplication factor has been calculated according to inner width which is shown in Figure 28. The range of inner width is 20.56 to 27.63 cm. The 20.56 cm is the size of the fuel assembly envelop. The 27.63 cm is the outermost dimension that the adjacent cell walls are attached to each other and there's no remained space for flux trap water. The difference between the maximum and minimum neutron multiplication factor is only 213 pcm although the inner width and flux trap size change about 7 cm. The total neutron flux inside the cell wall shows a sine shape in Figure 29. From the cell wall to the center of the flux trap, the neutron flux gradually rises as the distance from fuel assembly increases. The inner side of the cell wall, the neutron flux gets higher when high inner width except the cell wall attached at fuel assembly. The flux shows the highest value at the center position of the flux trap when the cell wall is departed from each other. When the cell walls are attached to each other, for 27.63 cm case, the flux shows the lowest value at the center of the flux trap. The absorption rate of water at the flux trap proportionally decreases as inner width increases from 2.4E-4 to 1.0E-5 as depicted in Figure 30. The absorption rate of stainless steel slightly increases but it does not noticeably change after 24 cm of inner width. The neutron thermalization at the cell wall enhanced as inner width increases. With higher inner width, the absorption of thermal neutrons decreases. As inner width increases, the amount of water increases inside the cell wall. Therefore, the moderation inside the cell wall increases and the thermal spectrum gets higher. Without neutron absorber, the spectrum variance at the flux trap is negligible according to inner width. So, the water gap performs a gap between neutron absorber not for flux trap.

For Gd 1 wt% case, the k_{eff} increases as the inner width of the cell wall increase in Figure 28. The neutron flux as a function of inner width has been analyzed in Figure 31. When the cell wall is attached at fuel assembly, the neutron flux continuously increases as sine shape (0 to pi/2). On the contrary, when the cell walls are attached to each other, two cell walls are attached, the neutron flux continuously decreases as cosine shape (0 to pi/2). Except for two conditions, the neutron flux shows 'V' shape. The neutron flux decreases as the distance from the fuel assembly increases until the cell wall. After the distance is far from the cell wall, the neutron flux increases. The neutron flux at the inner region of the cell wall with a large inner width shows higher than that of the cell wall with a smaller inner width. For the outer region, the neutron flux of large inner width shows lower than that of small inner width. The absorption rate at Gd 1 wt% cell wall and flux trap have been calculated in Figure 32. The absorption rate of the Gd 1 wt% cell wall shows a 'convex' shape. The reaction rate increases until 25 cm of inner

width and, then decreases after 25 cm of the cell wall. The absorption rate of flux trap water continuously decreases a large amount due to decreasing the amount of water at the flux trap. For Gd 1 wt% case, with neutron absorber, the neutron flux distribution at the cell wall does not be affected by inner width as described in Figure 36. The fast spectrum is dominant for all the inner widths. In Figure 37, the neutron thermalization at the flux trap enhances with a small inner width so the thermal neutron flux at the flux trap gets higher. This explains that the flux trap effectively traps thermal neutrons.

The difference between stainless steel and stainless steel with neutron absorber is the flux trap. The flux trap between neutron absorber decreases, therefore, neutron slowing down decreases. By the sequence of both effects, the neutron multiplication factor does not steadily decrease. Therefore, the optimum thickness for this storage system is 2 mm.

As inner width increases, the neutron flux increases and then decreases again. As the flux trap decreases, the absorption rate of water and neutron flux at the flux trap decreases. However, the amount of water that nears fuel assembly increases, therefore, the neutron flux inside the cell wall increases.

Although the absorption rate of the cell wall increases, the absorption rate of water at the flux trap decreases. Also, the neutron flux inside the cell wall increases, so the neutron multiplication factor increases as inner width increases.

4.2.3. Thickness

Finally, the k_{eff} as a function of thickness has been evaluated for the stainless steel and Gd 1 wt% case as shown in Figure 38. For both the stainless steel and Gd 1 wt% case, the k_{eff} decreases at a certain thickness and above certain thickness the k_{eff} increases as thickness increases. This behavior seems surprising at first because, as the cell wall becomes thicker, the amount of neutron poison increases, and therefore one would expect more neutron captures by a neutron absorber as thickness increases.

Therefore, the stainless steel with no neutron absorber case had been analyzed in advanced. For stainless steel condition, the multiplication factor decreases until the thickness of 1.0 cm. There is no strong neutron absorber in stainless steel, however, stainless steel still absorbs neutrons although it has a low neutron absorption cross section as described in Figure 39. The total neutron flux for stainless steel case is described in Figure 40. The neutron flux decreases as the thickness of the cell wall increase at a whole distance from the fuel assembly. The neutron flux is highest at the center position of flux trap for all cases. For thickness 0.01 cm case, the neutron flux continuously increases as distance increases. It seems that the cell wall is too narrow to absorb enough neutrons which affect the main neutron flux. For other thicknesses except for 0.01 cm, the neutron flux decreases until the cell wall position and after cell wall, the neutron flux increases as distance is far from the fuel assembly. For that, the absorption rate has been calculated at the stainless steel and water at the flux trap. From Figure 41, the absorption rate at stainless steel increases as increasing of the stainless steel thickness. However, the absorption rate of

water at the flux trap decreases as thickness increases. As the thickness of the cell wall increases, the amount of water decreases at the flux trap. Therefore, the absorption of neutrons from stainless steel increases when thickness increases. On the other hand, the absorption of neutrons from water decreases as thickness increases. The absorption rate of water at the flux trap is higher than that of the cell wall from 0.01 to 0.4 cm thickness. Although the multiplication decreases according to the thickness, the amount of decrement is not that large. The k_{eff} shows over 1.0 with all ranges of thickness of stainless steel. Therefore, with only stainless steel without neutron absorber, the criticality could not be maintained under 0.95.

As described earlier, the factors that control flux trap size are the thickness of the cell wall, the inner width of the cell wall and the pitch between fuel assemblies. The neutron flux spectra according to the thickness of the cell wall have been studied in advanced. When there is no neutron absorber, stainless steel case, the neutron thermal spectrum is dominant for all thicknesses from 0.01 to 0.9 cm as shown in Figure 45 and Figure 46. As thickness increases, the spectrum hardens at the cell wall and flux trap position.

For Gd 1 wt% case, which depicts stainless steel with neutron absorbing material case, the k_{eff} decreases at a certain thickness and then it increases as thickness increases as described in Figure 38. The amount of neutron absorber gradually rises, and the absorption cross section is high in the scale of 10^3 that makes lower k_{eff}. The total cross section of Gd 1 wt% is much higher than the stainless steel case due to Gd insertion compared with Figure 39 and Figure 42. Also, the absorption cross section of Gd 1 wt% is extremely higher than that of the scattering cross section at the thermal region. However, the graph does not correspond to the stainless steel case for neutron absorbing material case. The total neutron flux decreases at a certain distance and after that, the neutron flux increases as described in Figure 43. The outer region of the cell wall shows that the neutron flux decreases as thickness increases. However, the inner region of the cell wall shows that the neutron flux increases as thickness increases for thickness 0.2 to 0.9 cm. For thickness 0.01 cm, the neutron flux is the highest among all the distance and thicknesses. As described in Figure 38, the absorption rate at the Gd 1 wt% cell wall shows the same configuration in Figure 44. The absorption rate for the cell wall abruptly increases 0.01 cm to 0.2 cm thickness. After 0.2 cm thickness, the reaction rate slightly increases with thickness increment. For water at the flux trap, the absorption rate continuously decreases. The absorption rate of water at the flux trap has higher than that of the cell wall only at thickness 0.01 cm.

When neutron absorber exists, the Gd 1 wt% case, the thermal neutron flux dramatically decreases at cell wall when thickness increases as described in Figure 47. The thermal neutron cross section of Gd is quite high about 250,000 barns, therefore, almost all thermal neutrons are absorbed by Gd and epithermal and fast neutrons are left behind. At the flux trap position in Figure 48, the neutron flux distribution for the Gd 1 wt% case seems similar to the stainless steel case. The thermal spectrum is dominant for overall thickness and the spectrum hardens as thickness increases.

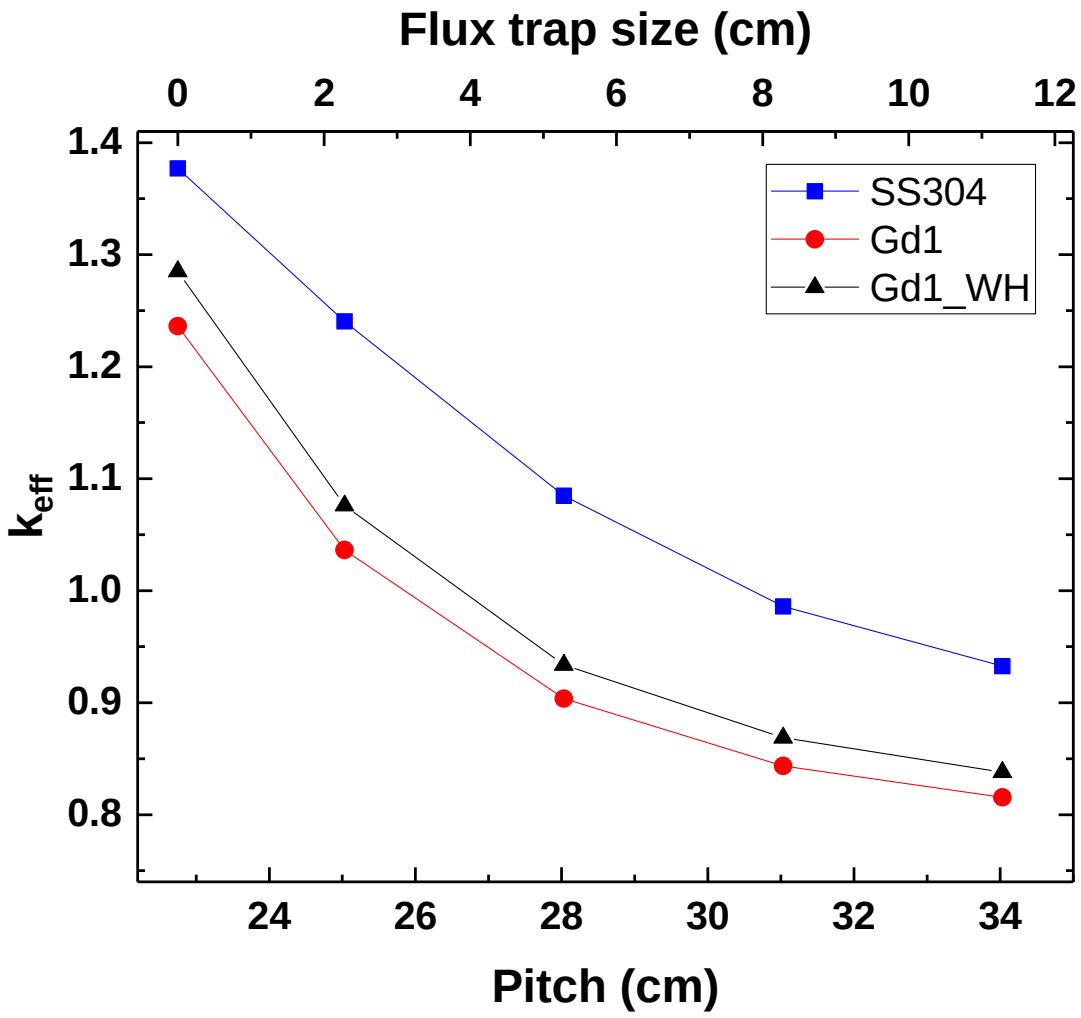

Figure 21 k_{eff} vs pitch for the stainless steel and Gd 1 wt% cases for PLUS7 and Westinghouse OFA 17x17

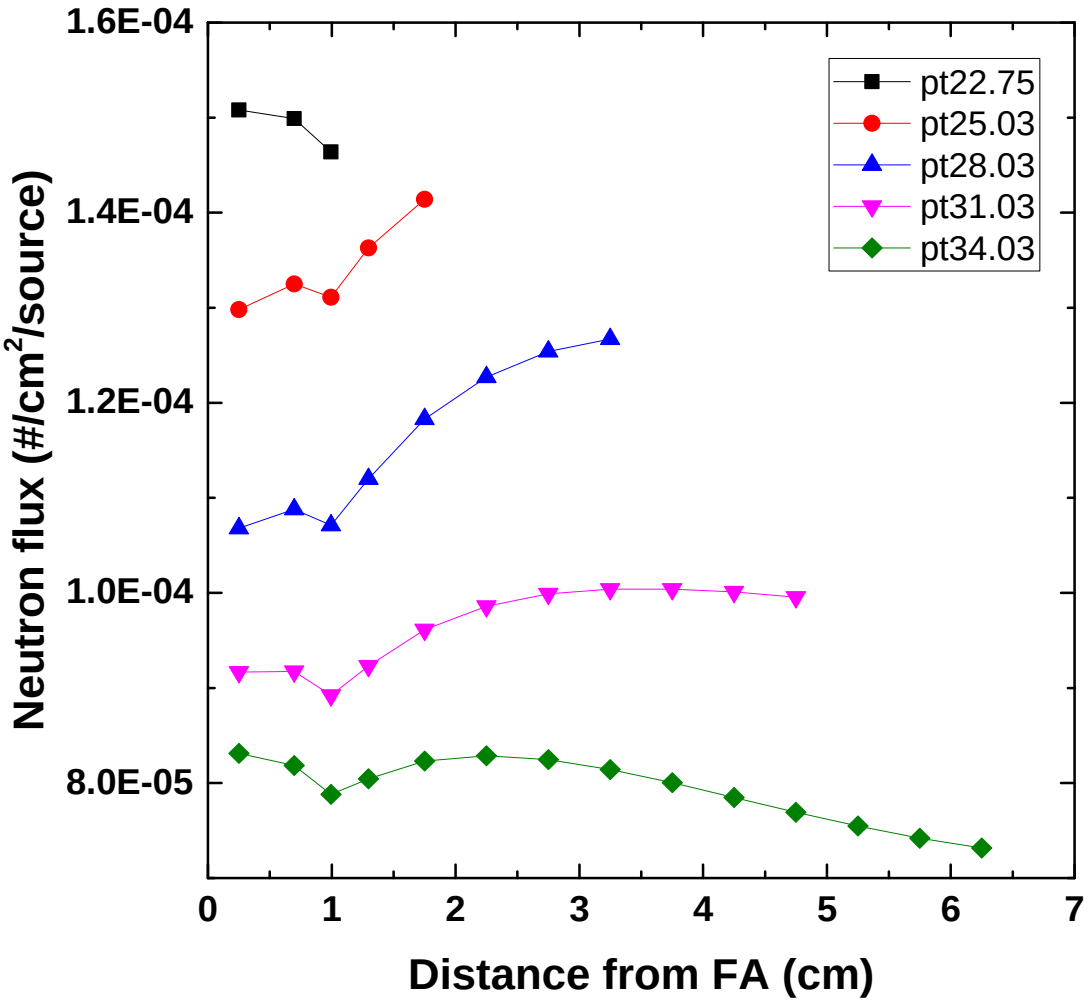

Figure 22 Neutron flux vs pitch of cell wall for the stainless steel case

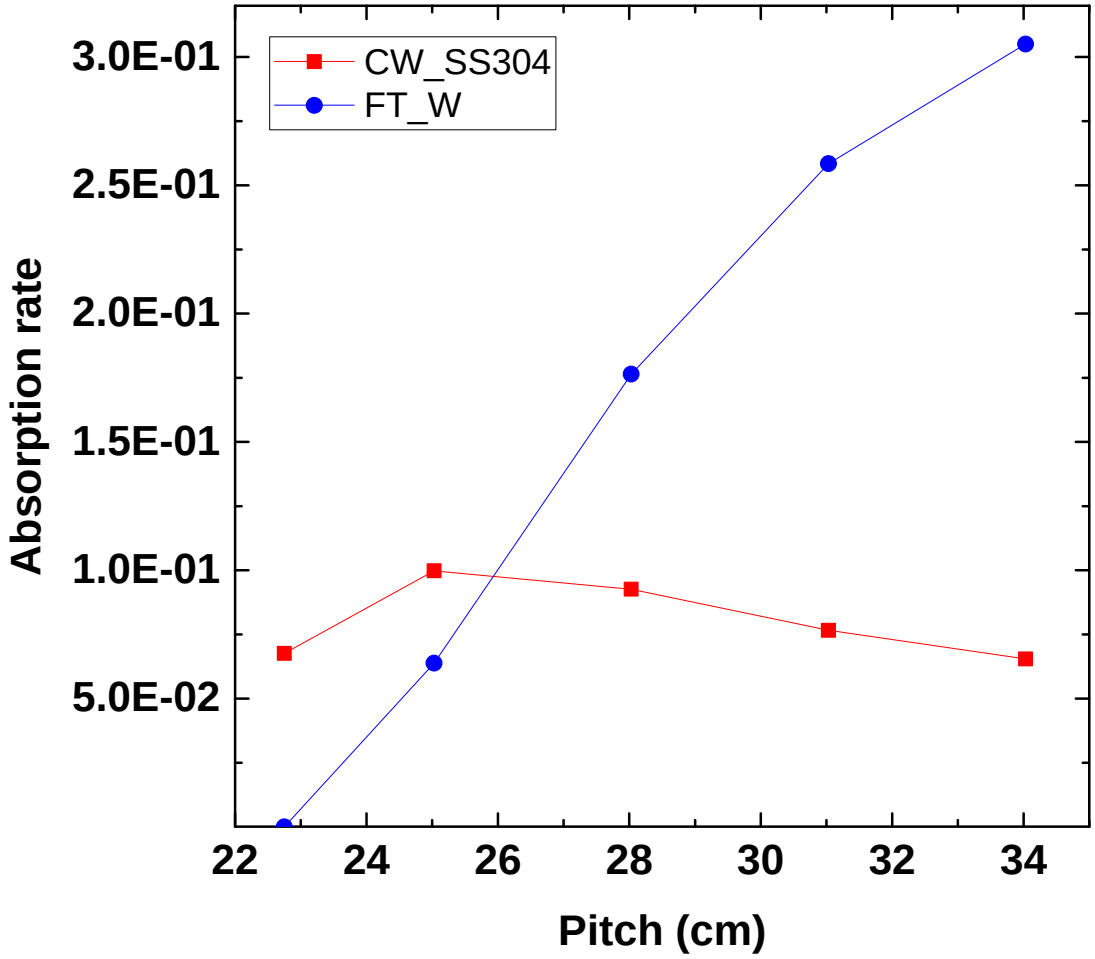

Figure 23 Absorption rate vs pitch of cell wall and water in flux trap for the the stainless steel case

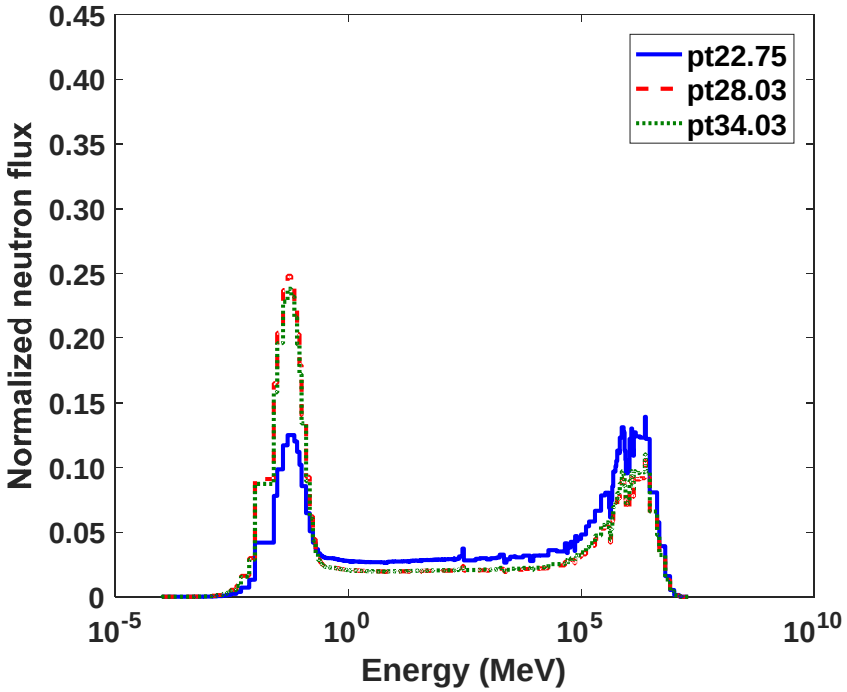

(a)

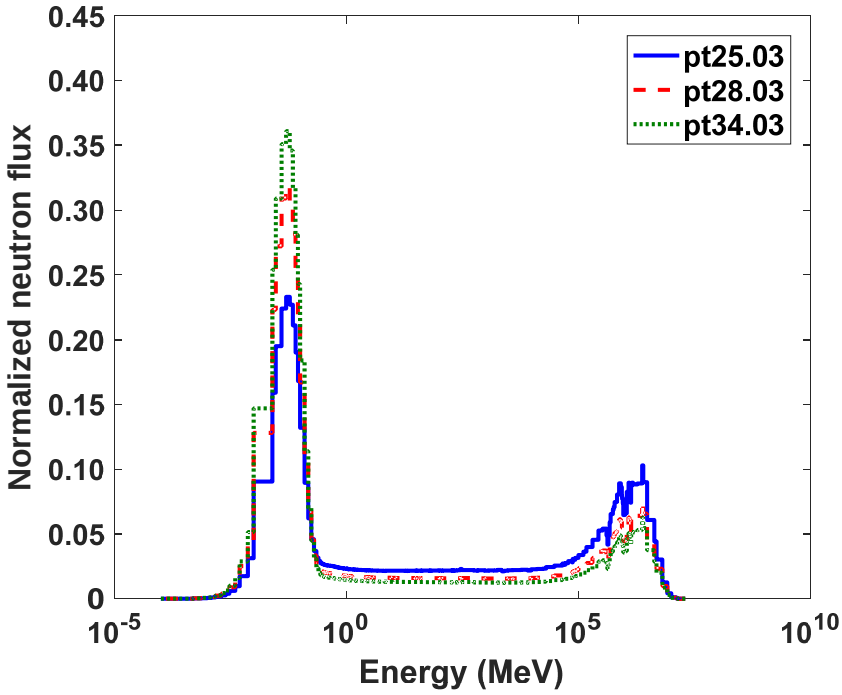

(b)

Figure 24 Neutron flux distribution vs pitch for the stainless steel case (a) Cell wall (b) Flux trap

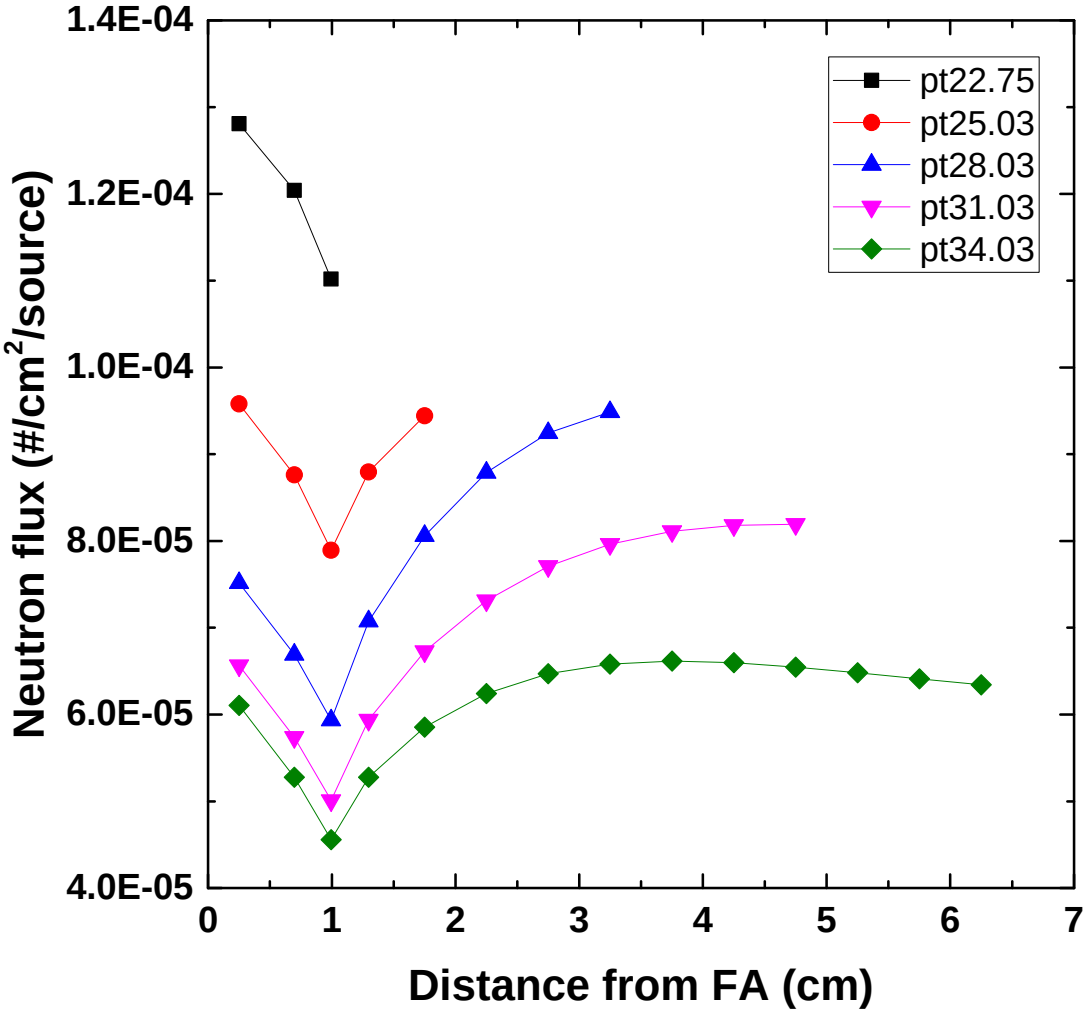

Figure 25 Neutron flux vs pitch of cell wall for the Gd 1 wt% case

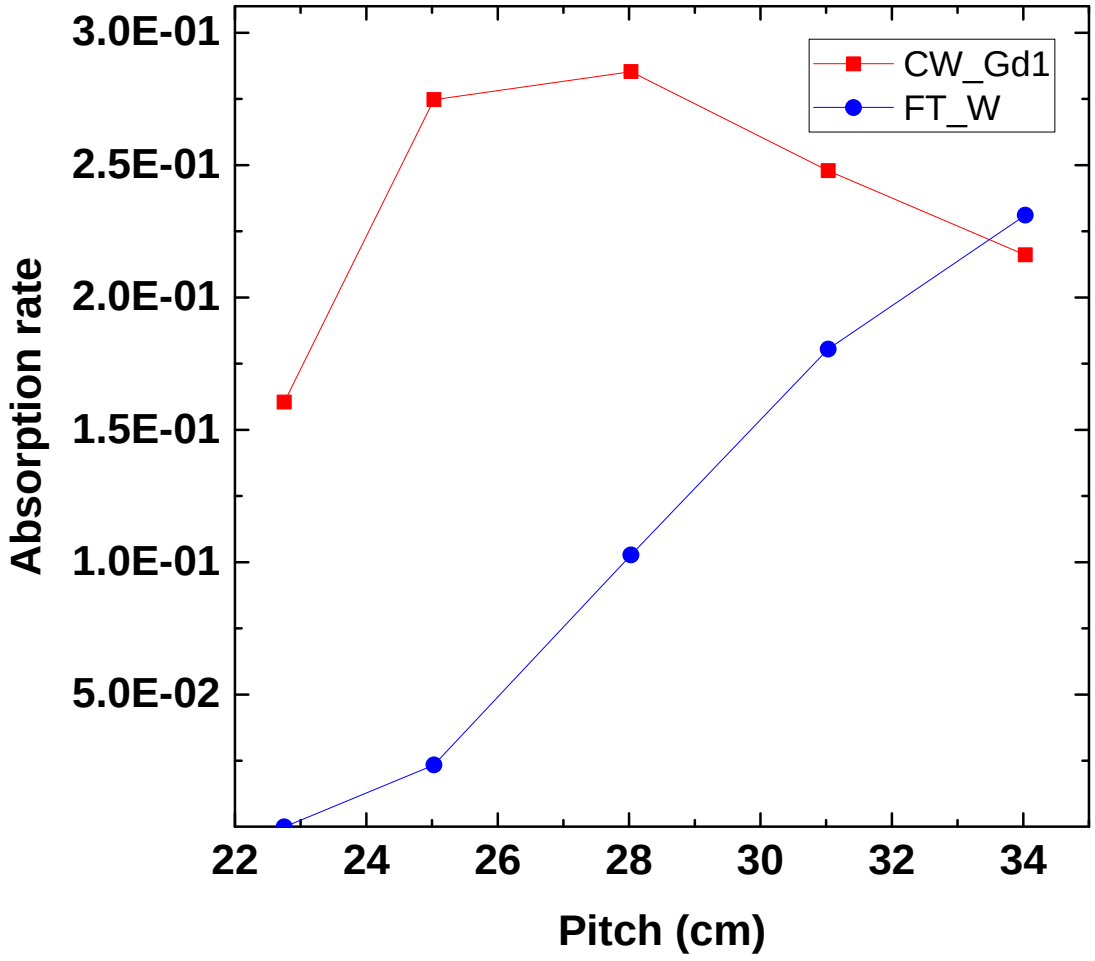

Figure 26 Absorption rate vs pitch of cell wall and water in flux trap for the Gd 1 wt% case

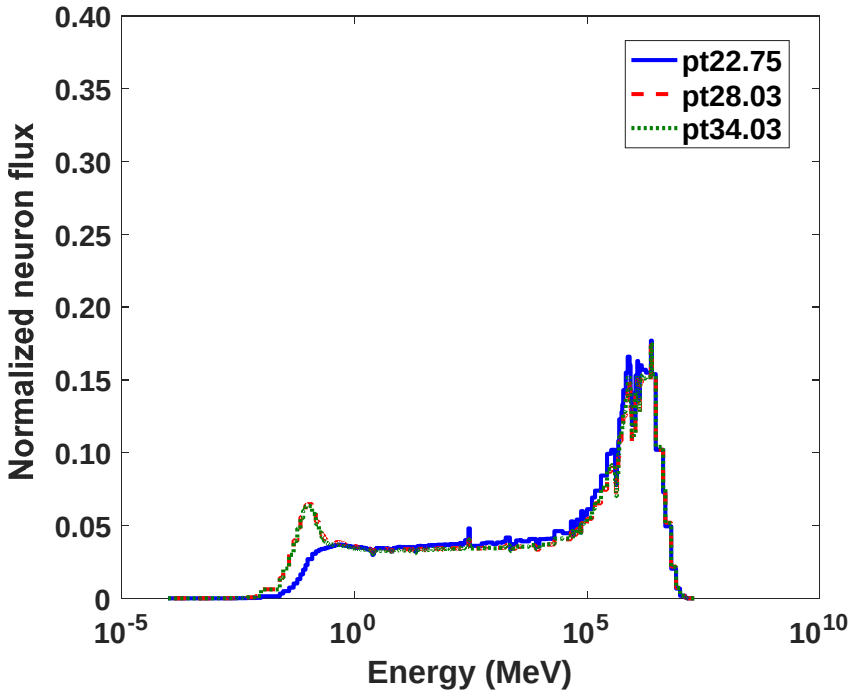

(a)

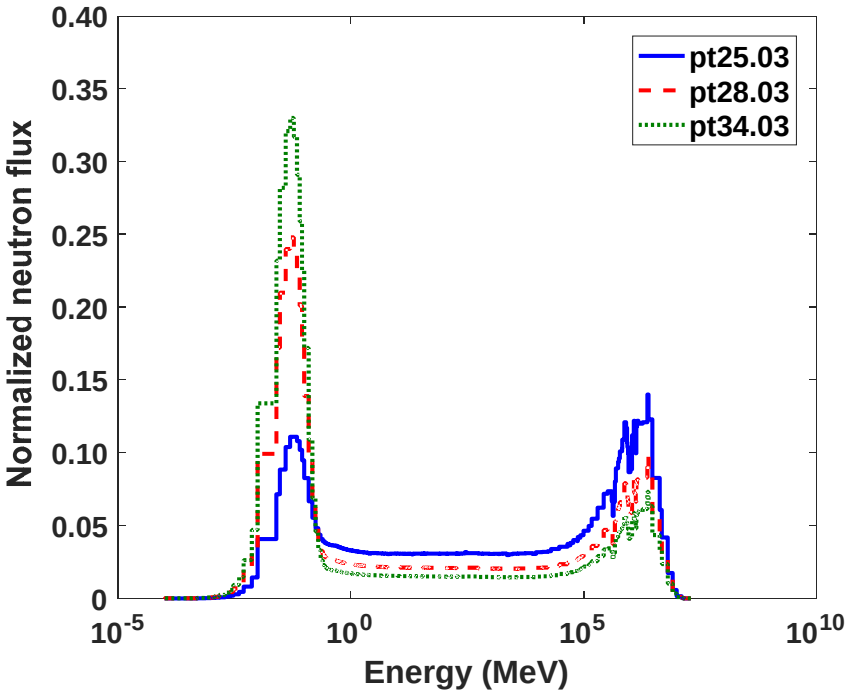

(b)

Figure 27 Neutron flux distribution vs pitch for the Gd 1 wt% case (a) Cell wall (b) Flux trap

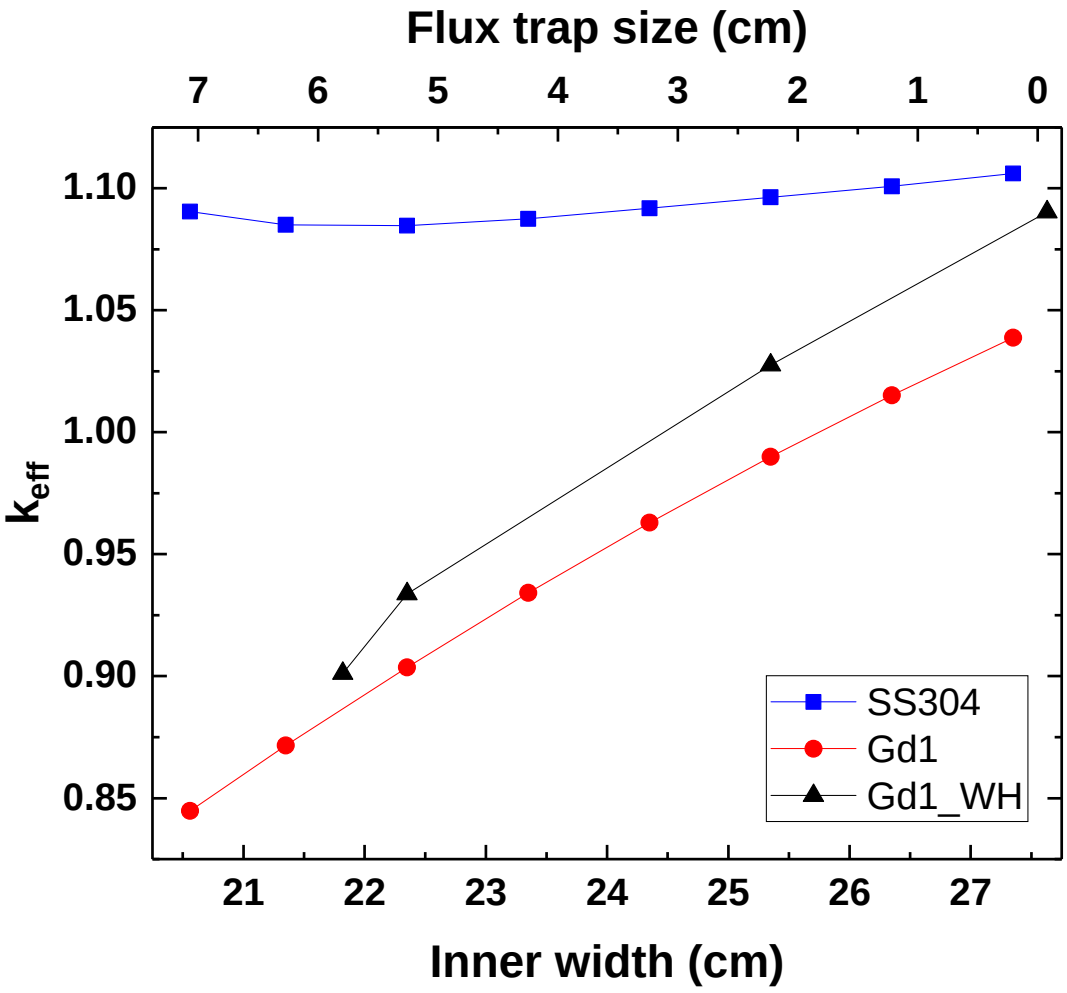

Figure 28 k_{eff} vs inner width for the stainless steel and Gd 1 wt% case for PLUS7 and Westinghouse OFA 17x17

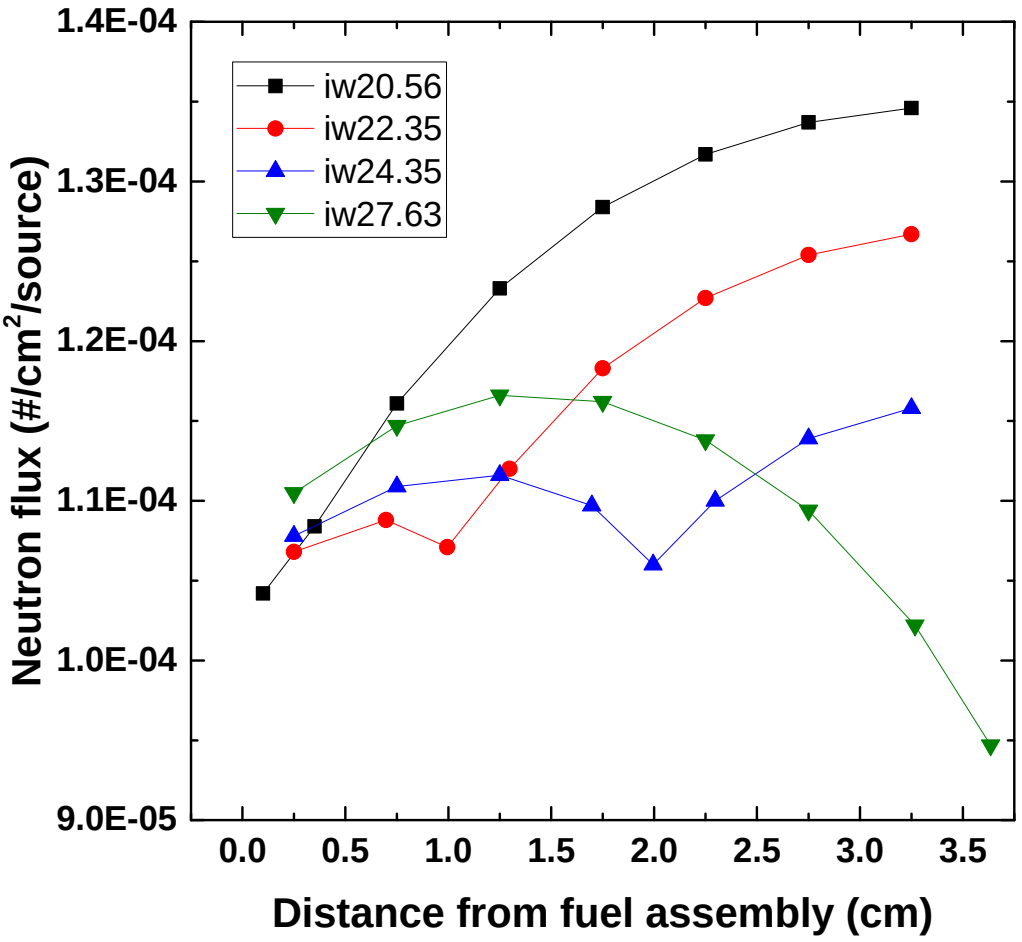

Figure 29 Total neutron flux vs inner width for the stainless steel case

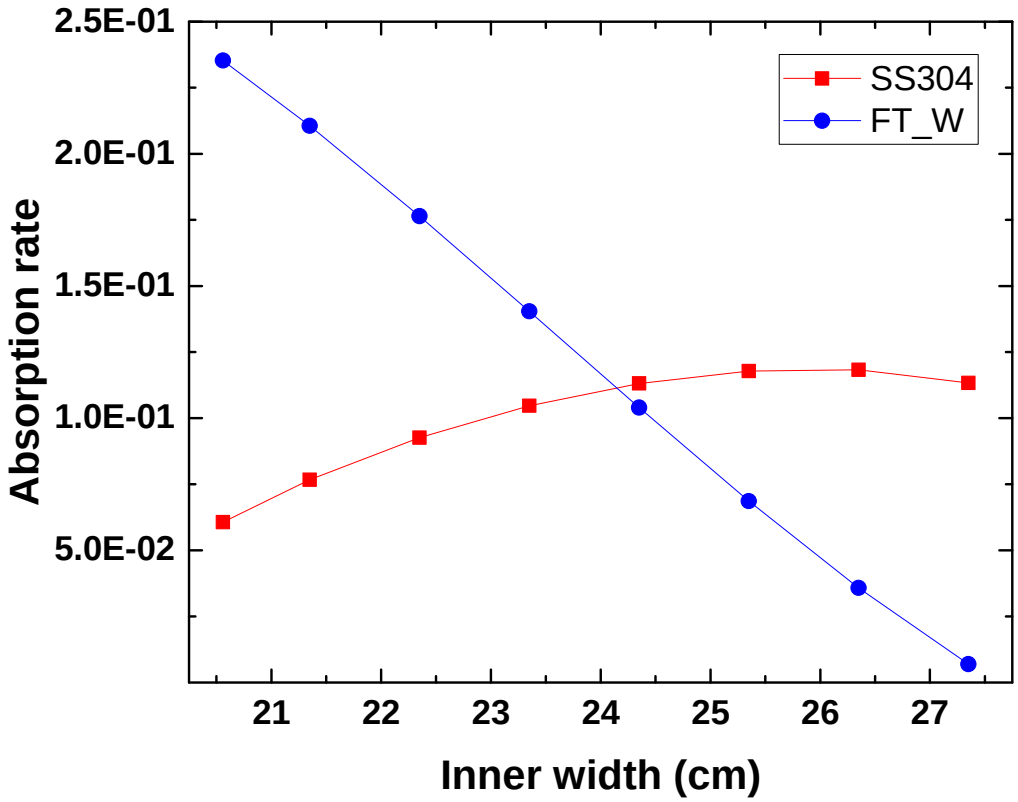

Figure 30 Absorption rate vs inner width for the stainless steel case

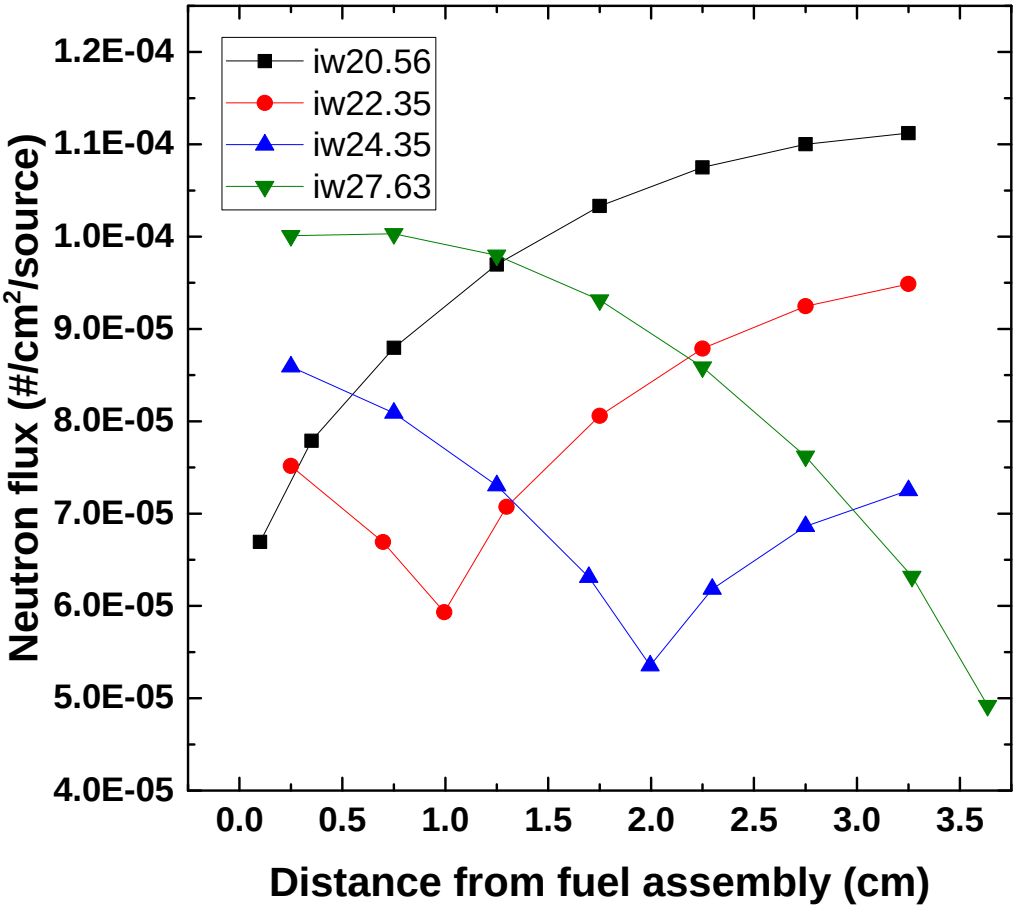

Figure 31 Total neutron flux vs inner width for the Gd 1 wt% case

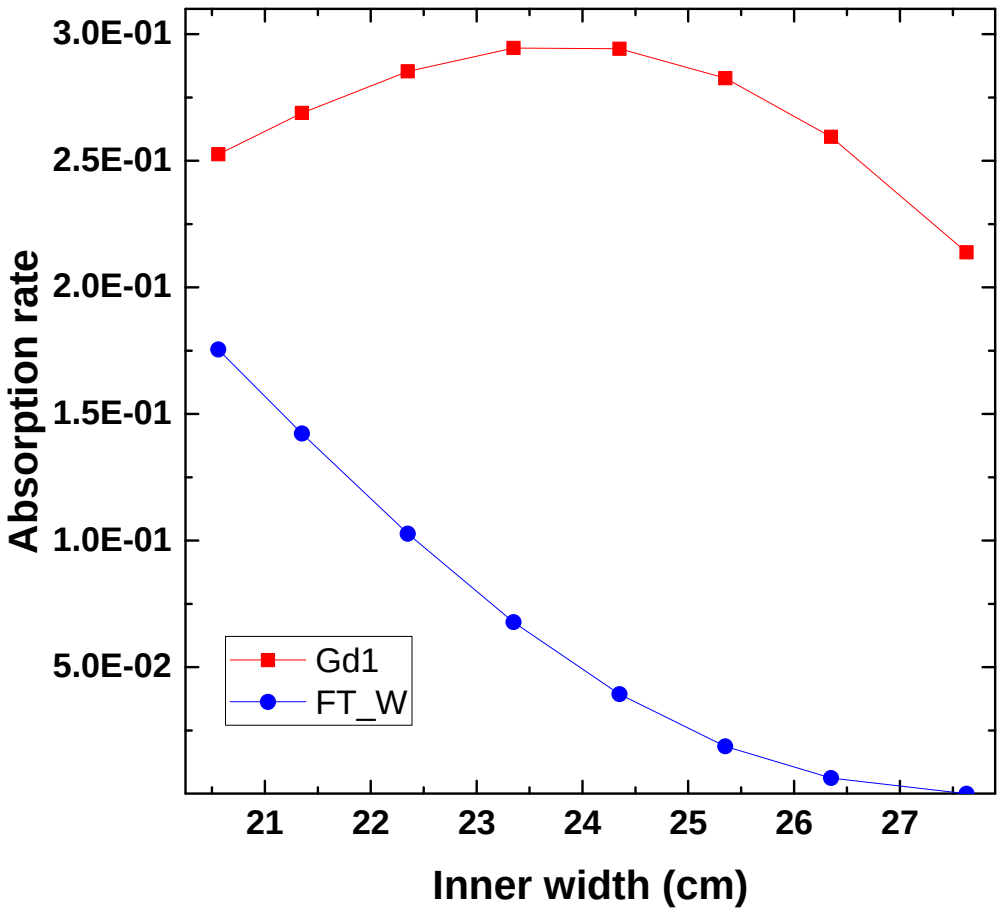

Figure 32 Absorption rate vs inner width of the cell wall and water in flux trap for the Gd 1 wt% case

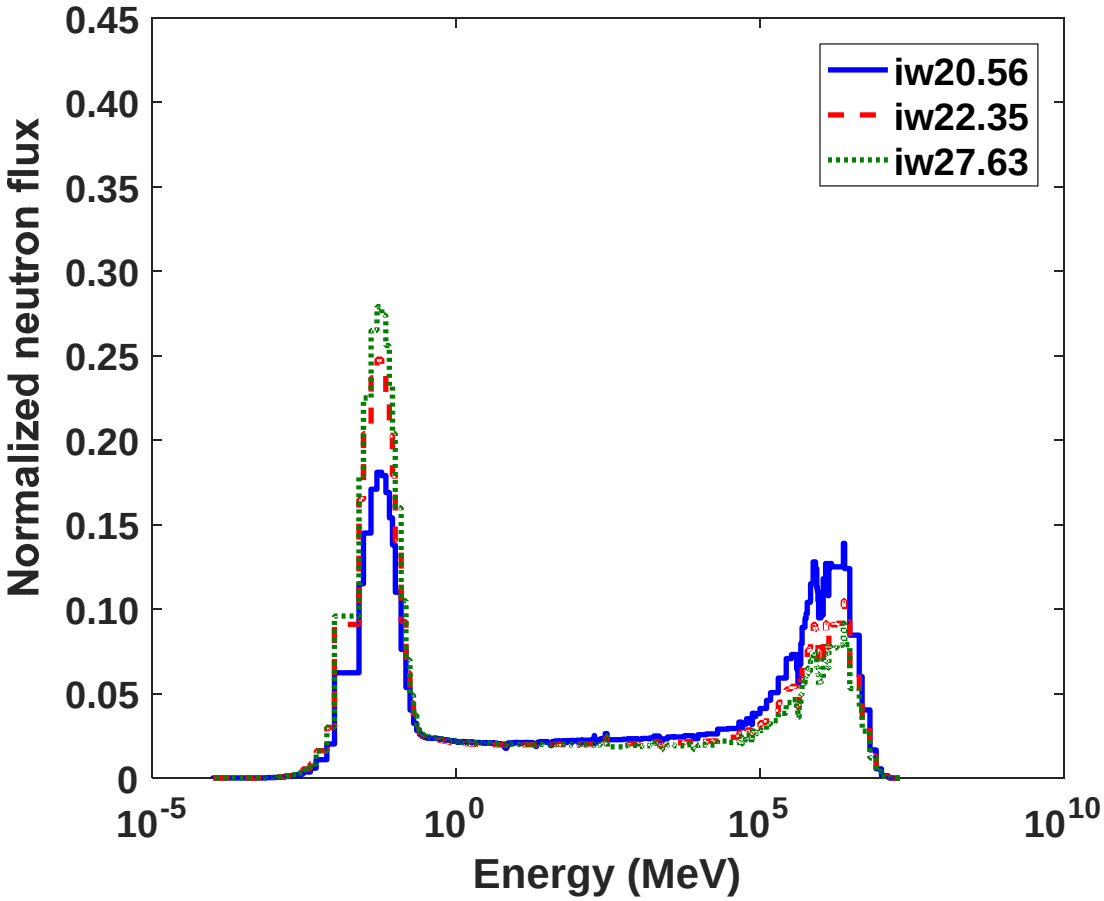

Figure 33 Neutron flux distribution vs inner width at cell wall for the stainless steel case

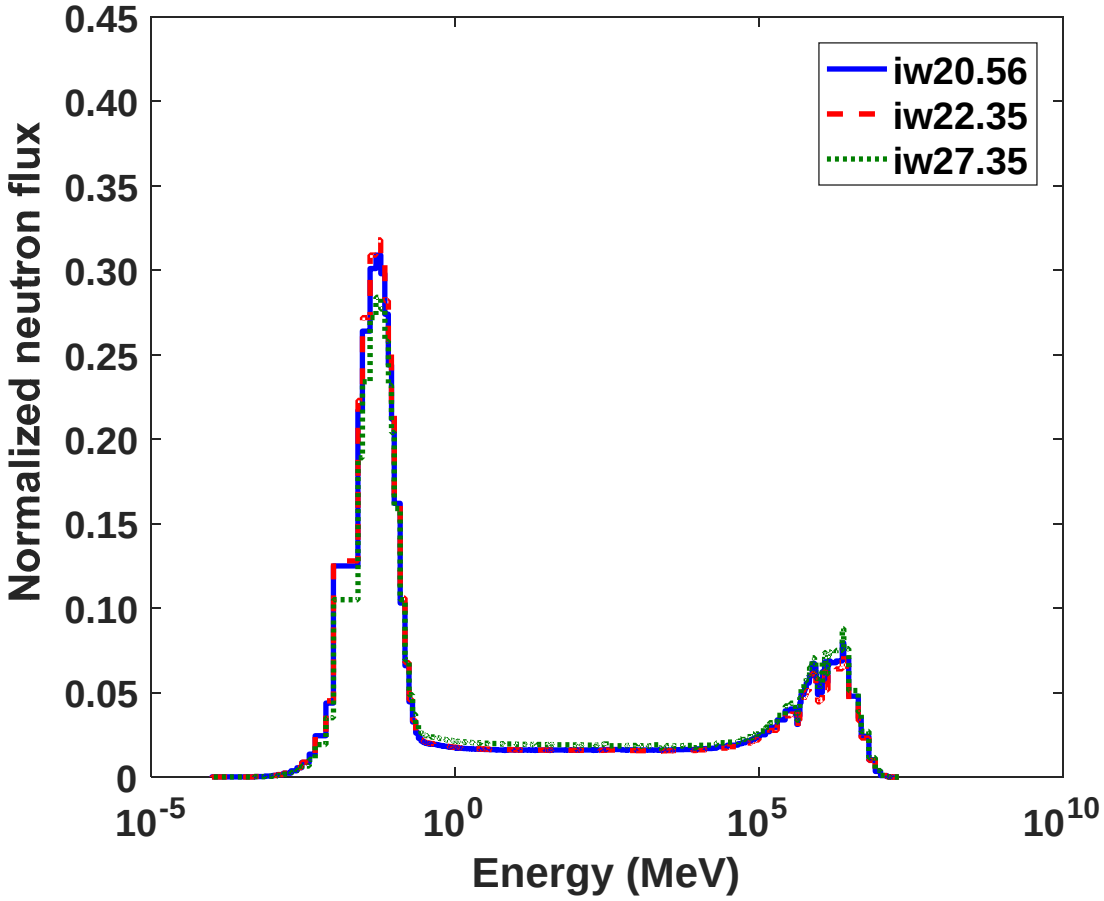

Figure 34 Neutron flux distribution vs inner width at flux trap for the stainless steel case

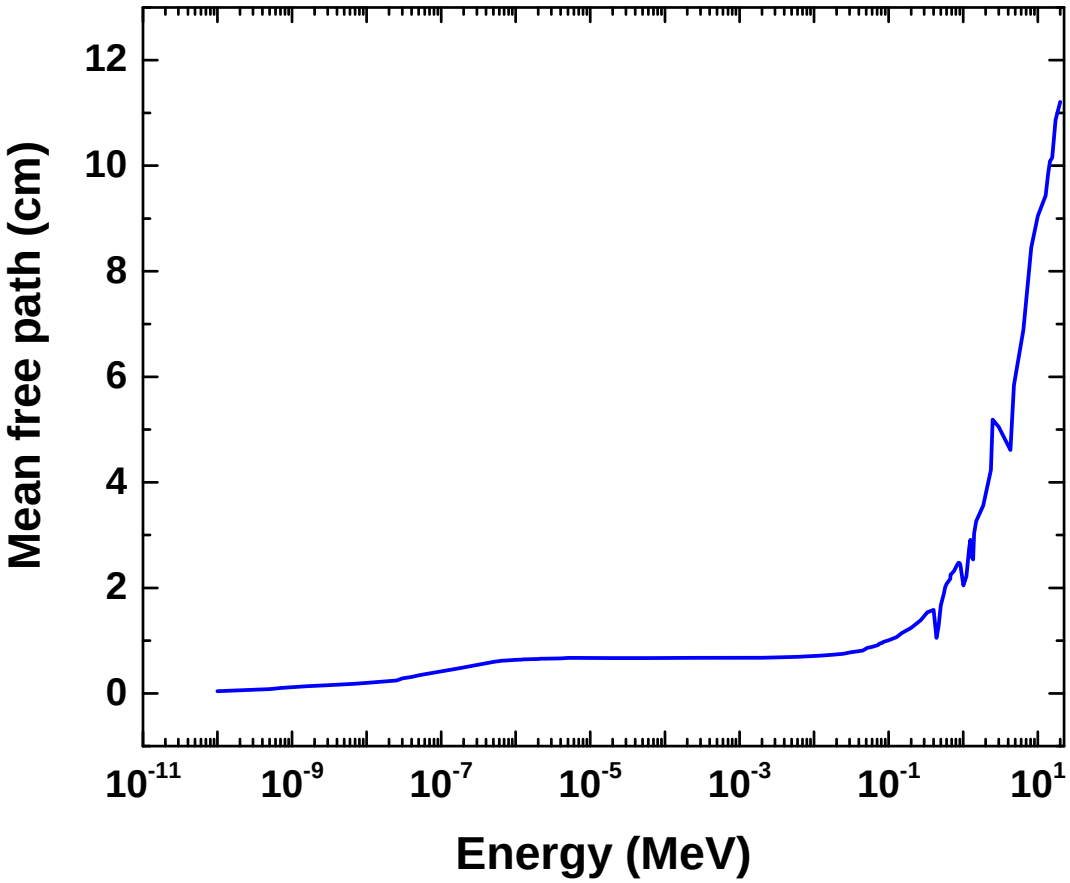

Figure 35 Mean free path vs energy in the water medium

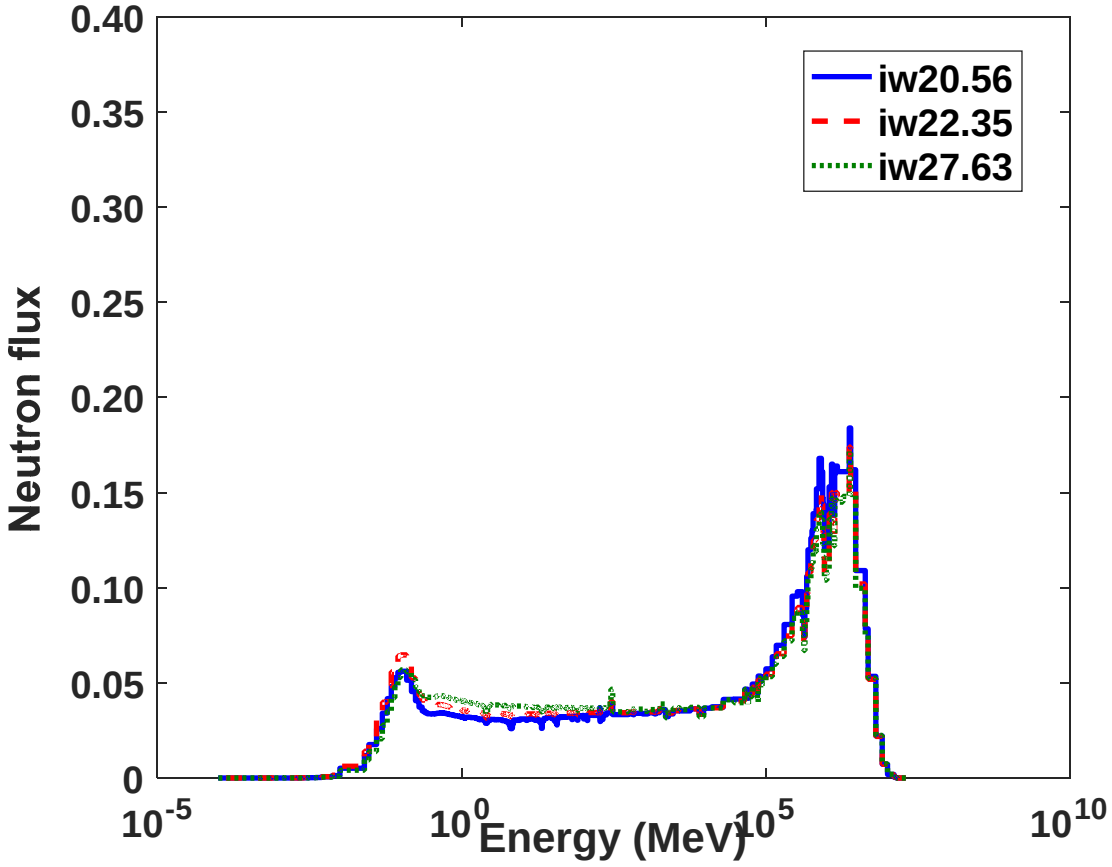

Figure 36 Neutron flux distribution vs inner width at cell wall for the Gd 1 wt% case

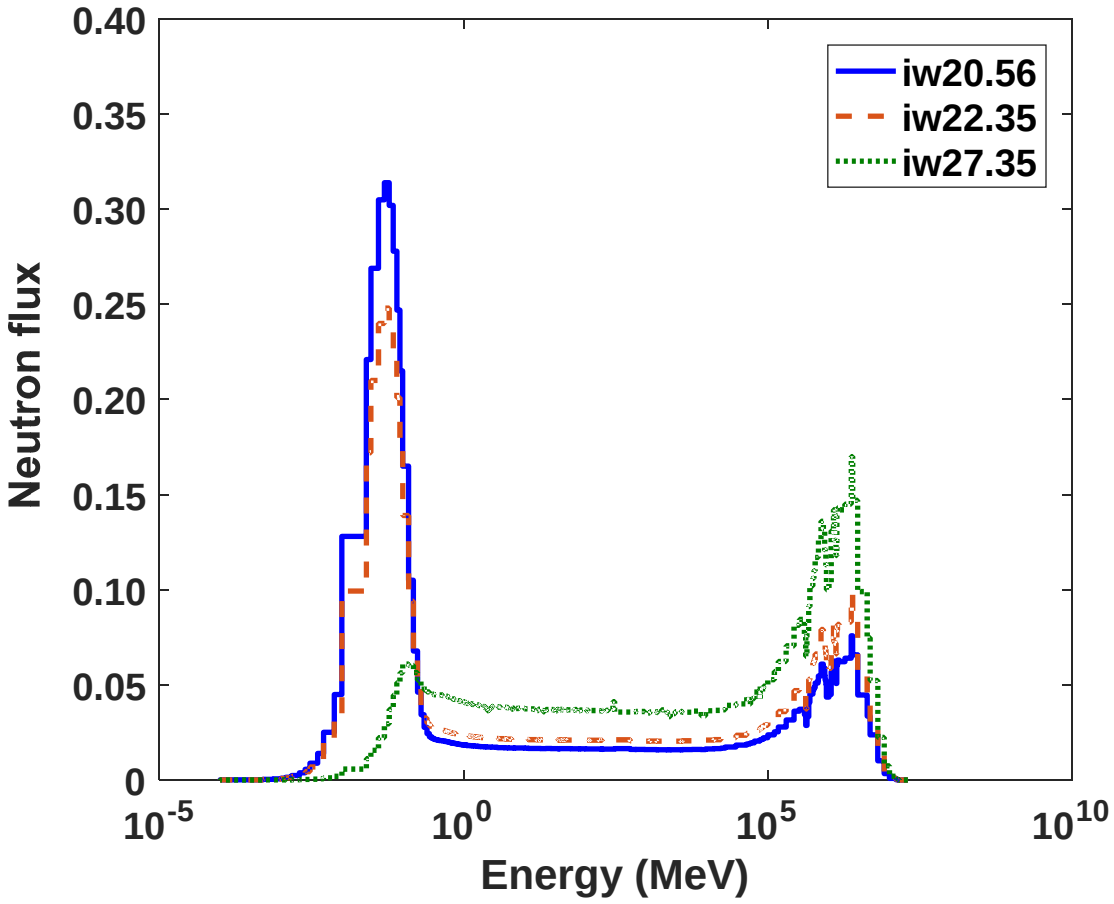

Figure 37 Neutron flux distribution vs inner width at flux trap for the Gd 1 wt% case

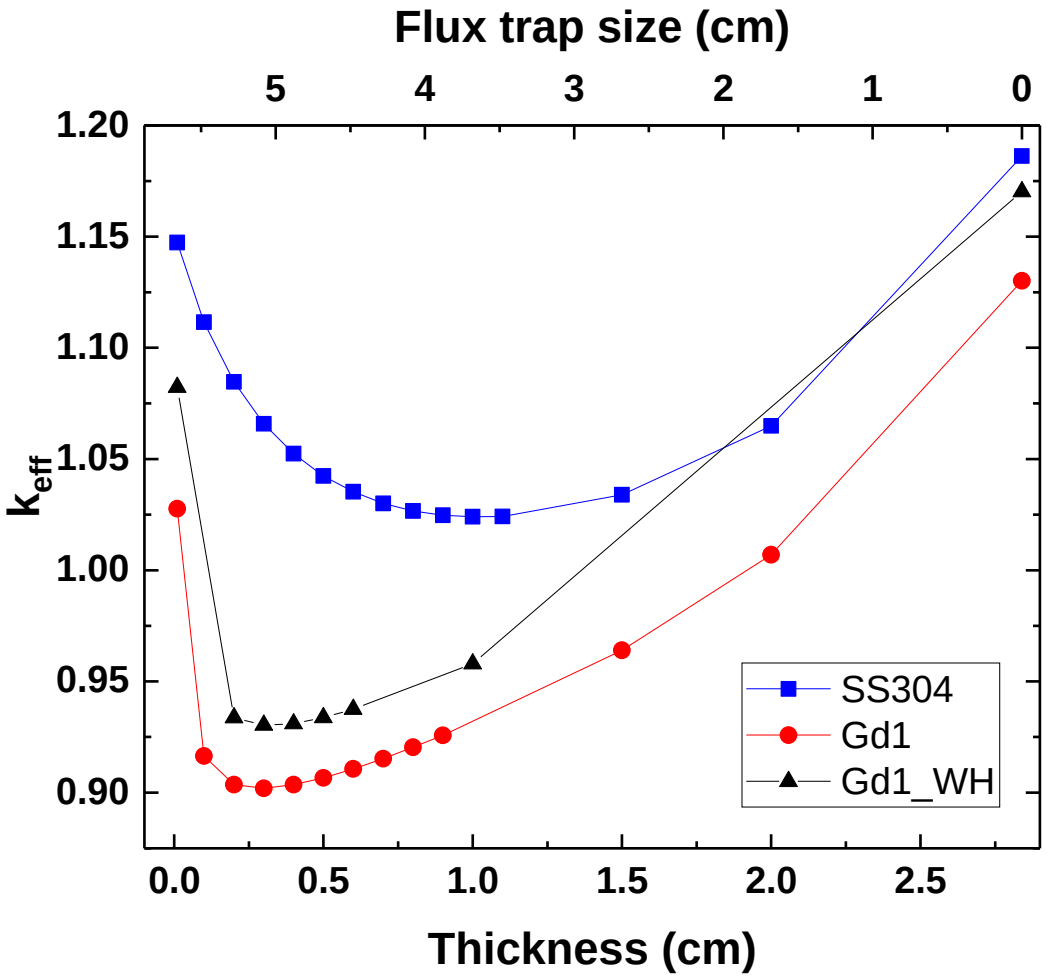

Figure 38 k_{eff} vs thickness of the stainless steel and Gd 1 wt% case for PLUS7 and Westinghouse OFA 17x17

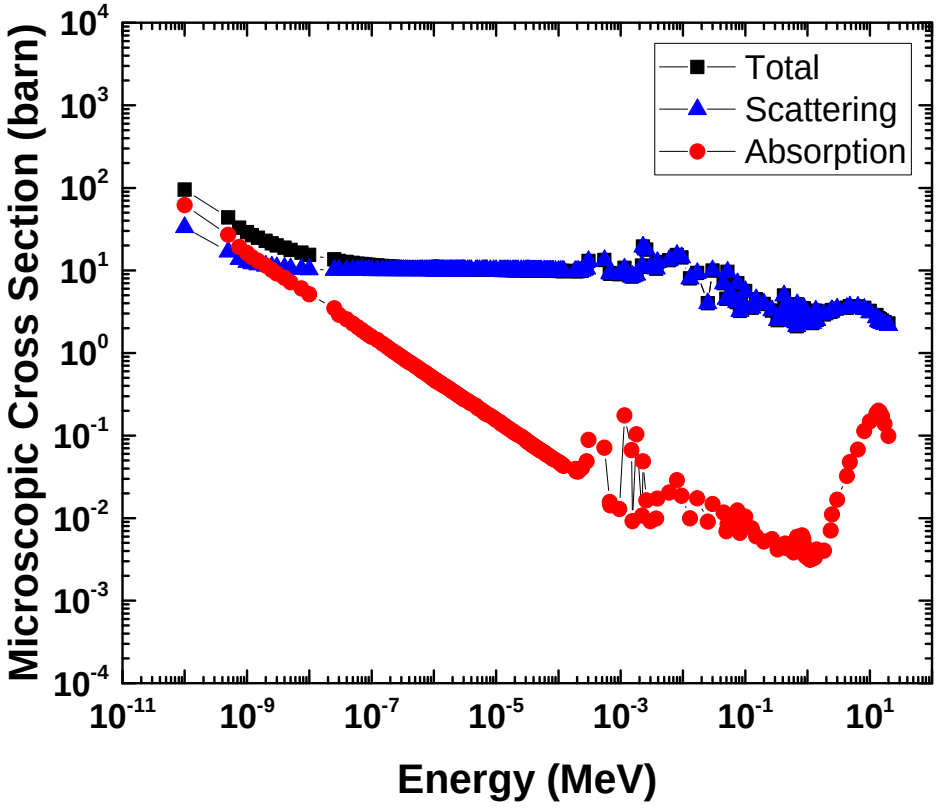

Figure 39 Total, scattering and absorption cross section of the stainless steel

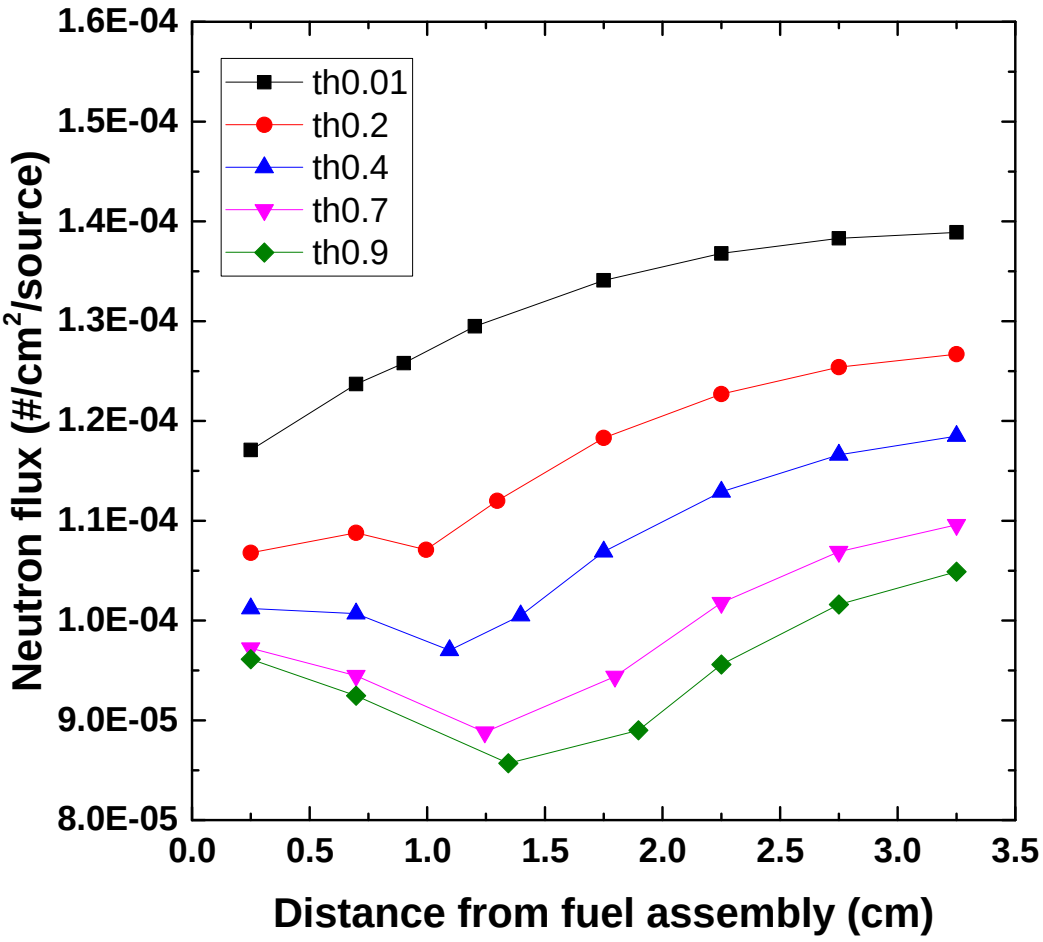

Figure 40 Total neutron flux of the stainless steel with various thickness of cell wall

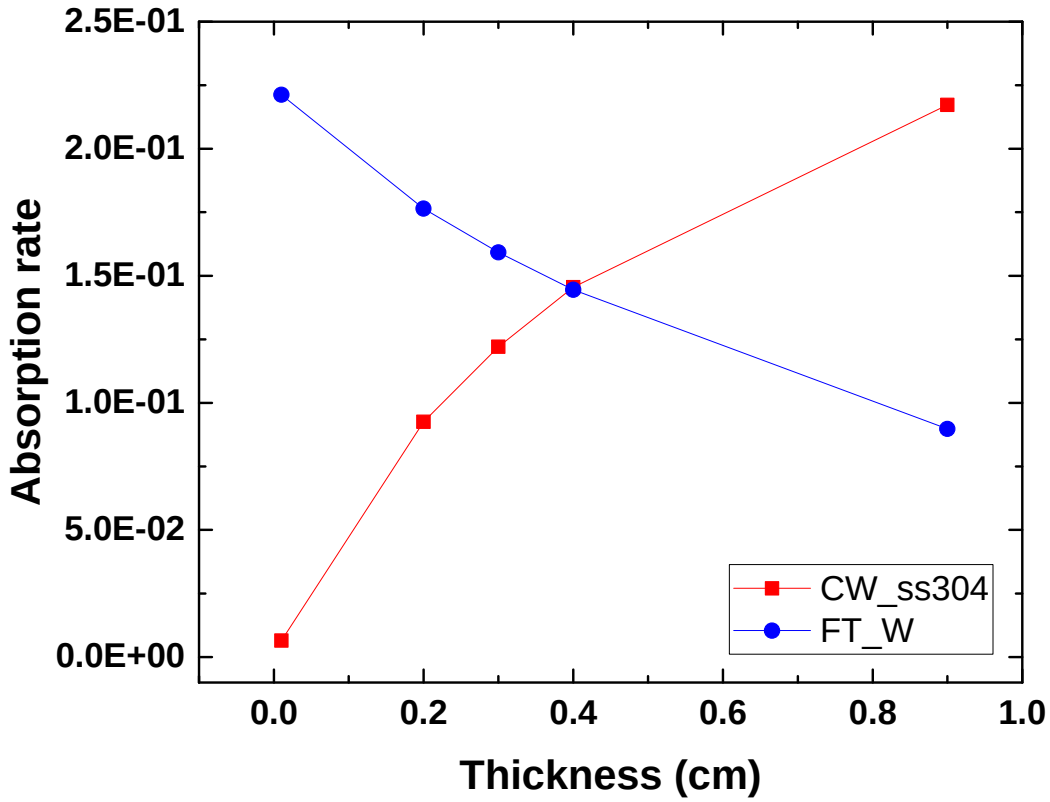

Figure 41 Absorption rate for the stainless steel with various thickness of cell wall

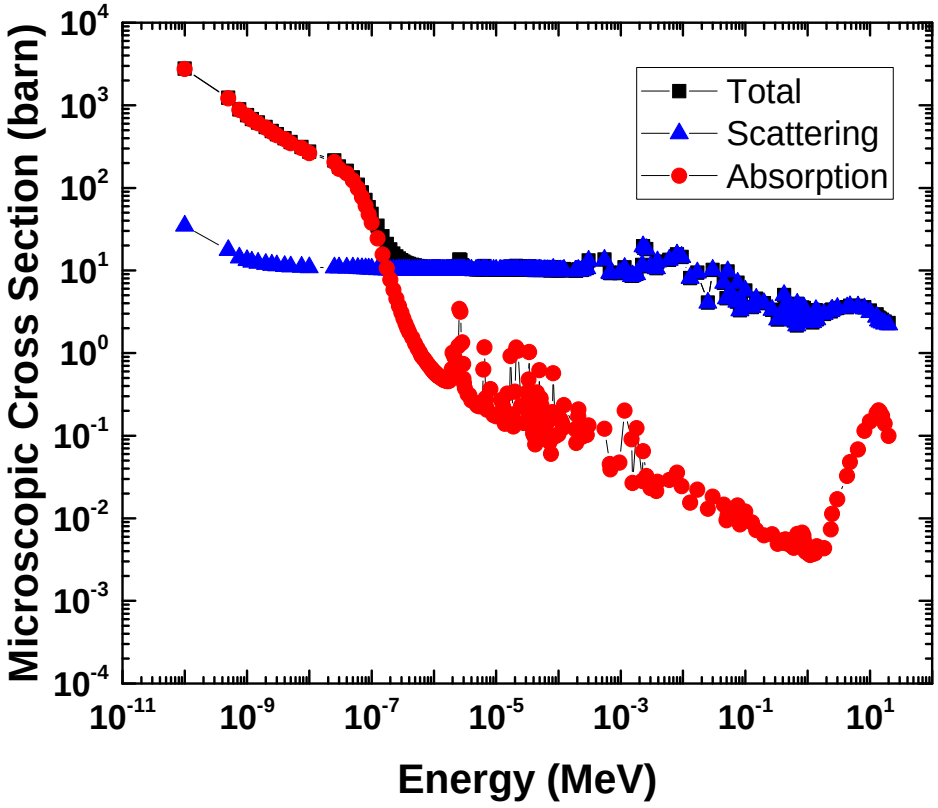

Figure 42 Total, scattering and absorption cross section of the Gd 1 wt%

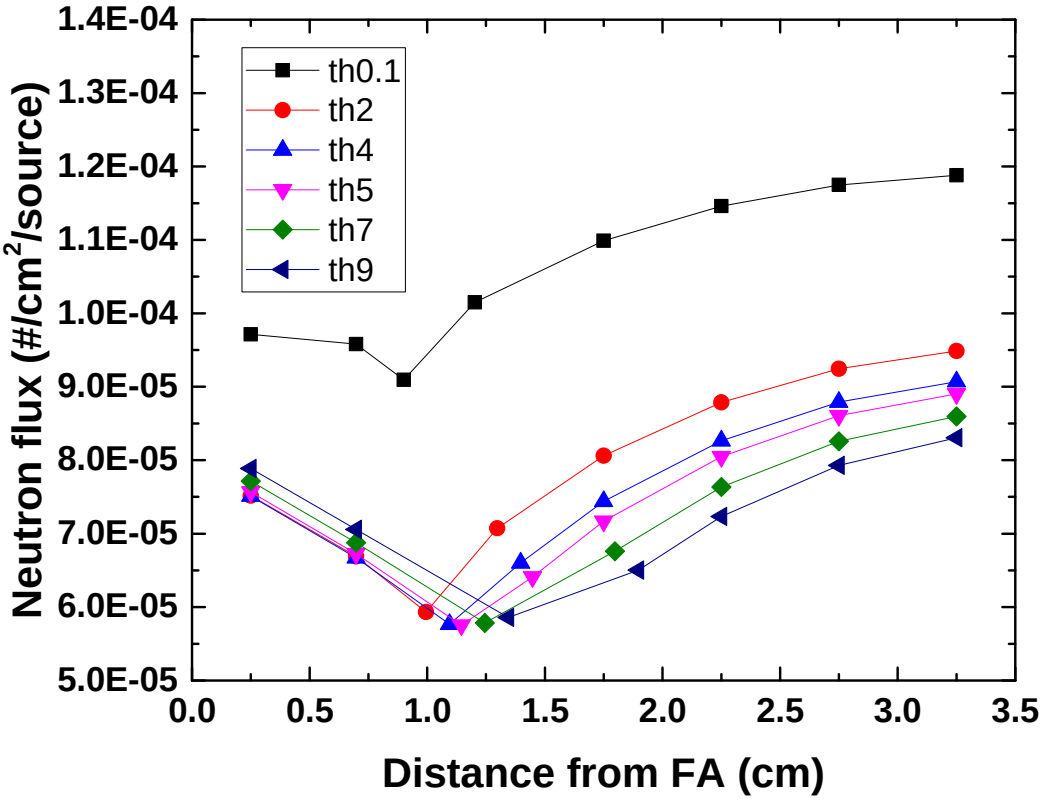

Figure 43 Total neutron flux of the Gd 1 wt% with various thickness of cell wall

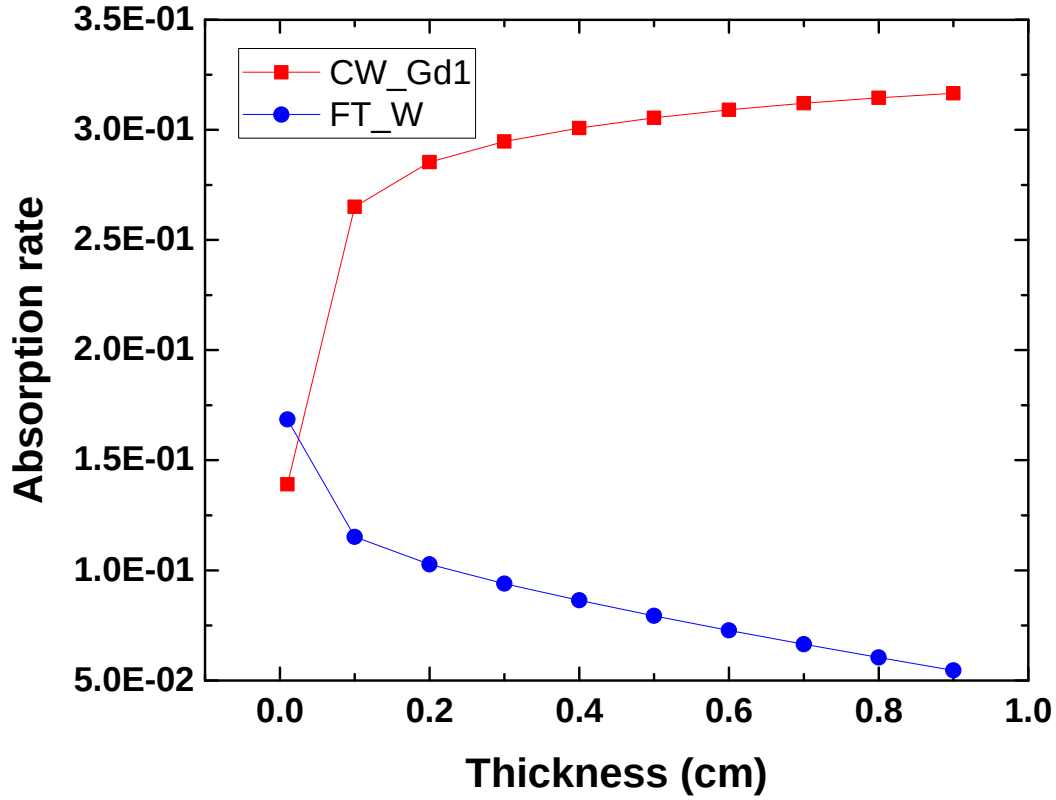

Figure 44 Absorption rate vs thickness of the cell wall and water in flux trap for the Gd 1 wt% case

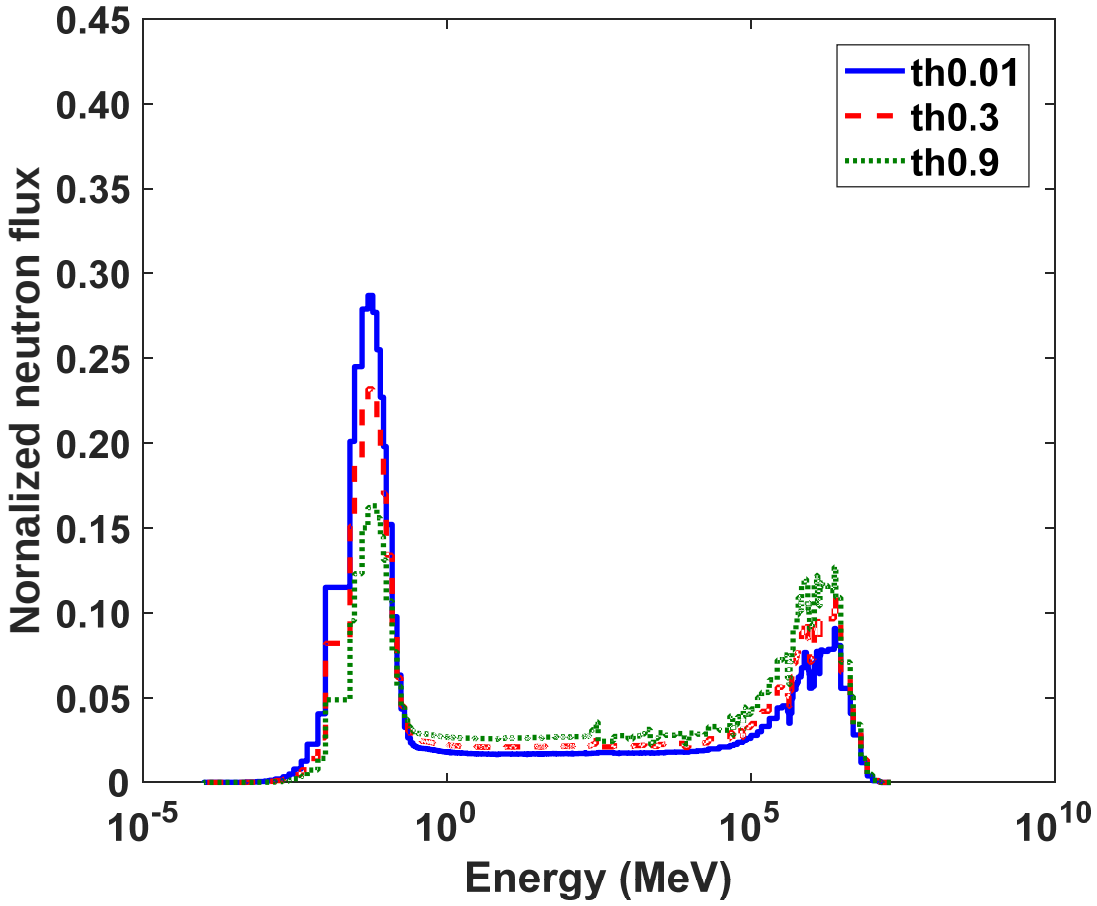

Figure 45 Neutron flux distribution vs thickness at cell wall for the stainless steel case

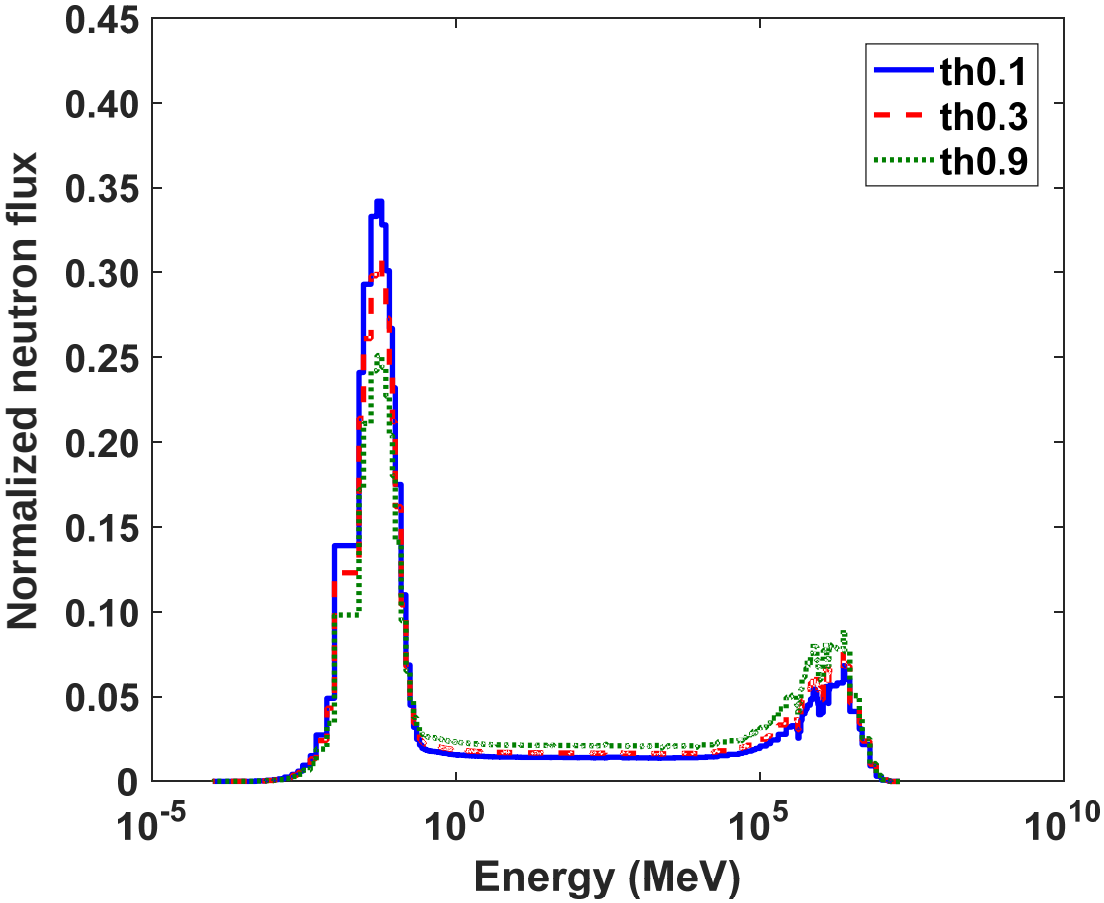

Figure 46 Neutron flux distribution vs thickness at flux trap for the stainless steel case

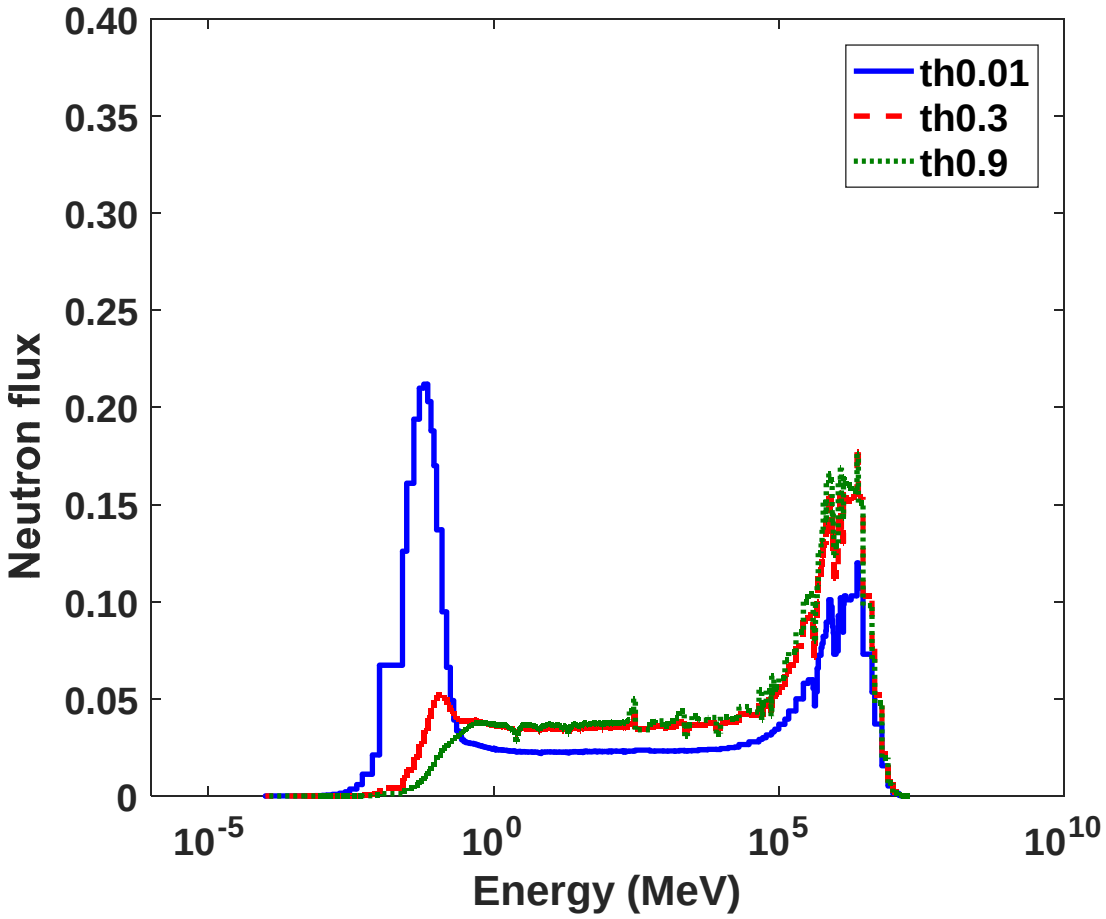

Figure 47 Neutron flux distribution vs thickness at cell wall of the Gd 1 wt% case

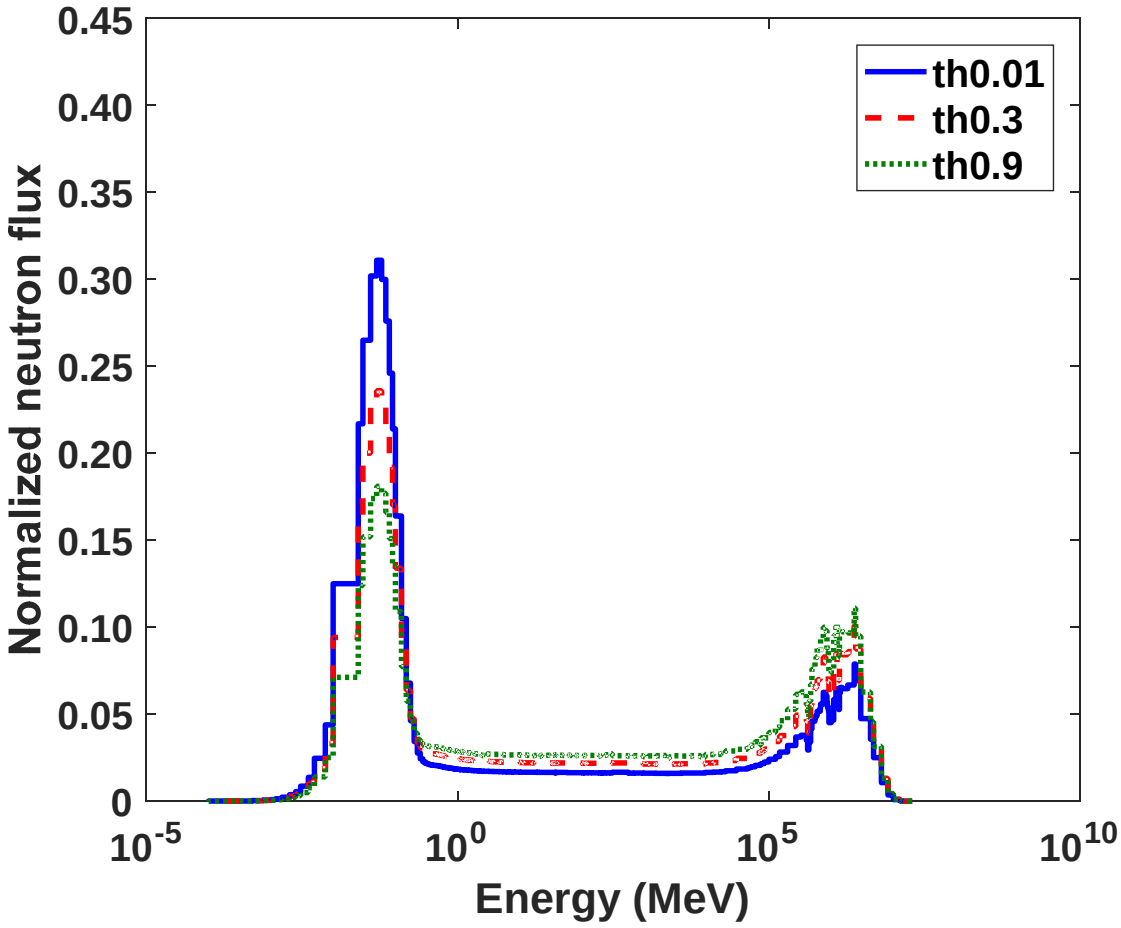

Figure 48 Neutron flux distribution vs thickness at flux trap of the Gd 1 wt% case

Chapter 5. Application to spent fuel transportation and storage system for criticality control

The new neutron absorber, Gd and B combined stainless steel, could be applied to spent fuel transportation and storage system. The reference models for spent fuel storage pool and spent fuel transportation and storage cask have been selected. The contents of neutron poison material should be decided by considering manufacturing possibilities. It is assumed that the maximum possible content of neutron absorbing materials is 1 wt% for Gd and 1 wt% for B from Chapter 3.

5.1. Spent fuel storage pool

The spent fuel is directly stored at the spent fuel storage pool after withdrawn from the nuclear reactor. In the spent fuel storage pool, the spent fuels are stored in two parts according to its reactivity. For region I, fresh fuel could be stored without any depletion. There are two neutron absorber panels between fuel assemblies. On the contrary, region II could store fuel assemblies with low reactivity. There is one neutron absorber panel between fuel assemblies. The selected design for the conventional spent fuel storage pool is Shin-kori units 3 and 4.

5.1.1. Region I

The region I racks are composed of a water flux trap between two neutron absorbers. The adopted geometrical parameters are from Shin-kori units 3 and 4 as described in Table 15. The neutron absorber for Shin-kori units 3 and 4 is Boral with 0.0220 g B-10/cm^2 for region I. In this study, the 75% credit for neutron absorber was applied, therefore, the concentration of B-10 used in the calculations is 0.0165 g B-10/cm^2 for region I. The cell and sheathing are composed of stainless steel.

The fresh fuel condition of 5 wt% enriched UO_2 fuel assembly was analyzed in region I. The density of nuclear fuel is 10.313 g/cm^3 (94.10TD). The water density is 1.0 g/cm^3 which depicts maximum density. The neutron absorber is Boral and the B-10 areal density is 0.0165 g B-10/cm^2 (75% neutron absorber credit). For conservative calculations, the soluble boron was not used in calculations. Also, the reflective boundary is utilized in a radial direction and a vacuum boundary is used for axial direction. The k_{eff} for Boral was 0.92796 ± 0.00030.

For the same performance with Boral, the various combinations of Gd and B were calculated for B contents of 0.5, 0.8 and 1.0 wt% as shown in Figure 49. The required Gd contents for B contents of 0.5, 0.8 and 1.0 wt% are 1.80, 1.25 and 0.9 wt% as summarized in Table 16. The total amount of neutron absorbing materials (both Gd and B) at each case is 2.30, 2.05 and 1.90 wt%. The required amount of Gd and B contents could be calculated through a linear function from Figure 50.

The possible composition could be implicated in the region I is Gd 0.9 wt% + B 1.0 wt%. Other compositions over the constraint of Gd 1 wt%. The Gd 0.9 wt% + B 1.0 wt% stainless steel was selected as an optimization study. The neutron multiplication factors were calculated as a function of inner width and thickness. As discussed in chapter 4, the k_{eff} shows the minimum value at the lowest inner width as summarized in Table 17. A free clearance between rack walls and fuel assemblies that takes into account the fuel assembly envelope and the manufacturing tolerances is needed. Considering those mechanical constraints, an optimum inner width of 21.2 cm is chosen. Also, the optimum thickness at the inner width of 21.2 cm is 0.45 cm. With an optimum inner width of 21.2 cm and an optimum thickness of 0.45 cm, the pitch could be reduced to 26.0 cm which has similar performance with Boral as shown in Figure 51.

B-10 could be enriched by up to 90%. With enriched B-10, the reactivity could be reduced, and the pitch might be more reduced than using natural B. The optimization study of thickness was conducted in Table 18. The optimum thickness is 0.5 cm with the inner width of 21.2 cm. With the optimum inner width of 21.2 cm and the optimum thickness of 0.50 cm, the pitch could be reduced to 24.9 cm as described in Figure 52. The code to code validation was performed with KENO V.a. and MCS in Table 19.

As represented in Figure 53, the total spent nuclear fuels stored in the region I are five modules; four for 8×9 and one for 7×9. The total number of fuel assemblies stored in the region I is 351. The total area covered by Boral for the region I is 269318.79 cm^2 calculated by Eq. (3) where the pitch is 27.7 cm. With the reduced pitch of 26.0 cm and 24.9 cm, 13.5 ~ 23.6% more fuel assemblies could be stored at the same space compared to Boral as calculated from Eqs. (4) and (5).

$$Total\ area = (\#\ of\ FA) \times (pitch)^2 \tag{3}$$

where:

$Total\ area = Total\ area\ covered\ (cm^2)$

$\#\ of\ FA = Number\ of\ fuel\ assemblies\ stored$

$pitch = Pitch\ size\ between\ fuel\ assemblies\ (cm)$

$$(\#\ of\ FA)_{GdB} = \frac{Total\ area}{(reduced\ pitch)^2} \tag{4}$$

where:

$(\#\ of\ FA)_{GdB} = Number\ of\ fuel\ assemblies\ stored\ for\ Gd\ and\ B\ stainless\ steel$

$reduced\ pitch = reduced\ pitch\ size\ from\ optimization\ study\ (cm)$

$$Increased\ capacity = \left(\frac{(\#of\ FA)_{GdB}}{(\#of\ FA)_{Boral}} - 1 \right) \times 100 \quad (5)$$

where:

$Increased\ FA$

$= Increased\ percent\ of\ capacity\ when\ switched\ to\ Gd\ and\ B\ stainless\ steel\ (\%)$

5.1.2. Region II

The region II racks have one neutron absorber between fuel assemblies. The adopted geometrical parameters are from Shin-kori units 3 and 4 as described in Table 15. The neutron absorber for Shin-kori units 3 and 4 is Boral with 0.0267 g B-10/cm^2 for region II. In this study, the 75% credit for neutron absorber was applied, therefore, the concentration of B-10 used in the calculations is 0.0220 g B-10/cm^2 for region II. The cell and sheathing are composed of stainless steel.

The fresh fuel condition of 5 wt% enriched UO_2 fuel assembly was analyzed for optimization study in region II. The density of nuclear fuel is 10.313 g/cm^3 (94.10TD). The water density is 1.0 g/cm^3 which depicts maximum density. The neutron absorber is Boral and the B-10 areal density is 0.0165 g B-10/cm^2 (75% neutron absorber credit). For conservative calculations, the soluble boron was not used in calculations. The boundary conditions are the periodic boundary for radial direction and vacuum boundary for axial direction. The k_{eff} for Boral was 1.20089 $\pm$ 0.00028.

The composition of Gd and B stainless steel is Gd 0.9 wt% + B 1.0 wt% with enriched B-10 90%. The optimization of inner width and thickness was performed for the inner width of 21.2 cm and 22.0 cm and thickness of 0.25 to 0.65 cm in Table 20. The reactivity for the inner width of 21.2 cm showed lower than that of 22.0 cm. The reactivity continuously decreases with increasing thickness of the cell wall. However, the pitch could not be reduced with increasing thickness of the cell wall. Therefore, the pitch with optimized dimension and Gd and B stainless steel could be reduced from 22.5 cm to 22.05 cm as described in Figure 54.

The region II could store enrichment from 1.5 to 5.0 wt%. Therefore, the fresh fuel condition of each enrichment was calculated in Figure 55. Only enrichment of 1.5 wt% could be stored without burnup. Therefore, the burnup credit is needed to be considered for storing over enrichment of 1.5 wt% for region II. The STARBUCS/SCALE code was used for depletion analysis. In STARBUCS calculation, the underneath burnup histories were considered.

- Average specific power: 38.365 MW/MTU
- No cooling time
- 18 axial profiles from NUREG/CR-6801
- Nuclide sets selected from NUREG/CR-7109 (Actinide only, actinide with 16 fission products and all nuclides)

The nuclide sets are summarized in Table 21. For three nuclide sets, the minimum required burnups according to enrichment were calculated. The upper safety limit is set as 0.90 and 0.95. From all nuclide sets, the loading curves show consistency with Boral and Gd 0.9 wt% + B 1.0 wt% (enriched B-10) stainless steel with optimized dimensions. In other words, the Gd 0.9 wt% + B 1.0 wt% (enriched B-10) stainless steel with optimized dimensions could be used in region II.

As described in Figure 53, there are thirteen modules of the rack in region II; four modules of 9x10, six modules of 10x10, two modules of 9x8 and one module of 9x9. The total number of fuel assemblies stored for Boral in region II is 1185. The increased capacity was calculated from Eq. (3)-(5). From the calculations, the capacity could be increased by about 4.05 %.

Table 15 Summary of dimensions of Shin-kori units 3 and 4

Component (cm)		Region I	Region II
Cell	Inner width	22.0	22.0
	Thickness	0.25	0.25
	Pitch	27.0	22.5
Neutron absorber	Width	18.0	18.0
	Thickness	0.25	0.25
Sheathing	Thickness	0.06	0.06

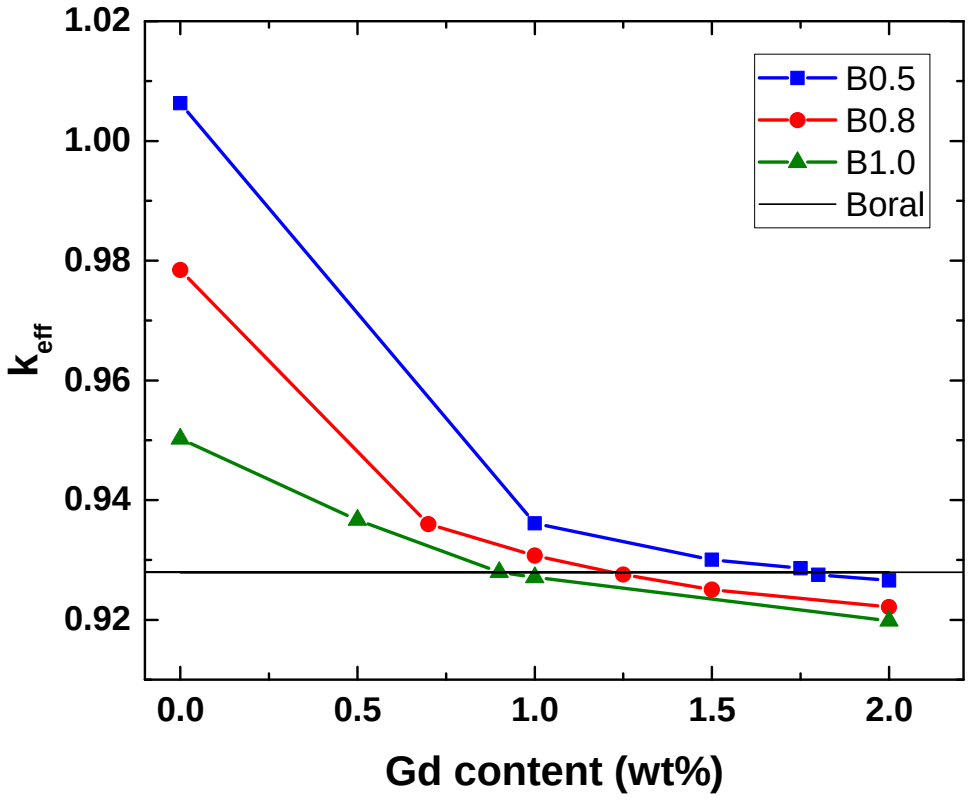

Figure 49 k_{eff} vs Gd content for B 0.5, 0.8 and 1.0 wt%

Table 16 Required neutron absorbing materials for the region I in Shin-kori units 3 and 4

B content (wt%)	Gd content (wt%)	Total (wt%)*
0.5	1.80	2.30
0.8	1.25	2.05
1.0	0.90	1.90

* Total amount of neutron absorbing materials (Gd+B)

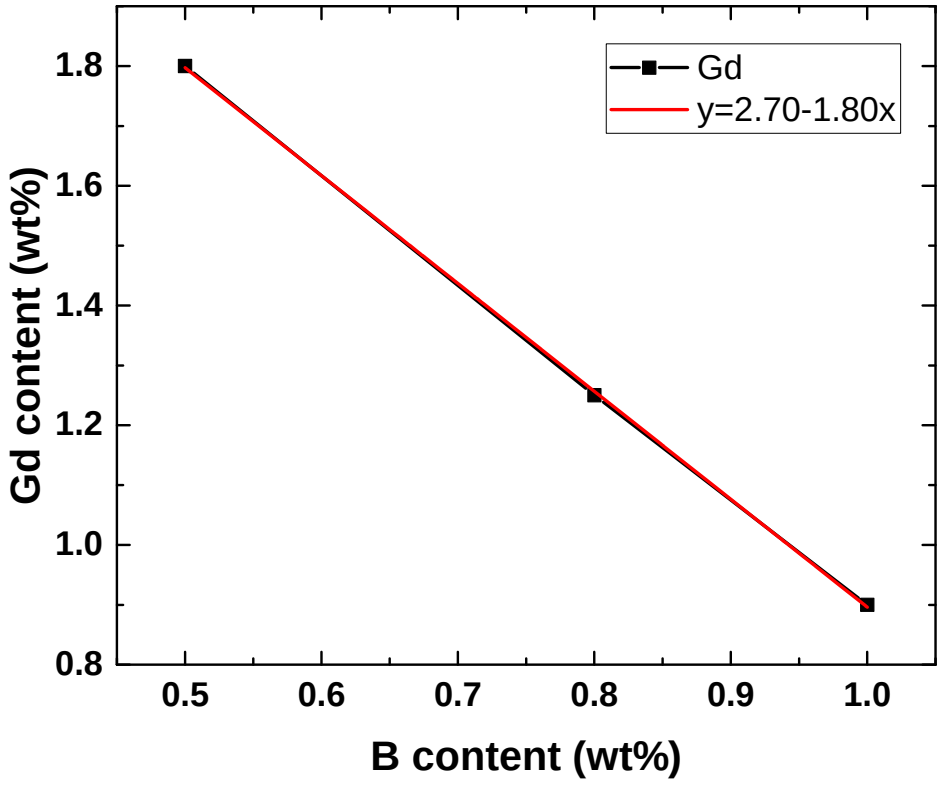

Figure 50 Required Gd contents as a function of B content for the region I in Shin-kori units 3 and 4 (x: B contents, y: Gd contents)

Table 17 k_{eff} vs cell wall thickness and cell inner width for the region I

Thickness (cm)	Inner width (cm)		
	21.2	21.5	22.0
0.15	0.91381	0.92401	0.94028
0.25	0.89714	0.90971	0.92797
0.35	0.89105	0.90378	0.92534
0.45	0.88920	0.90241	0.92409
0.50	0.88952	0.90285	0.92483

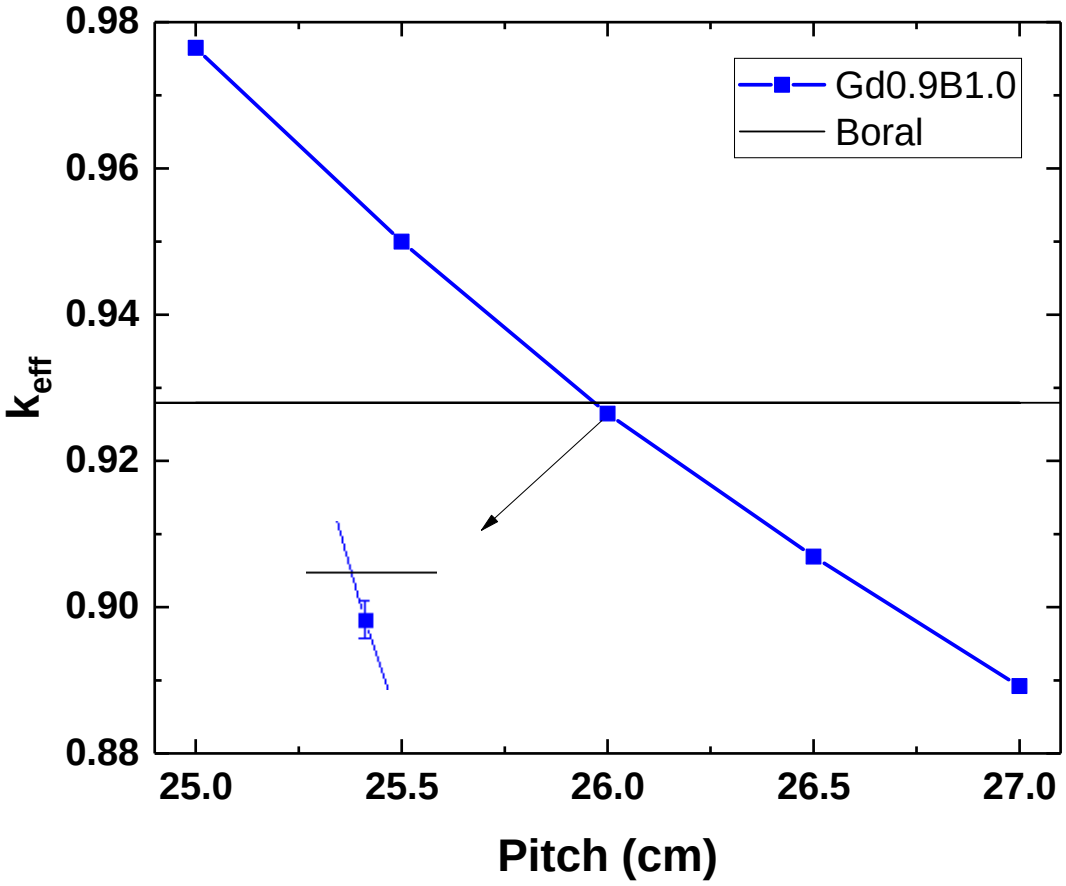

Figure 51 k_{eff} vs pitch for Gd 0.9 wt% + B 1.0 wt% stainless steel at cell inner width of 21.2 cm and the cell wall thickness of 0.45 cm

Table 18 k_{eff} vs cell wall thickness at cell inner width of 21.2 cm with enriched B-10 for the region I

Thickness (cm)	Inner width (cm)
	21.2
0.25	0.85320
0.35	0.84882
0.45	0.84762
0.50	0.84702
0.55	0.84748

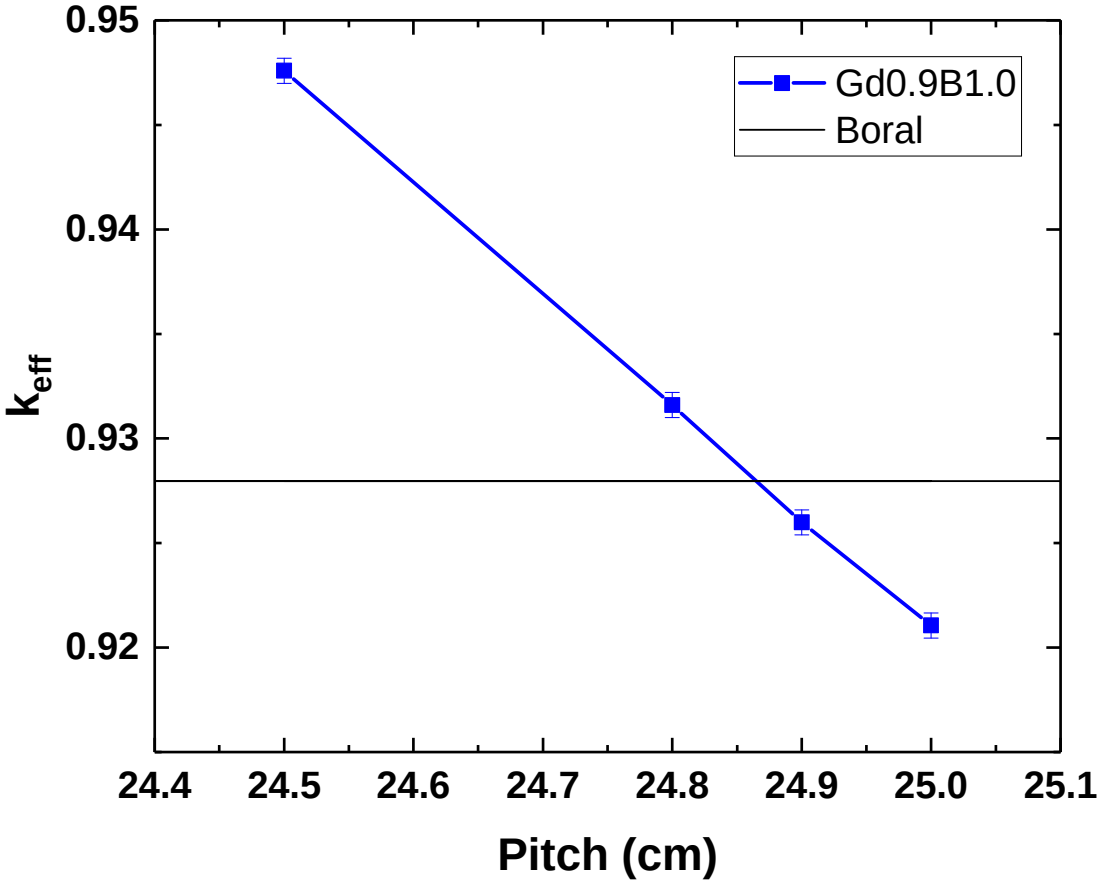

Figure 52 k_{eff} vs pitch for Gd 0.9 wt% + B 1.0 wt% with enriched B-10 90%

Table 19 k_{eff} calculated by KENO V.a. and MCS code for Gd 0.9 wt% + B 1.0 wt% with inner width of 21.2 cm, thickness of 0.50 cm and pitch of 24.9 cm

KENO V.a.	MCS
0.92599±0.00033	0.92353±0.00031

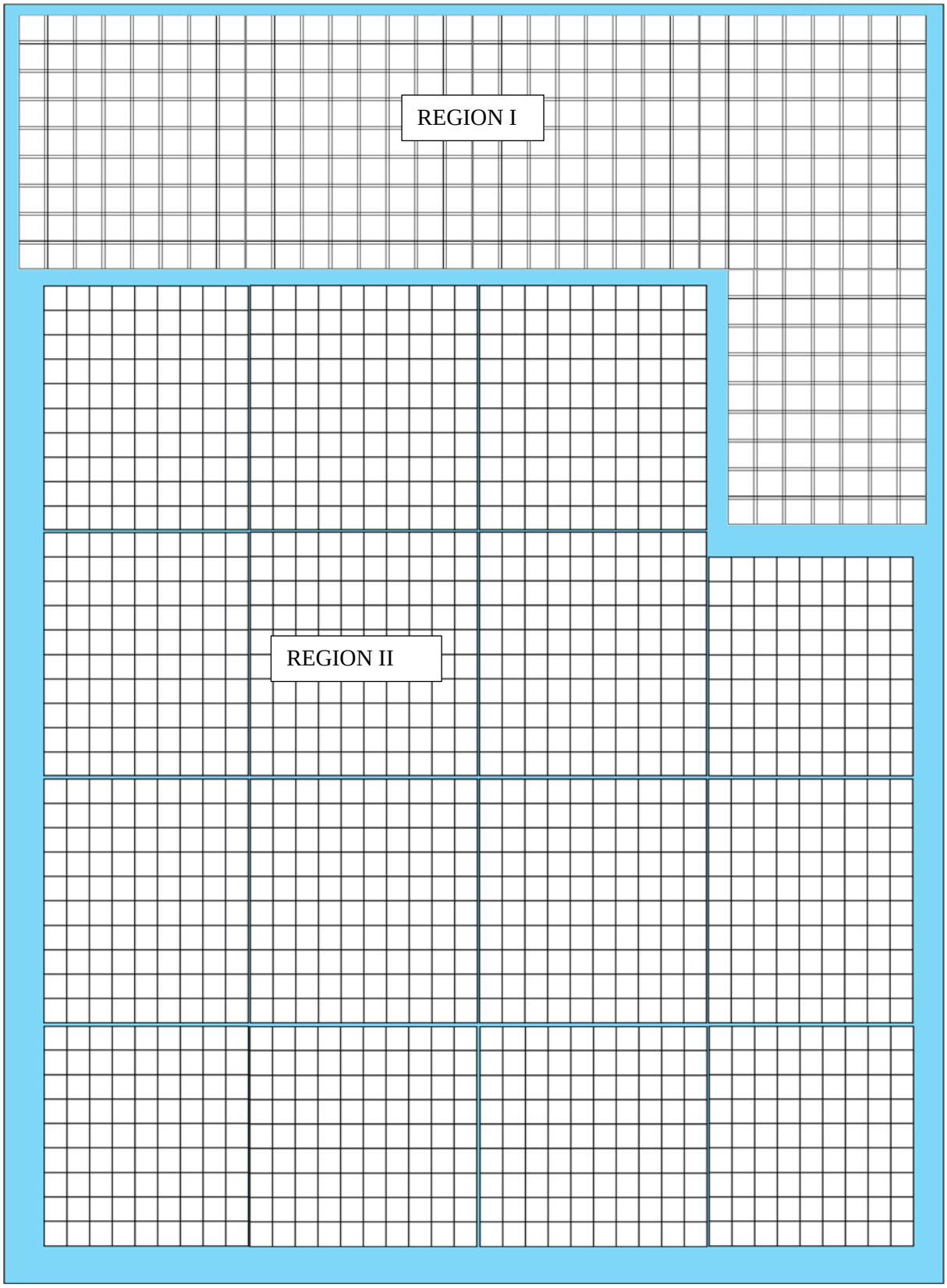

Figure 53 Arrange of spent nuclear fuel for spent fuel storage pool in Shin-kori units 3 and 4

Table 20 k_{eff} vs cell wall thickness and cell inner width for the region II

Thickness (cm)	Inner width (cm)	
	21.2	22.0
0.25	1.18530	1.18780
0.50	1.15229	1.15388
0.55	1.14764	1.14946
0.60	1.14363	1.14463
0.65	1.14005	1.14115

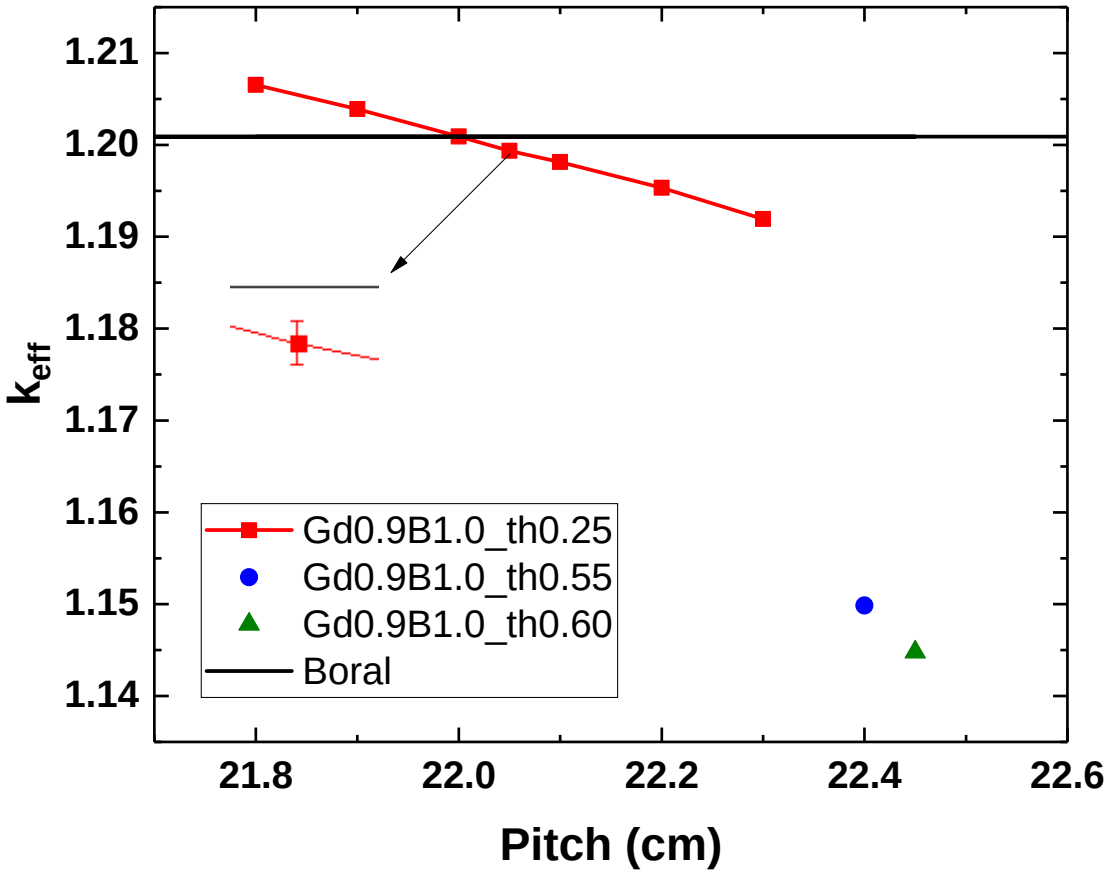

Figure 54 k_{eff} vs pitch for Gd 0.9 wt% + B 1.0 wt% with enriched B-10 90% for the region II

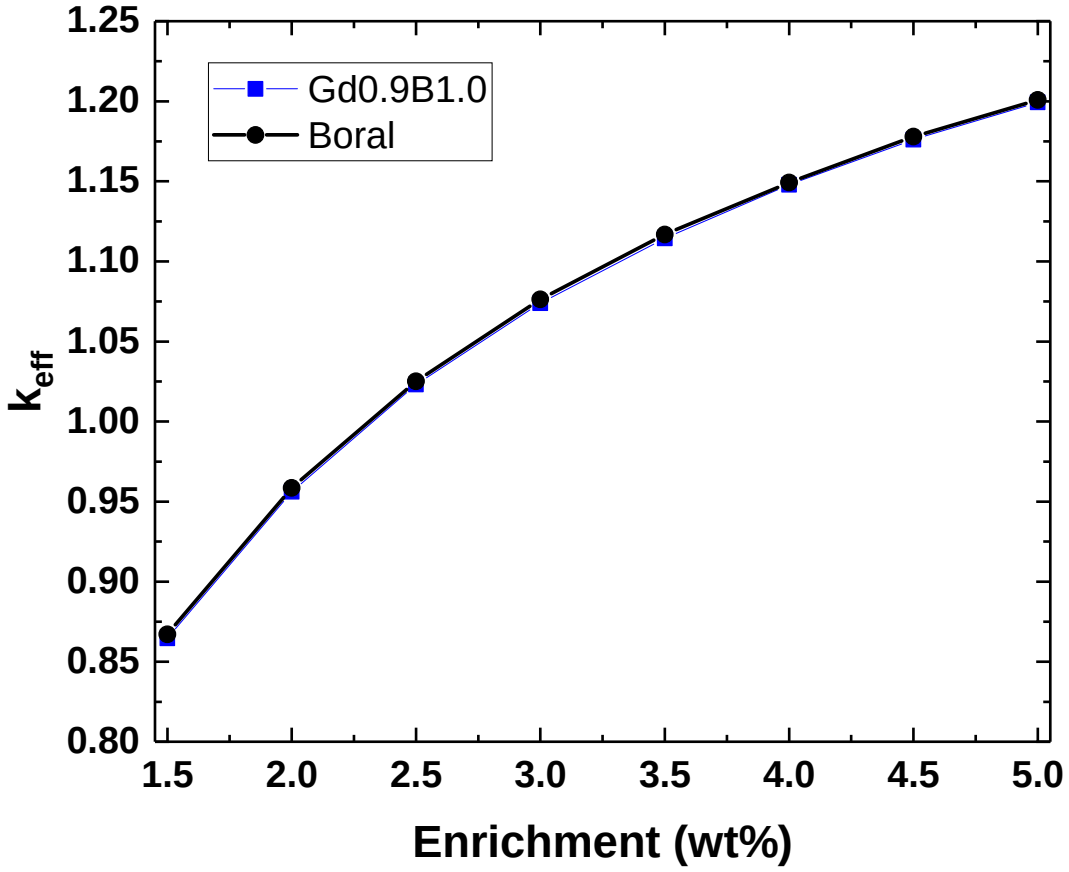

Figure 55 k_{eff} vs enrichment in fresh fuel composition for Boral and Gd 0.9 wt% + B 1.0 wt%

Table 21 Nuclide sets used in burnup credit [35]

Set of nuclides for actinide-only (12)			
U-234	U-235	U-236	U-238
Np-237	Pu-238	Pu-239	Pu-240
Pu-241	Pu-242	Am-241	Am-243
Set of nuclides for actinides and fission products (16)			
Mo-95	Tc-99	Ru-101	Rh-103
Ag-109	Cs-133	Nd-143	Nd-145
Sm-147	Sm-149	Sm-150	Sm-151
Sm-152	Eu-151	Eu-153	Gd-155

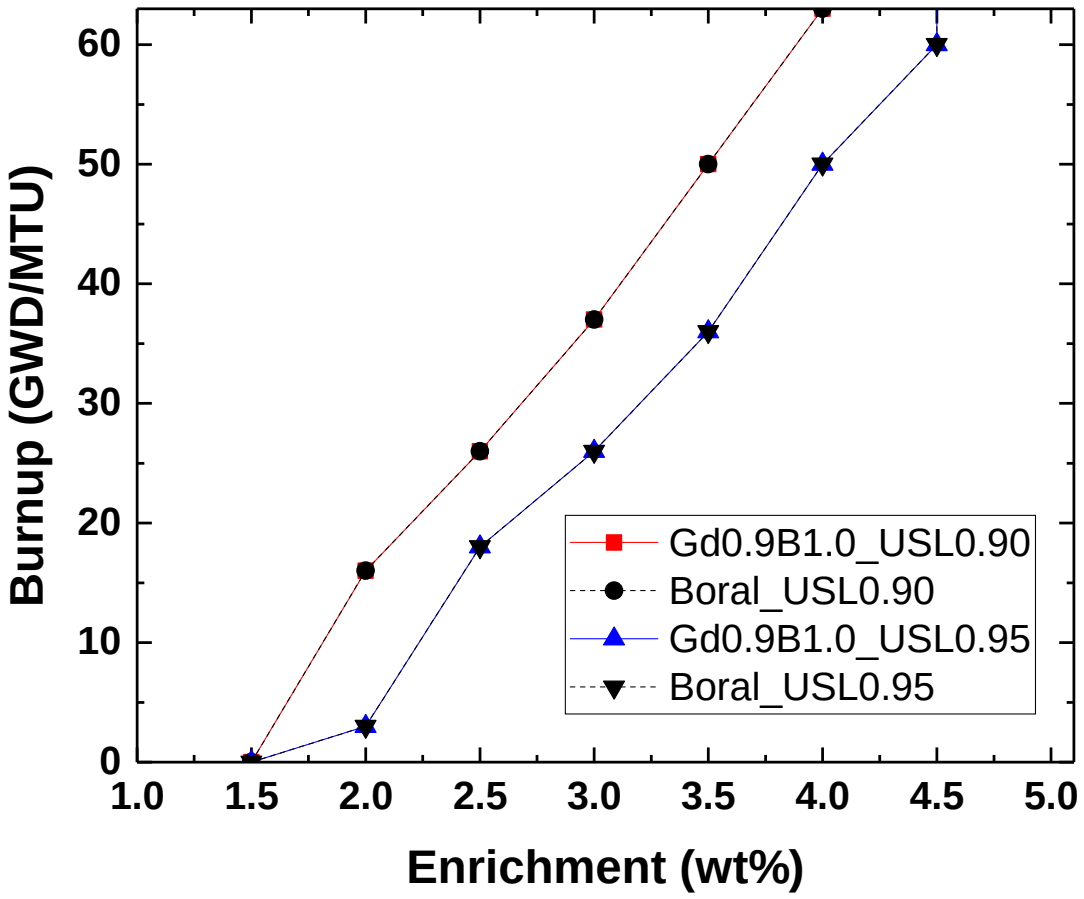

Figure 56 Loading curve for actinide only case

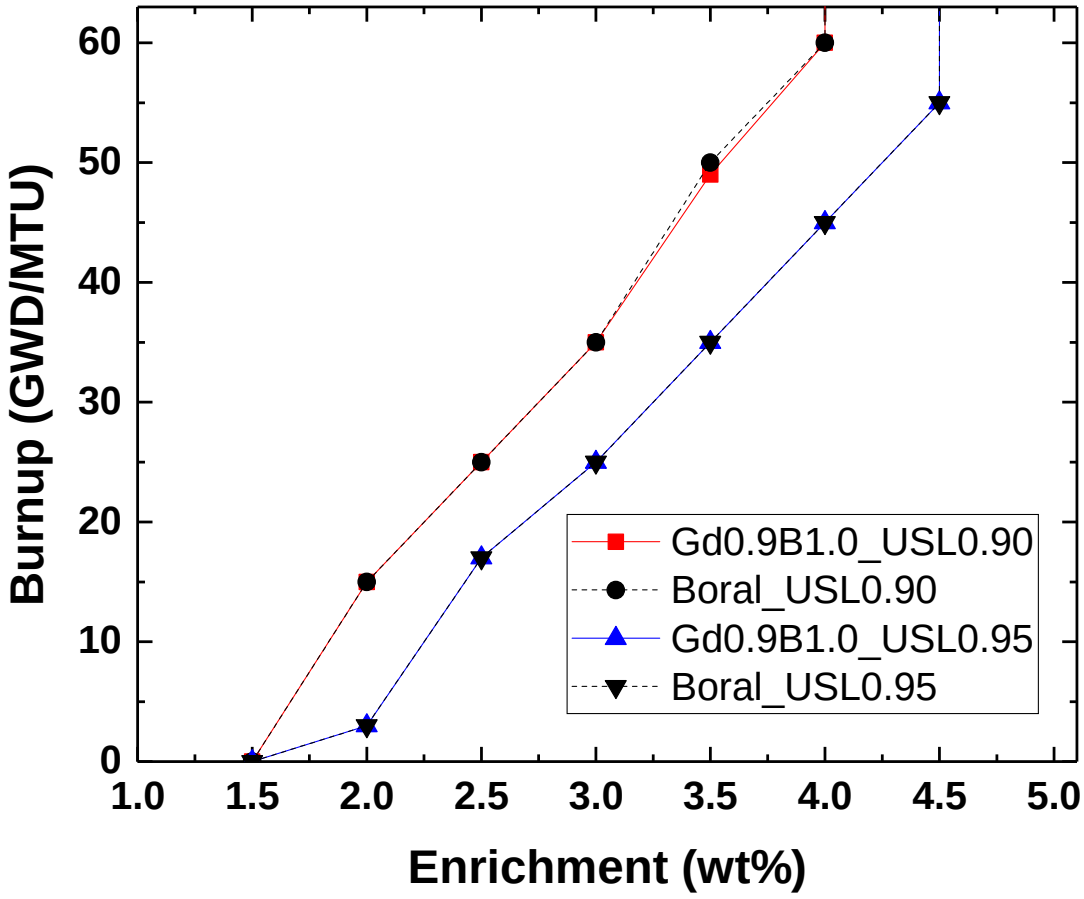

Figure 57 Loading curve for actinide with 16 fission products case

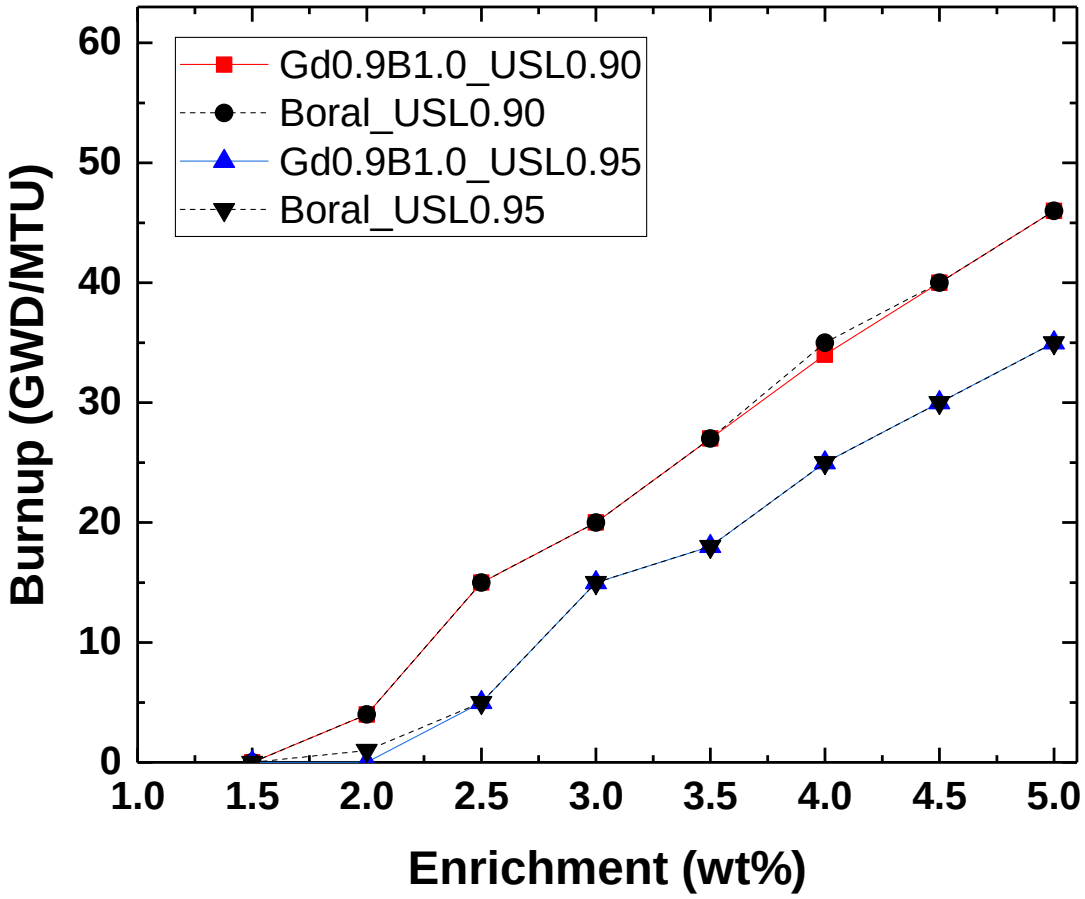

Figure 58 Loading curve for all nuclides case

5.2. Spent fuel transportation and storage cask

Representative models have been selected as KORAD-21 for flux trap type cask. KORAD-21 is developed by KOrea RADioactive waste agency (KORAD) in Korea. The details of KORAD-21 is previously explained in chapter 2. There are two neutron absorbers between adjacent fuel assemblies. It could accommodate 21 fuel assemblies. The fuel assemblies are stored at the center of the basket and the array of baskets is positioned inside the canister. Outside of the canister is a cask body, neutron shield, and outer shell. The cask body is carbon steel, the neutron shield is NS-4-FR resin and the canister and lids are stainless steel. The neutron absorber is METAMIC attached to the basket and sheathing covers it to protect.

The new neutron absorber of Gd and B based stainless steel has been adopted for neutron absorber in the spent fuel cask. The content of neutron absorber is applied by 75 % of the credit of neutron absorbing materials as followed by NUREG-1536. The credit of neutron poison material in fixed neutron absorbers could not be applied more than 75 percent unless the sufficient verifying presence of fabrication tests and uniformity of neutron absorber [22].

The reference neutron absorber of KORAD-21 is METAMIC which has 30.5 wt% of B_4C. The effective multiplication factor (k_{eff}) was 0.91476 ± 0.00021 under water moderation condition. The combination of Gd and B content has been calculated as described in Figure 59.

The required Gd contents have been evaluated for B contents of 0.6, 0.8 and 1.0wt% cases. It has been decided which has a similar performance with the reference neutron absorber. For B 0.6, 0.8 and 1.0wt% cases, the required Gd contents are 1.4, 0.7 and 0.35 wt%, respectively. The amount of total neutron absorbing materials is 2.00, 1.40 and 1.20 wt% for each B condition as summarized in Table 23. The required Gd content according to B content would be simply calculated by the polynomial fitting from Figure 60. The possible contents for KORAD-21 are Gd 0.7 wt% + B 0.8 wt% and Gd 0.35 wt% + B 1.0 wt% which are below constraints.

The Gd 0.35 wt% and B 1.0 wt% stainless steel was selected as representative composition because this case has the lowest total amount of neutron absorbing materials. The optimization study for Gd 0.35 wt% and B 1.0 wt% was conducted. The calculations are performed in the range of thickness 0.45 to 0.60 cm and inner width of 22.0 and 22.2 cm. The minimum k_{eff} was shown at the inner width of 22.0 cm and the thickness of 0.55 cm as described in Table 24.

With the reactivity reduction, the pitch could be reduced for dense storage. With the inner width of 22.0 cm and thickness of 0.55 cm, the pitch could be reduced to 27.3 cm for Gd 0.35 wt% + B 1.0 wt% stainless steel as shown in Figure 61. When the enriched B-10 90% is used, the reactivity could be much more reduced than natural B. With enriched B-10, the optimization study was conducted in Table 25. The optimum dimensions are 22.0 cm for inner width and 0.50 cm for thickness. With the optimized dimensions, Gd 0.35 wt% + B 1.0 wt% (enriched B-10) stainless steel could reduce pitch from 27.7 cm

to 26.0 cm as depicted in Figure 62. The area to store the same amount of fuel assemblies is reduced by about 5.0% ~ 11.89% by calculating from the Eq. (6).

$$Reduced\ area = \left(1 - \frac{(pitch)_{GdB}^2}{(pitch)_{Metamic}^2}\right) \times 100 \quad (6)$$

where:

$Reduced\ area = Area\ reduction\ by\ reducing\ pitch\ with\ Gd\ and\ B\ stainless\ steel\ (\%)$

$(pitch)_{GdB} = Pitch\ for\ Gd\ and\ B\ stainless\ steel\ (cm)$

$(pitch)_{Metamic} = Pitch\ for\ Metamic\ neutron\ absorber\ (cm)$

Table 22 Summary of dimensions for KORAD-21

Component (cm)		KORAD-21
Basket	Inner width	22.2
	Thickness	0.5
	Pitch	27.7
Neutron absorber	Width	18.0
	Thickness	0.3
Canister	Inner diameter	163.6
Cask body	Thickness	21.5

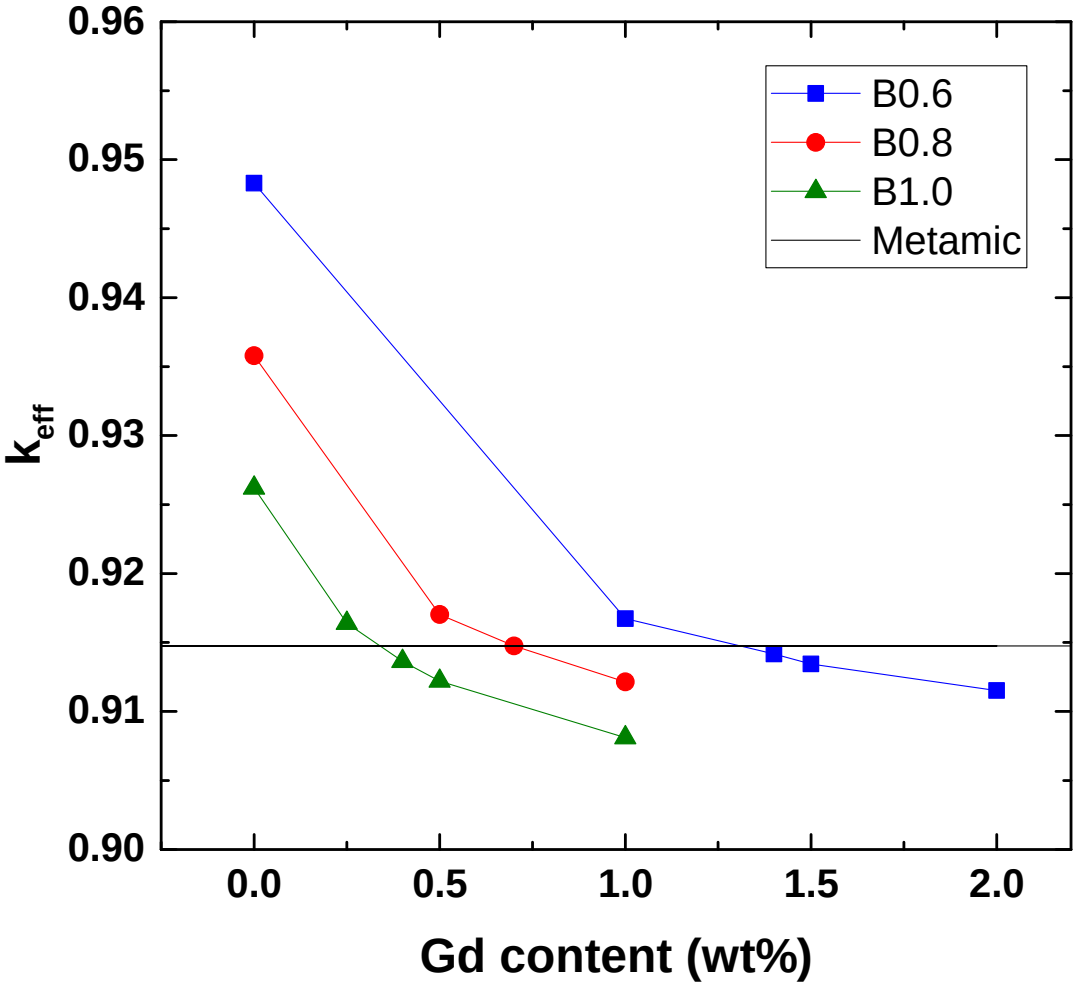

Figure 59 k_{eff} as a function of Gd and B contents for KORAD-21

Table 23 Required neutron absorbing materials for KORAD-21

B content (wt%)	Gd content (wt%)	Total*
0.6	1.40	2.00
0.8	0.70	1.50
1.0	0.35	1.35

*Total amount of neutron absorbing materials (Gd+B)

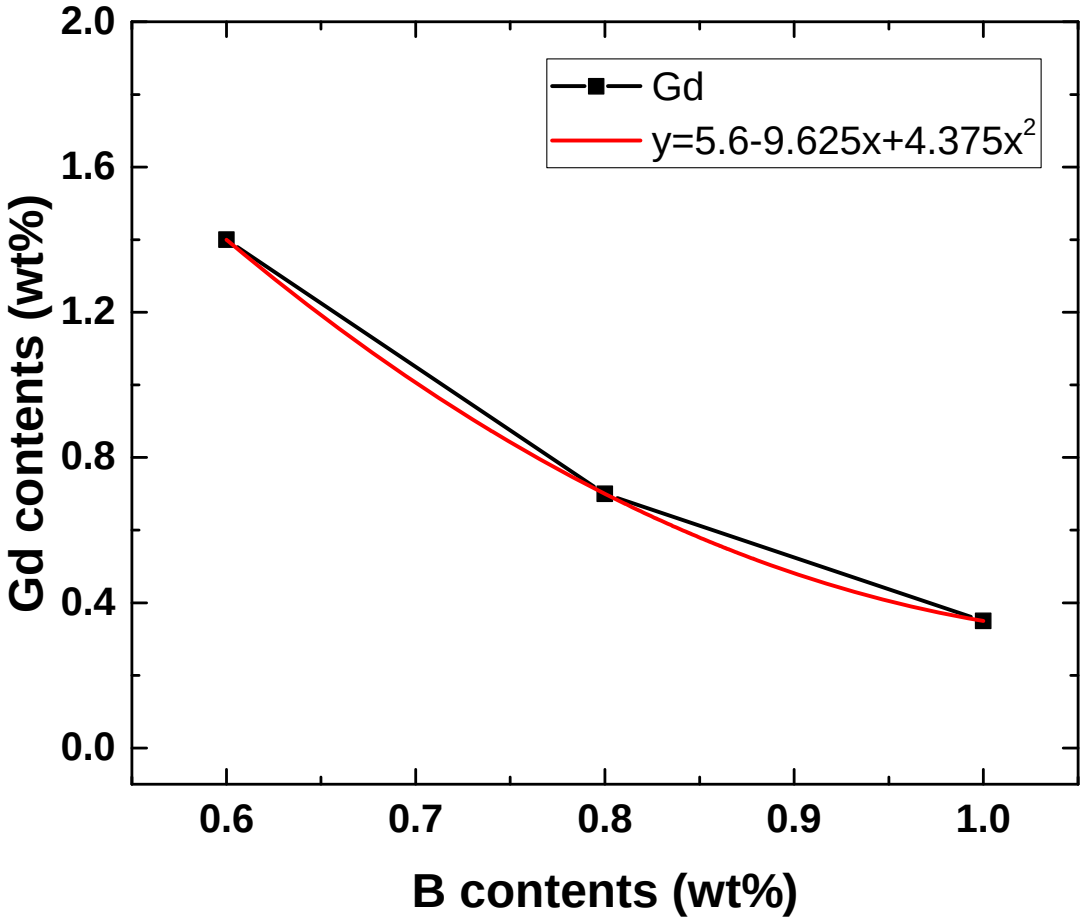

Figure 60 Required Gd contents as a function of B content for KORAD-21 (x: B contents, y: Gd contents)

Table 24 k_{eff} vs cell wall thickness and cell inner width for KORAD-21

Thickness (cm)	Inner width (cm)	
	22.0	22.2
0.40	0.90773	0.91571
0.45	0.90633	0.91478
0.50	0.90585	0.91444
0.55	0.90572	0.91460
0.60	0.90608	0.91514

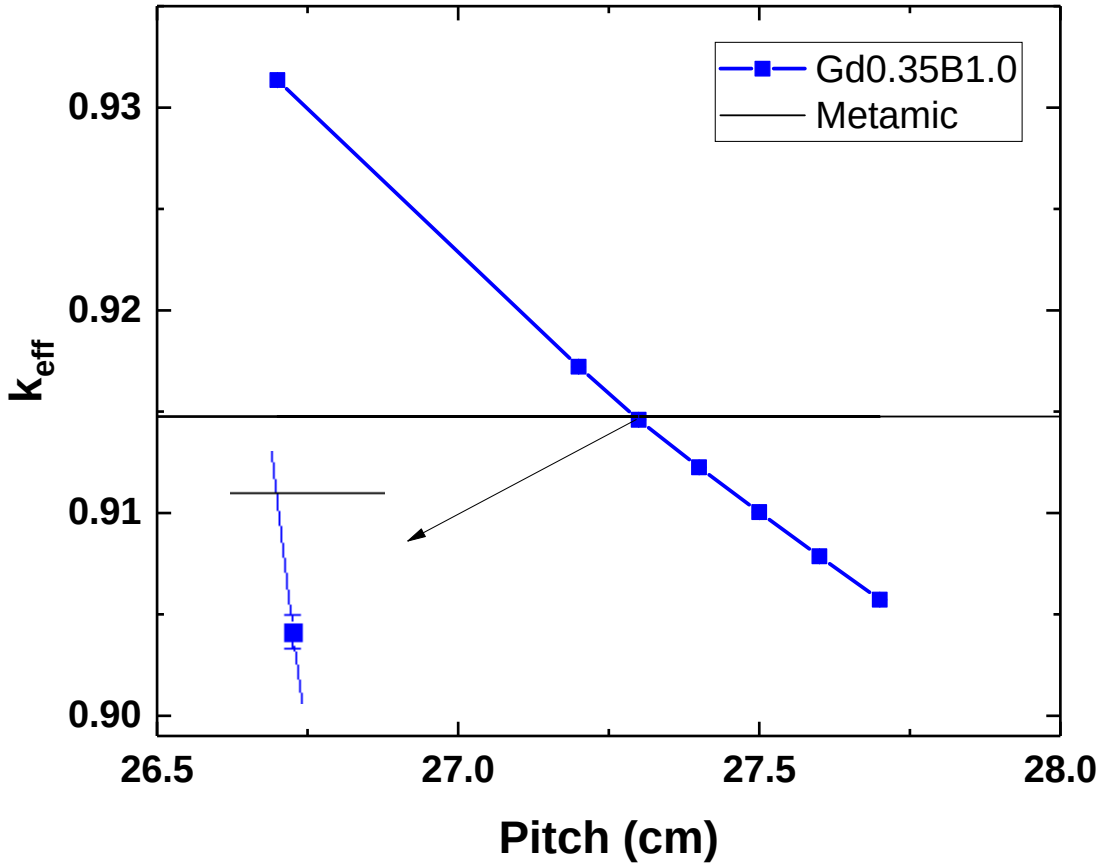

Figure 61 k_{eff} vs pitch for Gd 0.35 wt% + B 1.0 wt% at cell inner width of 22.0 cm and the cell wall thickness of 0.55 cm

Table 25 k_{eff} vs cell wall thickness at cell inner width of 22.0 cm for KORAD-21

Thickness (cm)	Inner width (cm)
	22.0
0.45	0.86260
0.50	0.86243
0.55	0.86297
0.60	0.86359

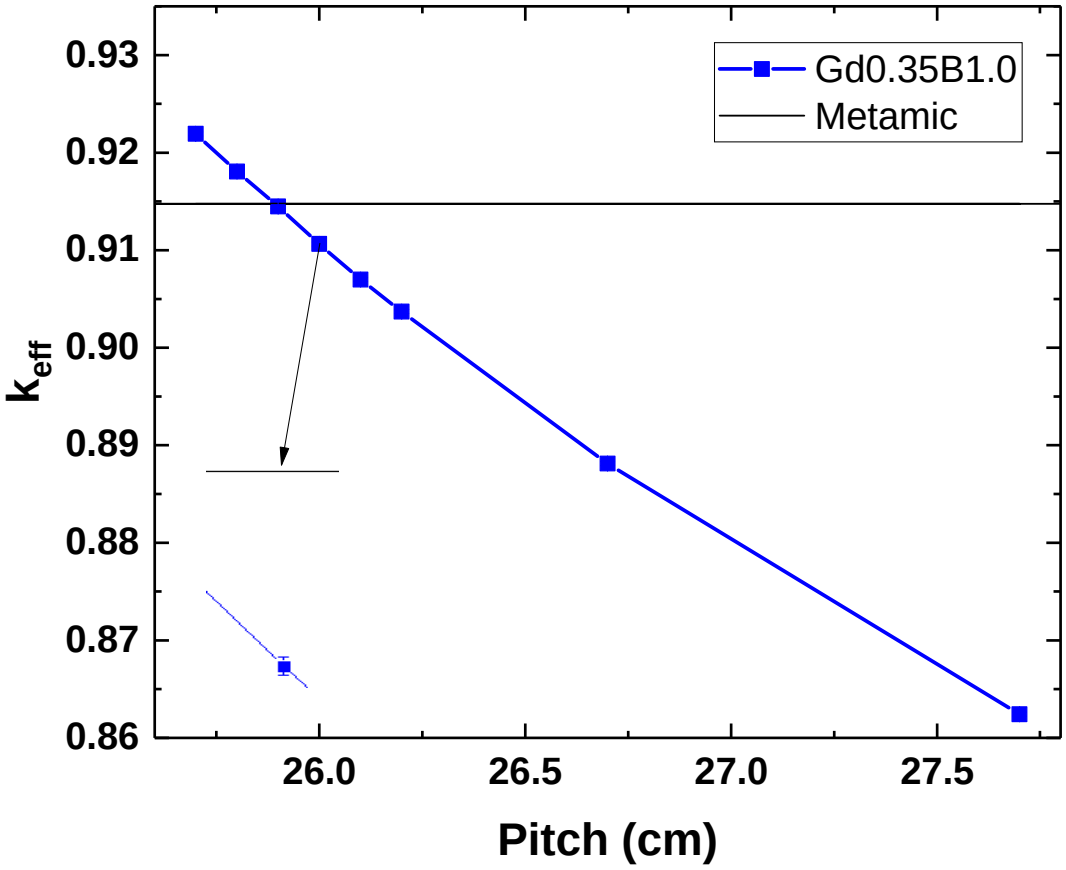

Figure 62 k_{eff} vs pitch for Gd 0.35 wt% + B 1.0 wt% (enriched B-10) at cell inner width of 22.0 cm and the cell wall thickness of 0.50 cm

Table 26 k_{eff} calculated by KENO V.a. and MCS code for Gd 0.35 wt% + B 1.0 wt% (enriched B-10) with inner width of 22.0 cm, thickness of 0.50 cm and pitch of 26.0 cm

KENO V.a.	MCS
0.91063±0.00009	0.90897±0.00010

Chapter 6. Accident analysis for spent nuclear fuel transportation and storage system

The spent fuel storage pool model and spent fuel transportation and storage cask model are the same as Chapter 5. The accident condition shows the most severe phenomenon in criticality. Therefore, the accident analysis should be conducted to be used as a neutron absorber in the SNF T&S system. Among various accident analysis, some cases are selected and conducted in this chapter.

6.1. Spent fuel storage pool

The spent fuel storage pool model is Shin-kori units 3 and 4. The neutron absorbing material content is Gd 0.9 wt% + B 1.0 wt% (enriched B-10) stainless steel.

6.1.1. Region I

The optimized dimensions for the region I are the thickness of 0.5 cm, the inner width of 21.2 cm and the pitch of 24.9 cm. The accident analysis for the region I is selected as a dropping of fuel assembly near the spent fuel pool rack. The fuel assembly could be dropped at the nearest cell between concrete as shown in Figure 63 (a).

The accident scenario is the dropping of the fuel assembly in a 16x1 array of fuel assemblies with neutron absorber. The boundary condition for the accident is the vacuum boundary at the concrete side, the reflective boundary for all other x-y directions and the vacuum boundary for axial direction. The concentration of B in borated water is 2150 ppm. The 4000 ppm of borated water is used during the operation. The k_{eff} for dropped fuel assembly accident is 0.80980 as summarized in Table 27. The k_{eff} shows lower than 0.95, therefore, the Gd 0.9 wt% + B 1.0 wt% could be used in Shin-kori units 3 and 4.

6.1.2. Region II

The optimized dimensions for region II are the thickness of 0.25 cm, the inner width of 21.2 cm and the pitch of 22.05 cm. The accident analysis for region II is selected as a misloading of the fuel assembly. The fuel assemblies stored in region II are the enrichment of 5.0 wt% and burnup of 46 GWD/MTU. The 46 GWD/MTU burnup is the minimum burnup required when the upper safety limit is 0.90. In a 2x2 array of fuel assemblies, the one fuel assembly of enrichment of 5.0 wt% for fresh fuel condition is misloaded in spent fuel rack as shown in Figure 63 (b). The B concentration of borated water is 2150 ppm which is almost a half value of 4000 ppm in operation. The neutron multiplication factor for Gd 0.9 wt% + B 1.0 wt% is 0.87343 in Table 27. It is lower than the regulatory limit of 0.95 so it could be

used in Shin-kori units 3 and 4 as a neutron absorber.

a

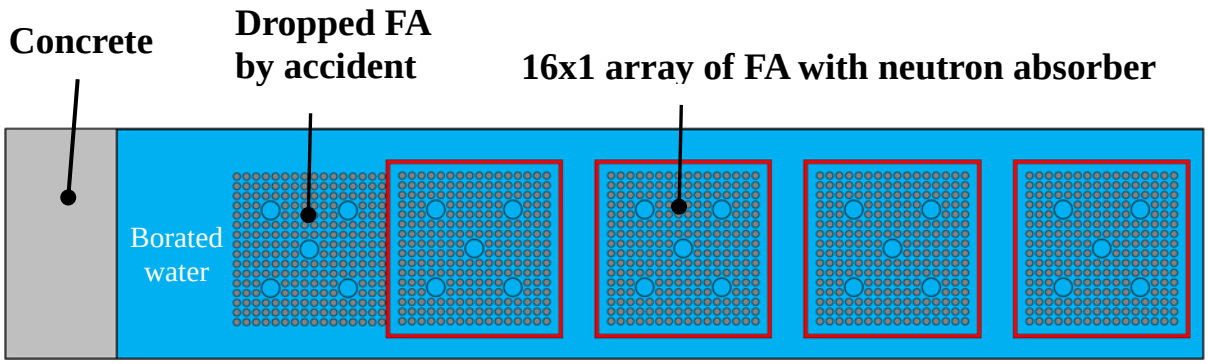

(a)

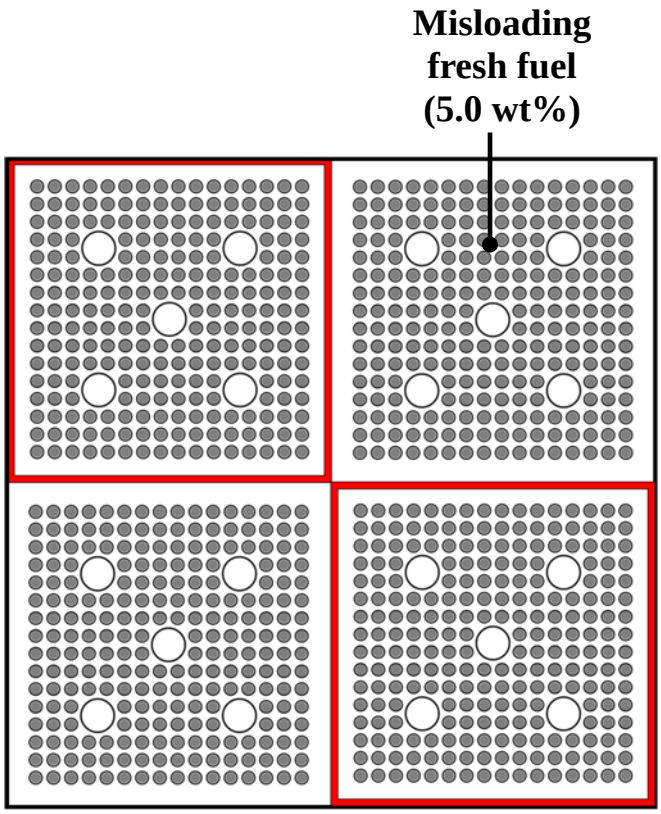

(b)

Figure 63 Accident conditions (a) Dropping of the fuel assembly in 16x1 array of fuel assemblies with neutron absorber at the region I (Only 4x1 array is described in figure and skipped for rest array of fuel assemblies) (b) Misloading of fuel assembly at region II

Table 27 k_{eff} for accident conditions for spent fuel pool storage

Condition	k_{eff}
Dropped FA	0.80980
Misloading of one FA	0.87343

6.2. Spent fuel transportation and storage cask

The spent fuel transportation and storage cask model is KORAD-21. The neutron absorbing material content is Gd 0.35 wt% + B 1.0 wt% (enriched B-10) stainless steel. The optimized dimensions are the thickness of 0.50 cm, the inner width of 22.0 cm and the pitch of 26.0 cm.

The accident cases studied in this chapter is eccentric positions of fuel assemblies, flooding with various water height and storing damaged fuel assembly. For the damaged fuel assembly, two conditions are considered missing one fuel rod and bare fuel rods.

For eccentric positioning of fuel assemblies, cell center positioning, cask centered positioning and cask periphery positioning are considered as described in Figure 64. The cask centered configuration is all assemblies in the basket are moved to the center of the cask. The cask periphery configuration is all assemblies in the basket are moved to the outside of cask. Among the three configurations, the cask centered configuration showed the highest multiplication factor as summarized in Table 28.

From the flooding accident, the cask could be flooded in the various height of the water as shown in Figure 65. The multiplication factor continuously increases with increasing the height of the water as shown in Figure 66. The 100% of flooded condition is the most severe case. When the water is flooded between pellet and cladding, the k_{eff} is 0.91793 in Table 28.

For storage of the damaged fuel, the missing one fuel rod in a fuel assembly and bare fuel rod are analyzed. The missing one fuel rod is at 8x8 position in Westinghouse OFA 17x17 fuel assembly as described in Figure 67. The fuel assembly with missing one fuel rod is applied to all fuel assemblies stored in the KORAD-21 cask. The neutron multiplication factor for missing one fuel rod is 0.91177. The bare fuel rods are missing of cladding at fuel rods as described in Figure 68 (a). One fuel assembly of bare rods and twelve fuel assemblies with bare rods are applied in KORAD-21. The configuration of twelve fuel assemblies with bare rods are illustrated in Figure 68 (b). The k_{eff} for twelve fuel assemblies of bare rods is 0.93116 in Table 28. All accident conditions ensure the safety limit of 0.95.

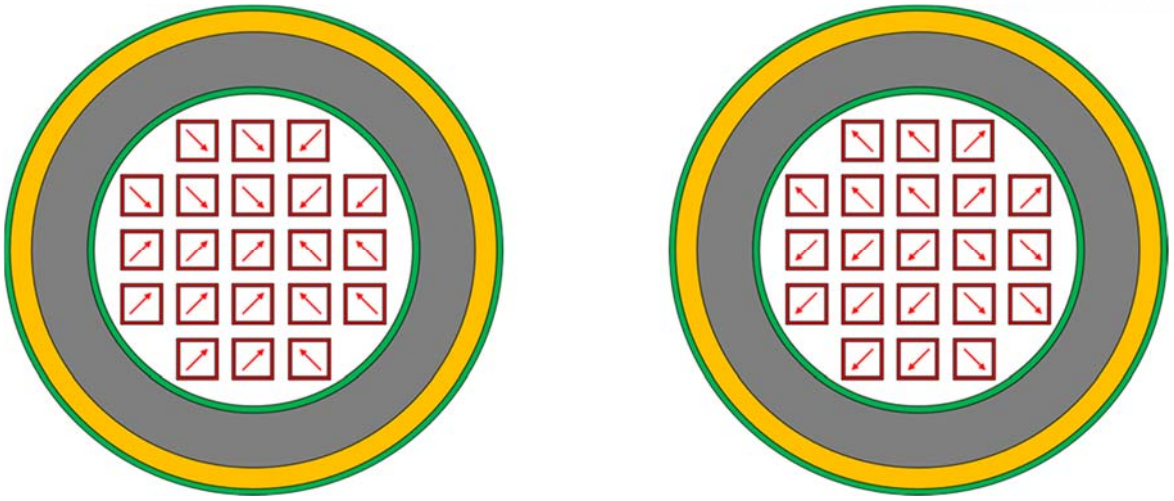

(a) (b)

Figure 64 Schematics of eccentric positions of fuel assemblies in cask (a) cask centered position (b) cask periphery position

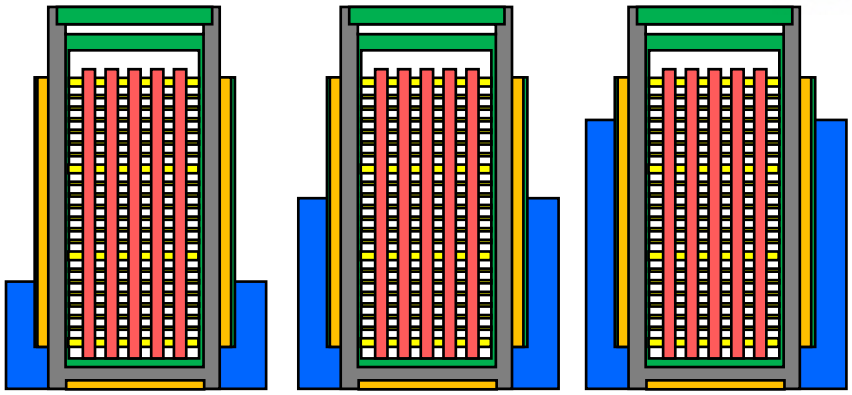

25% **48%** **75%**

Figure 65 Configuration of the various water height

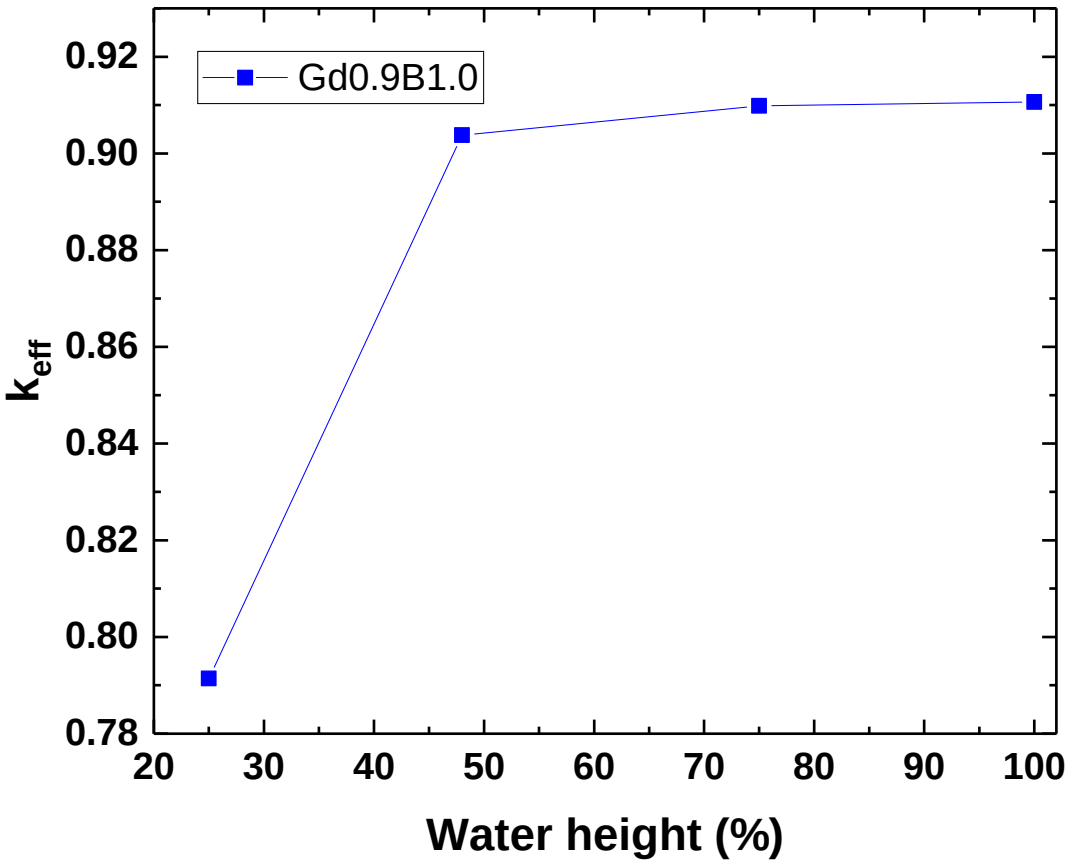

Figure 66 k_{eff} vs water height

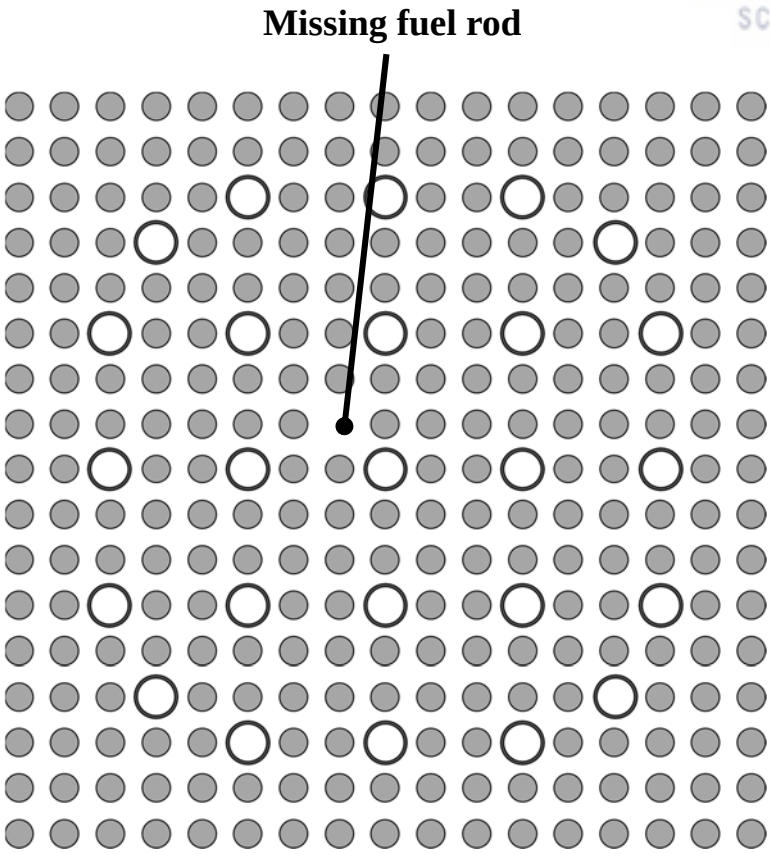

Figure 67 Missing one fuel rod at 8x8 position for the Westinghouse OFA 17x17 fuel assembly

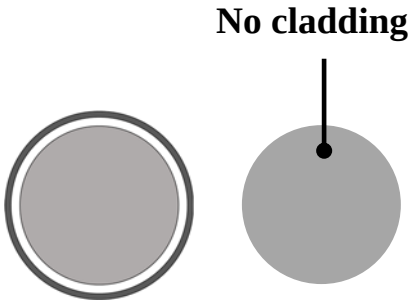

(a)

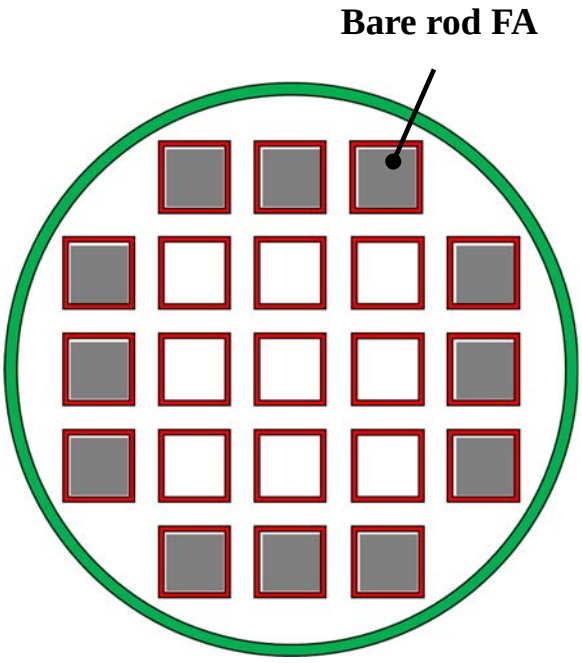

(b)

Figure 68 Configuration of bare rod fuel assembly (a) bard rod (b) orientation of 12 fuel assemblies for bare rod fuel assembly

Table 28 k_{eff} of accident conditions for KORAD-21

Condition		k_{eff}
Cell positioning	Cell center	0.91063
	Cask centered	0.91172
	Cask periphery	0.89262
Water between pellet and cladding		0.91793
Missing one fuel rod	8x8 position	0.91177
Bare rod	One fuel assembly	0.91384
	12 fuel assemblies	0.93116

Chapter 7. Conclusions

The application of Gd and B to neutron absorber could improve the criticality safety for spent fuel transportation and storage system due to their high thermal neutron absorption cross section. The Gd and B stainless steel was used as the integral type which is a single layer without separate neutron absorber or sheathing. Also, the manufacturing cost of the spent fuel transportation and storage system could be greatly reduced using the Gd and B stainless steel compared to Boral and Metamic. The cost-saver is the disappearance of the welding process between the cell wall and a sheathing containing a separate neutron absorber.

The sensitivity studies were conducted for optimizing design parameters of pitch between fuel assemblies, inner width of cell and thickness of the cell wall in spent fuel transportation and storage system. The selected dimensions are pitch 28.03 cm, inner width 22.35 cm, and thickness 0.2 cm. When analyzing each parameter, the other parameters are fixed. The composition of the cell wall was selected as two cases for no neutron absorber (stainless steel) and neutron absorber (Gd 1 wt%).

Firstly, the neutron multiplication factor continuously decreased with the increasing pitch from 22.75 cm to 34.03 cm with a constant inner width of 22.35 cm and thickness of 0.2 cm. As the distance between fuel assemblies increases, it is getting hard that the neutrons generated from fuel assembly impact on neighboring fuel assembly. Also, the total quantity of water between fuel assembly increases. Therefore, the absorption rate at the water gap increases and the thermalization of neutron enhanced. The enhanced thermalization at the water gap for SF transportation and storage system decreases the reactivity by trapping neutrons although the reactivity increases when neutron thermalization is enhanced for thermal reactors. This is because the water gap act as a flux trap that neutrons thermalized at the water gap are absorbed by neutron absorber before encountering fuel assemblies due to the short mean free path of thermal neutron.

Next, the k_{eff} proportionally increased with increasing inner width of the cell from 20.56 cm to 27.63 cm with a fixed pitch of 28.03 cm and thickness of 0.2 cm. The absorption cross section of Gd is extremely strong, therefore, the neutron flux steadily decreased in cosine shape from fuel assembly to cell wall (Gd 1 wt%). Due to the flux trap, the neutron spectrum hardening was noticed when inner width increases. Unlike the Gd 1 wt% case, the stainless steel has a low absorption cross section, thus, the neutron thermalization in the water region between fuel assembly and cell wall was enhanced with increasing inner width. Therefore, a large inner width makes the reactivity increase except for the inner width of 20.56 cm to 22.35 cm. When the inner width is between 20.56 cm to 22.35 cm, the distance between fuel assembly and the cell wall is 0 to 0.895 cm. The neutron mean free path below the fast energy region is lower than 1 cm. Therefore, the neutrons outside of the cell wall penetrate through stainless steel and encounter with fuel assembly at a shorter inner width in the region of 20.56 cm to

22.35 cm.

Finally, the reactivity showed the lowest at specific thickness according to contents of neutron absorber in the range of thickness 0.01 to 2.84 cm with a constant pitch of 28.03 cm and inner width of 22.35 cm. As the thickness increases, the flux trap continuously decreased, however, the k_{eff}s do not correspond to flux trap size. This is due to that the total quantity of stainless steel increases as thickness increases. Although stainless steel has a low neutron absorption cross section, it still has the ability to absorb neutrons. Therefore, the reactivity decreases with a large quantity of stainless steel, on the contrary, the reactivity increases with a small flux trap size. The optimum thickness for stainless steel was 1.0 cm. This phenomenon is much dramatically noticeable for the neutron absorber case, Gd 1 wt%. At the constant composition of Gd 1 wt%, the total quantity of Gd increases as thickness increases. Thus, a small increase in thickness makes a huge reduction in reactivity. However, the flux trap gradually decreases with increasing thickness. The optimum thickness for Gd 1 wt% was 0.3 cm.

For reducing reactivity, the pitch should be maximum, and the inner width should be minimum when neutron absorber exists. The thickness of the cell wall is needed to be analyzed for specific neutron absorber content. However, large pitch occupies large space to store the same amount of fuel assemblies. Only if the subcriticality is maintained, the pitch should be reduced for effective storage.

The new neutron absorber, Gd and B stainless steel with optimized dimension was applied to spent fuel transportation and storage cask and spent fuel pool storage rack. For the flux trap type transportation and storage system, the spent fuel pool of Shin-kori units 3 and 4 was selected for the spent fuel storage pool and the KORAD-21 was selected for spent fuel storage cask. The possible combination of Gd and B stainless steel and the optimized dimension were analyzed.

For the base dimension of Shin-kori units 3 and 4, the possible combination of Gd and B stainless steel is Gd 0.9 wt% + B 1.0 w%. The Gd 0.9 wt% + B 1.0 wt% was selected as optimization study for region I. Through optimization studies, the optimized inner width was 21.2 cm and the optimized thickness was 0.45 cm for natural B and 0.5 cm for enriched B. With combination of Gd and B stainless steel and optimized dimensions, the pitch could be reduced from 27.0 cm to 26.0 cm (natural B) and 24.9 cm (enriched B). 13.5 ~ 23.6% more fuel assemblies could be stored in the same space compared to Boral.

For the base dimension of Shin-kori units 3 and 4, the Gd 0.9 wt% + B 1.0 wt% (enriched B) was selected as the optimization study for region II. The optimized inner width was 21.2 cm and the optimized thickness is 0.5 cm. The pitch could be reduced from 22.5 cm to 22.05 cm. The 4.05% more fuel assemblies could be stored in the same space compared to Boral.

For the base dimension of KORAD-21, the possible combination of Gd and B stainless steel is Gd 0.7 wt% + B 0.8 wt% and Gd 0.35 wt% + B 1.0 w%. Among them, the Gd 0.35 wt% + B 1.0 wt% was selected as the optimization study. Through optimization studies, the optimized inner width was 22.0 cm and the optimized thickness was 0.55 cm (natural B) and 0.5 cm (enriched B). With the combination of Gd and B stainless steel and optimized dimensions, the pitch could be reduced from 27.7 cm to 27.3

cm (natural B) and 26.0 cm (enriched B). The 2.9 ~ 11.89% area covered by fuel assemblies is reduced in the same space compared to Metamic.

Maintaining subcriticality for accident conditions is critical. For SFP rack, the fuel assembly dropped in the region I and misloading of fresh fuel in region II were considered. For SFP cask, the eccentric position of the fuel assembly, flooding at various water height, flooding between pellet and cladding and loading of damaged fuel were analyzed. All accident conditions maintain subcriticality. The Gd and B stainless steel could ensure regulatory limits for accident conditions.

In conclusion, the Gd and B stainless steel with an optimized dimension could improve criticality control. This neutron absorber could applicable to both spent fuel cask and rack. Also, it could be stored more fuel assemblies in the same space.

Reference

[1] KHNP, “Spent nuclear fuel storage stauts of 2019 1st quarter,” *KHNP*, 2019. [Online]. Available: http://www.khnp.co.kr/board/BRD_000179/boardView.do?pageIndex=1&boardSeq=70138&mnCd=FN051304&schPageUnit=10&searchCondition=0&searchKeyword=.

[2] C. Dethloff, E. Gaganidze, V. V. Svetukhin, and J. Aktaa, “Modeling of helium bubble nucleation and growth in neutron irradiated boron doped RAFM steels,” *J. Nucl. Mater.*, vol. 426, no. 1–3, pp. 287–297, 2012.

[3] Y. Jung, K. Kim, and S. Ahn, “Helium bubble formation in neutron absorber irradiated in spent nuclera fuel pool,” in *Transactions of American Nuclear Society*, 2018, vol. 119, pp. 299–300.

[4] R. Nickel *et al.*, “Standard Specification for Alloy Plate , Sheet , and Strip 1,” ASTM B932-04, 2016.

[5] K.-O. Kim, “A Study on the Design and Its Application of Artificial Rare Earth (Re2O3) Based Neutron Absorber,” Hanyang University, 2012.

[6] S. H. Kim *et al.*, “An evaluation of the design and performance for a new neutron absorber based on an artificial rare-earth compound,” *Ann. Nucl. Energy*, vol. 85, pp. 461–466, 2015.

[7] S. H. Kim, J. H. Kim, C. H. Shin, J. K. Kim, H. S. Park, and S. Y. Kim, “A feasibility study on the criticality control method using radioactive vitrified forms for spent fuel storage,” *Nucl. Eng. Des.*, vol. 280, pp. 644–650, 2015.

[8] Y. Choi, Y. Baik, B. M. Moon, and D. S. Sohn, “Corrosion and Wear Properties of Cold Rolled 0.087% Gd Lean Duplex Stainless Steels for Neutron Absorbing Material,” *Nucl. Eng. Technol.*, vol. 48, no. 1, pp. 164–168, 2016.

[9] J.-H. Lim, “Development of Gd Containing Duplex Stainless Steel for Spent Nuclear Fuel Applications,” Sungkyunkwan University, 2016.

[10] B.-M. Moon, S.-W. Lee, M.-J. Kim, S.-R. Jung, Y.-J. Kim, and H.-D. Jung, “The Effect of Gadolinium on the Microstructures and Charpy Impact Properties of Super Duplex Stainless Steels,” *Metals (Basel).*, vol. 8, no. 7, p. 474, Jun. 2018.

[11] M. Y. Jung, Y. Baik, Y. Choi, and D. S. Sohn, “Corrosion and mechanical properties of hot-rolled 0.5%Gd-0.8%B-stainless steels in a simulated nuclear waste treatment solution,” *Nucl. Eng. Technol.*, vol. 51, no. 1, pp. 207–213, Feb. 2019.

[12] ORNL, “The High Flux Isotope Reactor (HFIR) User guide Rev 2.0,” 2015.

[13] C. J. Stanley and F. M. Marshall, “Advanced Test Reactor - A National Scientific User Facility,” in *Proceedings of the 16th International Conference on Nuclear Engineering*, 2008.

[14] F. Marshall, T. Allen, J. Benson, J. Cole, and M. Thelen, “Advanced Test Reactor National Scientific User Facility Partnerships,” 2012.

[15] H. Gerstenberg and I. Neuhaus, “A brief overview of the research reactor FRM II,” *Int. J. Nucl. Energy Sci. Technol.*, vol. 4, no. 4, p. 265, 2009.

[16] A. Axmann, K. Böning, and M. Rottmann, “FRM-II: The new German research reactor,” *Nucl. Eng. Des.*, vol. 178, no. 1, pp. 127–133, Dec. 1997.

[17] A. Röhrmoser, “Core model of new German neutron source FRM II,” *Nucl. Eng. Des.*, vol. 240, no. 6, pp. 1417–1432, Jun. 2010.

[18] K. N. CHOO, M. S. CHO, S. W. YANG, and S. J. PARK, “CONTRIBUTION OF HANARO IRRADIATION TECHNOLOGIES TO NATIONAL NUCLEAR R&D,” *Nucl. Eng. Technol.*, vol. 46, no. 4, pp. 501–512, Aug. 2014.

[19] “The operation status of nuclear facility of HANARO,” *KAERI*. [Online]. Available: https://www.kaeri.re.kr/board?menuId=MENU00386.

[20] M. Shahmohammadi Beni, T. C. Hau, D. Krstic, D. Nikezic, and K. N. Yu, “Monte Carlo studies on neutron interactions in radiobiological experiments,” *PLoS One*, vol. 12, no. 7, p. e0181281, Jul. 2017.

[21] H. D. Sohn and J. K. Kim, “Effect of stainless steel plate position on neutron multiplication factor in spent fuel storage racks,” *Nucl. Eng. Technol.*, vol. 43, no. 1, pp. 75–82, 2011.

[22] U.S.NRC, “Standard Review Plan for Spent Fuel Dry Storage Systems at a General License Facility Final Report,” NUREG-1536 Revision 1, 2010.

[23] M. B. Chadwick *et al.*, “ENDF/B-VII.0: Next Generation Evaluated Nuclear Data Library for Nuclear Science and Technology,” *Nucl. Data Sheets*, vol. 107, no. 12, pp. 2931–3060, 2006.

[24] J. C. Wagner, “Computational Benchmark for Estimation of Reactivity Margin from Fission Products and Minor Actinides in PWR Burnup Credit,” NUREG/CR-6747, 2000.

[25] A. Machiels, “Qualification of METAMIC® for Spent-Fuel Storage Application,” Palo Alto, CA, 1003137, 2001.

[26] K. Kim, S. Chung, and J. Hong, “Performance evaluation of METAMIC neutron absorber in spent fuel storage rack,” *Nucl. Eng. Technol.*, vol. 50, no. 5, pp. 788–793, Jun. 2018.

[27] A. Machiels and R. Lambert, “Handbook of Neutron Absorber Materials for Spent Nuclear Fuel Transportation and Storage Applications: 2009 Edition,” Palo Alto, CA, 1019110, 2009.

[28] “Neutron absorber material,” *Holtec Intenational*. [Online]. Available: https://holtecinternational.com/productsandservices/innovative-technologies/neutronabsorbermaterial/.

[29] ASTM International, “Standard Specification for Borated Stainless Steel Plate, Sheet, and Strip for Nuclear Application,” ASTM A887-89, 2014.

[30] W. L. Hurt, R. E. Mizia, T. E. Lister, P. J. Pinhero, C. V Robino, and J. N. Dupont,

"Development Of Neutron Absorbers To Support Disposal Of DOE SNF," in *2003 International High-Level Radioactive Waste Management Conference*, 2003.

[31] D. Loaiza, R. Sanchez, G. Wachs, W. Hurt, and R. Mizia, "Critical Experiment Analysis of Neutron Absorbing Ni-Cr-Mo-Gd Alloy Being Considered for the Disposal of SNF," *J. Nucl. Mater. Manag.*, vol. 32, no. 2, 2004.

[32] A. A. Galahom, "Study of the possibility of using Europium and Pyrex alloy as burnable absorber in PWR," *Ann. Nucl. Energy*, vol. 110, pp. 1127–1133, 2017.

[33] J. Choe, H. C. Shin, and D. Lee, "New burnable absorber for long-cycle low boron operation of PWRs," *Ann. Nucl. Energy*, vol. 88, pp. 272–279, 2016.

[34] K. J. R. Rosman and P. D. P. Taylor, "Isotopic Compositions of the Elements 1997," *Int. Union Pure Appl. Chem.*, vol. 70, no. 1, pp. 217–235, 1998.

[35] U.S.NRC, "An Approach for Validating Actinide and Fission Product Burnup Credit Criticality Safety Analyses — Criticality (keff) Predictions Office of Nuclear Regulatory Research," NUREG/CR-7109, 2011.

Acknowledgement

박사 과정을 진행하면서 저의 학위 논문이 잘 마무리될 수 있도록 도와주신 모든 분들께 감사의 인사를 드리고자 합니다.

학위 과정 내내 끊임없이 저를 지도해주신 손동성 교수님과 이덕중 교수님께 감사 인사를 드립니다. 또한, 저의 학위 수여를 위하여 아낌없는 조언을 주셨던 윤의성 교수님, 박창제 교수님 그리고 이현철 교수님께 감사의 인사를 전합니다.

언제나 저를 지지하고 응원해주었던 저의 가족 모두와 친구들 그리고 연구실원들 모두 감사합니다.

마지막으로 한정된 지면을 통해서 일일이 언급을 하지 못하였지만 그 동안 저를 도와주셨던 모든 분들께 감사 인사를 드리며, 모든 분들이 계셨기에 저의 학위가 잘 마무리될 수 있었습니다. 감사합니다.

2020년 1월

김미진